INFORMATION PRESERVATION METHODS FOR MODELING MICRO-SCALE GAS FLOWS

by

Quanhua Sun

A dissertation submitted in partial fulfillment
of the requirements for the degree of
Doctor of Philosophy
(Aerospace Engineering)
in The University of Michigan
2003

Doctoral Committee:

Professor Iain D. Boyd, Chair
Professor Graham V. Candler, University of Minnesota
Assistant Professor Andrew J. Christlieb
Professor Gerard M. Faeth
Professor Philip L. Roe

To my family and friends

ACKNOWLEDGMENTS

graduate secretary Margaret Fillion and other staff as well as other friends, who always offered me their generous help when in need.

I am deeply indebted to my family, especially to my wife, for their care, support, understanding, and love. Their constant cheers and words of encouragement have always helped me in many ways.

TABLE OF CONTENTS

LIST OF FIGURES

LIST OF TABLES

NOMENCLATURE

<u>English</u>

a speed of sound

B continuum breakdown parameter suggested by Garcia et al.

C_L lift coefficient

C_D drag coefficient

$\mathbf{c}$ molecule velocity vector

$\mathbf{c}'$ molecular thermal velocity vector

c molecular speed

c_r relative speed between two molecules

d diameter of a molecule

e energy

$\mathbf{F}$ external force vector per unit mass

f velocity distribution function

$\mathbf{h}$ heat flux vector

$\mathbf{I}$ unit tensor

Kn Knudsen number

k Boltzmann constant

L characteristic length

m mass of a molecule

N number of molecules

n	number density of molecules
P	continuum breakdown parameter suggested by Bird
Pr	Prandtl number
p	pressure tensor
p	scalar pressure
Q	physical quantity
q	heat flux vector
R	specific gas constant
Re	Reynolds number
r	physical space vector
S	surface area
T	thermodynamic temperature
T_a	additional temperature in the energy flux model
t	time
u	velocity in x direction
V	flow velocity vector
V	gas flow speed
Vol	volume
v	velocity in y direction

Greek

α	angle of attack
χ	collision deflection angle in the collision plane
δ	mean molecular spacing
δ_{ij}	kronecker delta

ε	internal energy
ϕ	continuum breakdown parameter suggested by Tiwari
γ	ratio of specific heats
κ	coefficient of heat conduction
λ	mean free path of molecules
μ	viscous coefficient
θ	collision deflection angle in the collision plane
ρ	mass density
$\sigma d\Omega$	differential cross-section
$\boldsymbol{\tau}$	shear stress tensor
τ_0	mean collision time
ξ	number of degrees of freedom

Subscripts

buf	related to buffer cells
c	related to cell
GLL	gradient-length local
IP	related to IP cells
i	particle index
NS	related to N-S cells
n	component normal to surface
res	related to reservoir cells
s	surface condition or component parallel to surface
w	wall condition
∞	free stream condition

Superscripts

$\overline{(\ )}$ statistical average

$(\ )'$ pre-collision

$(\ )''$ post-collision

$(\ )^{in}$ related to incident particles

$(\ )^{re}$ related to reflected particles

CHAPTER I

INTRODUCTION

Micro-scale gas flow is a new research field driven by microsystems technology. Experiments have shown that fluid mechanics of micro-scale gas flows are not the same as those experienced in the macroscopic world. In order to understand micro-scale gas flows, many numerical methods have been developed. However, these methods either lack on physics or are numerically expensive. In this thesis, a general-purpose numerical approach is developed for modeling micro-scale gas flows with reasonable efficiency and accuracy. First, a particle approach called the "information preservation" (IP) method is developed that has a relatively low numerical cost for a kinetic method. Second, a hybrid approach is introduced that couples the IP method and a continuum approach, which limits the numerical cost by using the continuum approach in continuum regions and maintains the physical accuracy by applying the IP method in the other computational regions. Finally, an application of the hybrid approach to study micro-scale gas flows is included in this thesis.

1.1 Background

Micro-scale gas flow is a rapidly growing research field being driven by microsystems technology (Senturia, 2001). This technology is opening doors to a micro scale world and is generating numerous topics for almost all engineering fields (Epstein and Senturia, 1997), including aerospace, biological, chemical, electrical, material, and mechanical engineering.

Microsystems, or microelectromechanical systems (MEMS), are devices that have a characteristic length of less than 1 millimeter but more than 1 micron, that combine mechanical and electrical components, and that are fabricated using integrated circuit batch processing technologies. These systems have many advantages due mainly to their small size. They can be batch-manufactured with very low costs. They require little energy to operate. They miniaturize systems and improve their performance. Microsystems also enable new functions in some areas. Because of these advantages, microsystems are finding increased applications in a variety of industrial and medical fields, with a potential worldwide market in the billions of dollars (French, 2000; Ehrfeld and Ehrfeld, 2001).

Many applications of microsystems involve gas flows. Typical of such applications include micro-turbines (McNeely, 1998; Blankinship, 2001), chemical sensors (Hagleitner et al., 2001), micro-propulsion for spacecraft (Rossi et al., 2001), micro sensors and micro actuators to sense and control small-scale vortex structure for increasing the aerodynamic efficiency and maneuverability of aircraft (Lofdahl and Gad-el-Hak, 1999; Gad-el-Hak, 2001; Choi et al., 2002), and hand-held gas chromatography systems for the detection of trace concentrations of air-borne pollutants (Kolesar and Reston, 1998).

However, our understanding of micro-scale gas flows lags far behind the rapid progress in the fabrication and application of microsystems (Ho and Tai, 1998; Gad-el-Hak, 1999; Beskok, 2001; Karniadakis and Beskok, 2002). Experiments have shown that the fluid mechanics of micro-scale gas flows are not the same as those experienced in the macroscopic world. For instance, the pressure distribution in a long micro-channel was observed to be nonlinear (Pong et al., 1994), and the measured flowrate in a micro-channel was higher than that predicted from a conventional continuum flow model (Arkilic, 1997). The frictional force between the rotor and the substrate of a micro motor (Fan et al., 1988) is found to be a function of the contact area instead of the normal force

(Ho and Tai, 1998). The dynamic response of micromachined accelerometers operating at atmospheric conditions was observed to be over-damped (Gad-el-Hak, 1999).

Therefore, it is necessary to investigate the fluid mechanics of micro-scale gas flows, to better understand microsystems and optimize their performance. First, theoretical analysis can use the Boltzmann equation to explain basic physics of micro-scale gas flows because this equation is considered the governing equation for such flows. However, this equation is far too complicated to analyze practical micro-scale gas flows. Therefore, drastic approximations are often made to the Boltzmann equation. Thus analytic results obtained from these approximations can only qualitatively predict micro-scale gas flows. Second, experiments have been used to study simple geometry problems, including flows in micro-channels and micro-nozzles (Harley et al., 1995; Bayt, 1999). Experiments on complicated geometries (Freeman et al., 1998), however, are focused on overall performance of microsystems, because the small physical dimensions of microsystems make detailed studies about flow fields difficult. Therefore, such study is not sufficient to optimize microsystems because of the lack of detailed information. Finally, an effective method of studying micro-scale gas flows is numerical simulation. Conventional continuum-based computational techniques have extended their validity by adopting slip boundary conditions. Kinetic approaches are also used because continuum methods are not valid for many micro-scale gas flows. However, conventional kinetic approaches are numerically too expensive to simulate most practical micro-scale gas flows. Therefore, it is necessary to reduce the computational cost for kinetic approaches or even to combine a less expensive kinetic approach with a continuum method for simulating micro-scale gas flows.

1.2 Fluid Mechanics of Micro-Scale Gas Flows

We mentioned above that fluid mechanics at micro scales behave differently from those at macro scales. This behavior follows because the characteristic length or the scale

of a flow is an important parameter for many physical phenomena, including flow regimes, surface forces, and surface effects.

Flows can be characterized by the Knudsen number (Kn), which is the ratio of the mean free path of the gas molecules to the smallest characteristic length of the flow. Generally speaking, when the Knudsen number is less than 0.01, the flow is in the continuum regime. When the Knudsen number is between 0.01 and 0.1, the flow is in the slip regime. In this slip regime, a flow can still be described by continuum equations except that a slip velocity, or a temperature jump boundary condition, or both, should be adopted. This requirement is due to an insufficient number of collisions between incident and reflected molecules relative to the wall. When the Knudsen number is between 0.1 and 10, the flow is in the transitional regime where intermolecular collisions and collisions between molecules and walls are of the same importance. When the Knudsen number exceeds 10, however, the flow is in the free-molecular regime where collisions between molecules are rare.

For air at standard conditions, the equilibrium mean free path length is roughly 65 nanometer. If a macro-scale gas flow having a characteristic length of 1 meter is considered, then the Knudsen number of the flow is much less than 0.01 and the flow can be described by continuum equations. However, if the flow is a micro-scale gas flow having a characteristic length of 1 micron, then the Knudsen number is on the order of 0.1, and rarefied effects are important and must be included in modeling micro-scale gas flows.

Surface forces are prominent when the flow scale is small, which can be characterized by the surface-to-volume ratio ($S/Vol \approx L^2/L^3 = 1/L$). This ratio changes from 1 m^{-1} to 10^6 m^{-1} as the characteristic length scale of a system is varied from 1 meter to 1 micron. As a result, if a surface force acts on a flow, then the force is more important at micro scales. Therefore, surface force effects play important roles at micro scales. Surface roughness and inhomogeneities also are significant for micro-scale gas flows.

The momentum and thermal accommodation coefficients of the surface become two dominant parameters when describing micro-scale gas flows.

Therefore, a length in the micro-scale is the main characteristic of micro-scale gas flows. Methods to study such flows must be able to capture the main physics of these flows. Another characteristic of these flows is that such flows are generally slow, which means that variations of flow fields are not always prominent. Therefore, valid methods must have the ability to reduce the numerical error or the statistical scatter.

1.3 Previous Related Studies

In order to understand micro-scale gas flows, many numerical approaches have been developed. They can be categorized into three types of approach as follows: continuum approach, particle approach, and hybrid approach.

Continuum approaches for modeling micro-scale gas flows involve the solution of continuum equations with slip boundary conditions. Many conventional computational fluid techniques can be used to solve continuum equations, including the finite volume method (Versteeg and Malalasekera, 1996) and the finite element method (Reddy and Gartling, 1994). Because micro-scale gas flows generally exhibit rarefied phenomena, a wall boundary condition having a slip velocity, or a temperature jump, or both, is generally required to extend the application of continuum approaches to model flows in the slip regime.

Professor Karniadakis' group developed a Navier-Stokes solver (μFlow code) using the spectral element method (Karniadakis and Sherwin, 1999). They use a slip boundary condition (Beskok, 1996; Beskok and Karniadakis, 1999) that is valid over the entire Knudsen number range. They studied the rarefied gas effects for flows in channels, pipes and ducts (Karniadakis and Beskok, 2001), which showed that a continuum-based approach can be employed to simulate micro flows in the continuum and slip regimes.

Hennighausen (2001) developed a numerical method that integrates the compressible Navier-Stokes equations on a deforming grid by utilizing upwind differences and a finite volume approach. The boundary condition used is a Maxwellian-type slip boundary condition. A preconditioning technique was also implemented in order to speed up the convergence for low Reynolds number flows. This approach has been used to design and simulate the flow about a prototype micro air vehicle.

Aluru and Li (2001) developed a meshless method for solving the Navier-Stokes equations, which may be suitable for truly complex-geometry MEMS flows. The so-called finite cloud method combines collocation with a fixed kernel technique for the construction of interpolation functions over a scattered set of points. The method can solve general partial differential equations, and good results have been obtained using this approach for examples having elasticity, heat transfer, thermoelasticity, Stokes flows or piezoelectricity. This method has been developed recently, and has not yet been employed routinely for MEMS applications.

There are other continuum approaches for modeling micro-scale gas flows (Myong, 2001; Wang, 2002). However, applications of these approaches are limited by the validity of the continuum equations. Generally speaking, these methods, including approaches that solve the Burnett equations, e.g., Liou and Fang (2001), can only be used to model flows in either the continuum regime or the slip regime. As a result, approaches based on kinetic theory are desired to model micro-scale gas flows in order to capture all the possible physics associated with these flows.

The direct simulation Monte Carlo (DSMC) method (Bird, 1994) is one of the most successful numerical approaches for simulating rarefied gas flows. This method has been applied to simulated micro-scale gas flows. However, the statistical scatter associated with this method prevents its application for many practical micro-scale gas flows, because of its huge numerical expense. Attempts have been made to modify this

method in order to simulate micro-scale gas flows with lower or affordable computational cost.

Fan and Shen (1999) proposed an information preservation (IP) method for low-speed rarefied gas flows based on the DSMC method. The IP method uses the molecular velocities in the DSMC method as well as an information velocity that records the collective velocity of the large number of molecules that a simulated particle represents. The information velocity is modeled during the simulation, and is sampled as the flow velocity. This method has been used to simulate Couette flow, Poiseuille flow and Rayleigh flow in all flow regimes with satisfactory results (Fan and Shen, 2001). These applications to low-speed flows shows that the IP method can save computational time by several orders of magnitude compared with a similar DSMC simulation, which promotes effective use of the IP method for micro-scale gas flows. This method has been recently developed and applied to simulate low-speed micro-channel flows (Cai et al., 2000) and to investigate the flows around a NACA0012 airfoil (Fan et al., 2001) using an isothermal assumption. However, in order to model general micro-scale gas flows, the isothermal assumption must be removed, and a general principle must be established to update the preserved information.

Pan and his co-workers have also developed two modified DSMC methods. In one of the modified DSMC methods (Pan et al., 2000), the velocity of gas molecules as well as the stress and the temperature of the gas flows is split into two parts. One part is determined using a macroscopic model and the other is obtained using the DSMC algorithm. Simulations of micro Couette flows show that this modified DSMC method exhibits much smaller statistical scatter than the original approach. In the other modified DSMC method (Pan et al., 2001), a molecular block model was proposed based on the relationship between the statistical scatter and the mass of the gas molecule. The reference diameter and the number density of the so-called big molecule are determined by ensuring that the mean free path and dynamic viscosity of the big molecule are equal

to those of the real constituent molecules. However, neither of these modified DSMC methods has been widely tested.

Kaplan and Oran (2002) proposed another technique to reduce the statistical scatter associated with the DSMC method. It involves a postprocessing operator by applying a filter to extract the solution from a noisy DSMC calculation. The filter, called flux-corrected transport, uses a high-order, nonlinear monotone convection algorithm. Simulations show that filtering in this way removes high-frequency statistical fluctuations and can extract a solution from a noisy DSMC calculation for a low speed Couette flow.

These modified DSMC methods do predict good results for test examples with affordable computational cost. However, a more efficient approach for simulating micro-scale gas flows (especially for external flows) is to develop a hybrid approach that combines the physical accuracy of kinetic methods with the numerical efficiency of continuum approaches. Micro-scale gas flows have domains where continuum equations are still valid, especially for external subsonic flows. Continuum approaches are generally several orders of magnitude more efficient than the DSMC method; therefore, a hybrid approach can reduce the computational cost of a numerical simulation, by limiting the DSMC method to the regions where the kinetic equations must be applied, and using continuum approaches in the rest of the computational domain.

In the past ten years, many studies of hybrid techniques have been reported. There exist weakly coupled schemes (Hash and Hassan, 1996a; Lumpkin et al., 1996) for which a continuum approach provides a boundary condition for a particle method. There are also overlapping coupling strategies for which a particle method provides a boundary condition for a continuum scheme (Bourgat et al., 1996), or even provides transport coefficients for a continuum method (Oh and Oran, 1998). However, non-overlapping coupled schemes may give better performance for accuracy and efficiency. Wadsworth and Erwin (1990, 1992) first demonstrated such a scheme by simulating one-dimensional shock waves and considering two-dimensional slit flows using a property extrapolation

technique. Hash and Hassan (1996b) performed detailed studies of a hybrid code and suggested that the Mashak condition is a better coupling technique. However, in a later paper, Hash and Hassan (1997) pointed out that the large statistical scatter from the DSMC method precluded the application of the Mashak condition to low speed flows. Related coupling schemes are also available in the literature (Tallec and Mallinger, 1997; Alder, 1997; Hadjiconstantinou, 1999; Flekkøy et al., 2000; Aktas and Aluru, 2002). For further development of hybrid methods, adaptive hybrid schemes are therefore proposed, especially for unsteady rarefied flows. Roveda et al. (1998) described an Euler/particle approach that can analyze unsteady flows by coupling an adaptive discrete velocity (ADV) Euler solver and the DSMC method with an adaptive interface. In a following paper, Roveda et al. (2000) successfully simulated an unsteady pressure driven slit flow with this scheme. There are other adaptive hybrid schemes, such as the adaptive domain decomposition method proposed by Tiwari and Klar (1998) and the adaptive mesh and algorithm refinement (AMAR) method developed by Garcia et al (1999).

Most of the hybrid schemes, however, exhibit scatter difficulties with the particle methods. Sampling a large number of particles is generally adopted by most authors with multiple time steps (Wadsworth and Erwin, 1990; Hash and Hassan, 1996; Aktas and Aluru, 2002), ghost cells (Roveda et al., 1998), or local average from multiple cells (Flekkøy et al., 2000). Then a large sampling size is required for low speed flows, which can be numerically expensive to couple two methods for each time step. As a result, for general micro scale gas flows, a kinetic method having a small statistical scatter must be coupled with a continuum solver in a hybrid approach.

1.4 Specific Objectives of the Study

Although many numerical approaches have been developed recently, there is at present no general-purpose approach for modeling micro-scale gas flows. Some available methods are too computationally expensive, and some are not able to capture physics

accurately. Fortunately, there are some approaches that show potential for modeling micro-scale gas flows with efficiency and accuracy, such as the information preservation (IP) method. Hence, the first objective of this thesis is to develop the IP method for modeling general micro-scale gas flows.

The second objective of this thesis is to develop a hybrid approach for modeling micro-scale gas flows. As continuum approaches are generally more efficient than particle methods including the IP method, the best method for modeling micro-scale gas flows is to develop a hybrid approach that combines the efficiency of a continuum approach in regions where continuum equations are still valid and the accuracy of the IP method for the rest of the computational domain.

The third objective of this thesis is to investigate an external micro-scale gas flow since there are few such investigations so far. We intend to study the aerodynamic characteristics of a micro-scale airfoil.

1.5 Thesis Organization

The remaining chapters are organized as follows:

In Chapter II, the kinetic description of gas flows will be reviewed, and typical numerical approaches will be evaluated with respect to their capabilities for modeling micro-scale gas flows. Detailed descriptions will be given for two numerical approaches: the direct simulation Monte Carlo (DSMC) method and a continuum approach solving the Navier-Stokes equations. These represent respectively a pure particle approach and a pure continuum approach.

In Chapter III, the information preservation (IP) method will be developed based on the DSMC method, with the intention to model general micro-scale gas flows with moderate efficiency and accuracy. The principle to update the preserved information will be explained, and models will be introduced when describing the preserved information. Some advantages and disadvantages of the IP method will also be discussed.

In Chapter IV, evaluation of the IP method will be performed by comparing results obtained from the IP and DSMC method for several benchmark problems. These problems are the thermal Couette flow, high-speed Couette flow, Rayleigh flow, and a flow over a NACA0012 airfoil.

In Chapter V, a hybrid approach will be introduced by coupling the IP method and a continuum approach. The emphasis will be on the determination and implementation of the continuum/particle interface.

In Chapter VI, flows are simulated over a micro-scale flat plate having zero thickness and a 5% thickness using the hybrid approach. Drag on the plate with zero thickness will be studied and the aerodynamic characteristics of the 5% flat plate will be investigated.

In Chapter VII, we will present summary, conclusions, and discuss recommendations for future research.

CHAPTER II

OVERVIEW OF TYPICAL NUMERICAL APPROACHES FOR
MODELING MICRO-SCALE GAS FLOWS

In this chapter, an overview is given for the kinetic description of gas flows and related numerical approaches. Typical approaches are then evaluated emphasizing micro-scale gas flows. It turns out that particle approaches and continuum approaches are both feasible for investigating micro-scale gas flows; therefore, a detailed description is given of the particle and continuum methods that are used in this thesis.

2.1 Kinetic Description of Gas Flows and Related Numerical Approaches

Conflicting views on matter as either continuous or discrete date back at least to early Greek philosophy: Aristotle insisted on the continuous point of view whereas Democritus proposed the discrete, atomistic standpoint. Modern physics has reconciled these conflicting views by considering continuum descriptions as local averages of the underlying discrete atoms. In this section, an overview is given of numerical approaches for modeling gas flows, ranging from the discrete to the continuum methods.

2.1.1 Molecular Models and Several Characteristic Lengths

Gases are generally described as a myriad of discrete molecules (monatomic, diatomic, or polyatomic). Physics has shown that both single molecules and inter-molecular interactions are very complicated due to the inner structure of molecules. However, in view of the large number of molecules in most cases, it is almost impossible, and fortunately unnecessary, to address all the details of molecules and their interactions. Therefore, several molecular models have been suggested for practical applications,

including the simplest hard sphere (HS) model, the widely used variable hard sphere (VHS) model (Bird, 1981), and the recently proposed generalized soft sphere (GSS) model (Fan, 2002). These models treat molecules as tiny spheres with a fixed or variable diameter (d), and molecular interactions occur only when two molecules are in contact.

From the view point of fluid mechanics, there are three characteristic lengths associated with molecules: the diameter of molecules, the mean molecular spacing, and the mean free path of molecules. It is clearer to describe these lengths if discussion is limited to a simple gas that consists of a single chemical species where all molecules are assumed to have the same structure. Corresponding concepts for gas mixtures, however, are not too difficult to obtain.

The mean molecular spacing, δ, defines the average volume available to a molecule, which can be described as $\delta = n^{-1/3}$ (n is the number density of molecules). If the ratio of the mean molecular spacing to the characteristic dimension of a flow, L, is small, statistical fluctuations can be neglected. This requires that enough molecules (say 10^6 molecules) should be within the volume of interest for a gas to be modeled macroscopically.

The diameter, d, of molecules defines their cross-section for collisions and is model-dependent. For instance, the diameter in the HS model may be different from the diameter in the VHS model. In addition, the diameter of an individual collision can also be energy-dependent, such as in the VHS model. If the diameter is much less than the mean molecular spacing, the dilute approximation can be used. This approximation states that only a small part of the space is occupied by molecules, when the scale of the ratio of the molecular diameter to the molecular spacing is small (e.g., it can be adopted when $d/\delta < 1/7$). This means that effects on a molecule from other molecules are small, and it is very highly probable that only one other molecule is involved with a molecule in case that there is a strong effect. Therefore, for a dilute gas, molecular interactions are commonly treated as binary collisions.

The mean free path, λ, is the average distance traveled by a molecule between collisions. It can be calculated for the HS model as $\lambda = 1/\left(\sqrt{2}\pi d^2 n\right)$. The ratio of the mean free path to the characteristic dimension, which is called the Knudsen number ($Kn = \lambda/L$), defines the degree of rarefaction of a gas. The Knudsen number is generally considered to be an important parameter identifying the validity of continuum approaches.

The overall effects of these characteristic lengths to related approximations in fluid mechanics are illustrated in Figure 2.1, following Bird (1994). It shows: the dilute approximation can be used when the ratio of the molecular spacing to the molecular diameter is larger than 7; continuum approaches are valid when the Knudsen number is less than 0.01; statistical fluctuations can be neglected when the ratio of the characteristic length of a flow to the mean molecular spacing is larger than 10.
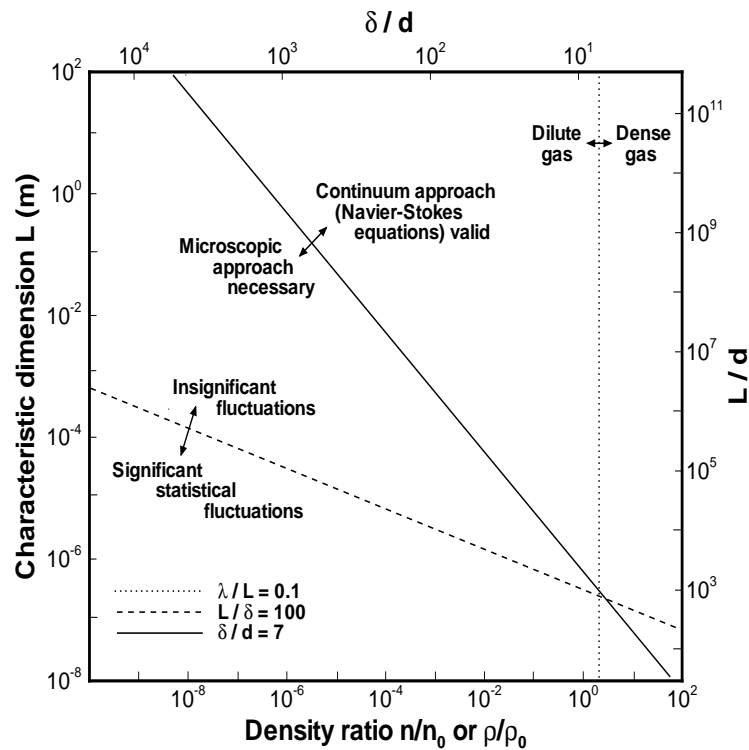
Figure 2.1. Effective limits of major approximations in fluid mechanics

2.1.2 Molecular Dynamics

Because a gas is composed of molecules, a fundamental way to model a gas flow is to trace the movement of all molecules; this can be done using molecular dynamics (Haile, 1993).

A molecular dynamics simulation involves simultaneous tracking of a large number of simulated molecules within a region of simulated physical space. There are three main aspects of a typical molecular dynamics simulation. First of all, probabilistic procedures are required for setting the initial state. Generally, molecules are randomly distributed according to certain distribution functions for their location, velocity and internal state. Next, a potential energy function is needed to determine the force on a molecule due to the presence of other molecules. Collisions occur whenever the spacing between any pair of molecules decreases to the assumed cutoff limit of their force field. Third, all simulated molecules obey Newton's equations of motion.

Macroscopic flow properties are obtained by averaging the molecule information over a space volume. The size of a space volume can be selected so that it will not result in significant statistical fluctuations nor smear out the gradient of a property. In principle, the space volume should have dimensions much larger than the mean molecular spacing and much smaller than the characteristic dimension. As a result, the mass density, ρ, defined as the mass per unit volume of the gas, can be expressed as $\rho = Nm/\Delta Vol$, where N is the number of molecules having a mass m within unit volume, ΔVol. The flow velocity, $\mathbf{V}$, the average velocity of all molecules in a volume, can be calculated as $\mathbf{V} = \sum_{i=1}^{N} \frac{\mathbf{c}_i}{N}$, or $\mathbf{V} = \bar{\mathbf{c}}$. The scalar pressure, p, is normally defined as the average of the three normal components of the pressure tensor, $\mathbf{p}$, which is the momentum flux based on the molecular thermal velocity ($\mathbf{c}' = \mathbf{c} - \mathbf{V}$). The expression for the pressure p is then giving by $p = \frac{1}{3}\rho\left(\overline{c^2} - V^2\right)$. The thermodynamic temperature T is essentially an

equilibrium gas property. However, the expression $T = \dfrac{m}{3k}\left(\overline{c^2} - V^2\right)$ is still valid for the

translational temperature in a non-equilibrium situation (Bird, 1994).

With the help of the previous expressions, macroscopic properties can be obtained from a molecular dynamics simulation. However, it is highly inefficient to use the molecular dynamics method for most practical applications, because a large number of molecules must be simulated, and the computation of an element of trajectory for any molecule requires consideration of all other molecules as potential collision partners. As a result, molecular dynamics is limited to flows where the continuum and statistical approaches are inadequate.

2.1.3 Velocity Distribution Function and the Boltzmann Equation

It is desired to have a mathematical description for all the molecules in a flow. Maxwell used a velocity distribution function $f(\mathbf{c})$ to describe the probability of a molecule to have a certain velocity at a certain location and time. It appears that a complicated velocity distribution function is required to specify the velocity for all molecules involved. However, for a dilute gas, it is possible to use a velocity distribution function for a single molecule due to molecular chaos. Any macroscopic quantity can then be easily obtained using the velocity distribution function. For instance, if Q is a microscopic quantity of a molecule, then the corresponding macroscopic average can be obtained using $\overline{Q} = \int_{-\infty}^{\infty} Q f \, \mathrm{d}\mathbf{c}$. Hence, the velocity distribution function must be known for all times and locations to fully describe a flow.

The Boltzmann equation that describes the time evolution of the velocity distribution function of molecules can be written as follows:

$$\frac{\partial}{\partial t}(nf) + \mathbf{c} \cdot \frac{\partial}{\partial \mathbf{r}}(nf) + \mathbf{F} \cdot \frac{\partial}{\partial \mathbf{c}}(nf) = \int_{-\infty}^{\infty}\int_{0}^{4\pi} n^2\left(f^* f_1^* - f f_1\right) c_r \sigma \, \mathrm{d}\Omega \, \mathrm{d}\mathbf{c}_1 \qquad (2.1)$$

where n is the number density, t is the time, $\mathbf{r}$ is the physical space vector, $\mathbf{c}$ is the velocity space vector, $\mathbf{F}$ is the external force per unit mass, c_r is the relative speed

between a molecule of class $\mathbf{c}$ and one of class $\mathbf{c}_1$, $\sigma d\Omega$ is the differential cross-section for the collision of a molecule of class $\mathbf{c}$ with one of class $\mathbf{c}_1$ such that their post-collision velocities are $\mathbf{c}^*$ and $\mathbf{c}_1^*$, respectively, and functions f, f_1, f^* and f_1^* are the corresponding velocity distribution functions for the molecule and its collision partner before and after such collision. This equation is a seven-dimensional integro-differential equation. The first term describes the change rate of the number of molecules. The second and third terms describe the change of the number of molecules due to molecular movement and due to an external force field. The term on the right hand side is called the collision term, which generally provides the main difficulty for solving this equation. This term describes the change of the molecules due to molecular collisions.

The Boltzmann equation provides a mathematical means to describe a gas flow. It is possible to solve this equation for simple problems, especially when molecular collisions can be neglected. However, it is a significant challenge to calculate the collision term in the equation for general flows. In some situations, the collision term can be modeled, and the model equation (e.g., the BGK equation (Bhatnagar et al., 1954)) can predict flow properties with good accuracy.

2.1.4 Moments of the Boltzmann Equation and the Transfer Equation

The collision term in the Boltzmann equation provides the change of the number of molecules in a phase space element due to molecular collisions. However, the mass, momentum and energy of two molecules do not change during a collision. Therefore, it is desired to derive equations for these conserved quantities from the Boltzmann equation.

The average of a quantity may be obtained by multiplying the velocity distribution function by that quantity, followed by integrating the product over all velocity space. These averages are referred to as the moments of the distribution function. Similarly, a moment of the Boltzmann equation can be obtained by multiplying the

equation by a quantity, Q, and then integrating the resulting equation over all velocity space as illustrated by Equation 2.2.

$$Q\frac{\partial}{\partial t}(nf)+Q\mathbf{c}\cdot\frac{\partial}{\partial \mathbf{r}}(nf)+Q\mathbf{F}\cdot\frac{\partial}{\partial \mathbf{c}}(nf)=Q\int_{-\infty}^{\infty}\int_{0}^{4\pi}n^2\left(f^*f_1^*-ff_1\right)c_r\sigma d\Omega d\mathbf{c}_1 \qquad (2.2)$$

If $\mathbf{F}$ is assumed to be independent of $\mathbf{c}$, then Equation 2.2 can be expressed as follows:

$$\frac{\partial}{\partial t}\left(n\overline{Q}\right)+\nabla\cdot\left(n\overline{\mathbf{c}Q}\right)-n\mathbf{F}\cdot\overline{\frac{\partial Q}{\partial t}}=\Delta[Q] \qquad (2.3)$$

where $\Delta[Q]=\int_{-\infty}^{\infty}\int_{-\infty}^{\infty}\int_{0}^{4\pi}n^2Q_1\left(f_1^*f^*-f_1f\right)c_r\sigma d\Omega d\mathbf{c}d\mathbf{c}_1$. This equation is often called the transfer equation or the equation of change.

It can be shown that $\Delta[Q]$ has several alternative forms (Gombosi, 1994). One alternative form is illustrated in Equation 2.4:

$$\Delta[Q]=\frac{1}{2}\int_{-\infty}^{\infty}\int_{-\infty}^{\infty}\int_{0}^{4\pi}n^2\left(Q^*+Q_1^*-Q-Q_1\right)f_1fc_r\sigma d\Omega d\mathbf{c}d\mathbf{c}_1 \qquad (2.4)$$

where Q,Q_1,Q^*,Q_1^* is the quantity associated with collision partners and their post-collision partners, respectively. Then $\Delta[Q]$ is caused by the change of the quantity Q of the collision pair during a collision.

When the quantity Q is a collision invariant, the collision integral $\Delta[Q]$ must be zero; this property greatly simplifies the transfer equation. The transfer equations for mass (m), momentum ($m\mathbf{c}$) and energy ($\frac{1}{2}mc^2$) are then expressed as follows:

$$\frac{\partial}{\partial t}(\rho)+\nabla\cdot(\rho\mathbf{V})=0 \qquad (2.5)$$

$$\frac{\partial}{\partial t}(\rho\mathbf{V})+\nabla\cdot(\rho\mathbf{V}\mathbf{V})=-\nabla p+\nabla\cdot\mathbf{\tau} \qquad (2.6)$$

$$\frac{\partial}{\partial t}\left(\frac{1}{2}\rho\left(V^2+3RT\right)\right)+\nabla\cdot\left(\frac{1}{2}\rho\left(V^2+3RT\right)\mathbf{V}\right)=-\nabla\cdot\mathbf{h}-\nabla\cdot(p\mathbf{V})+\nabla\cdot(\mathbf{V}\cdot\mathbf{\tau}) \qquad (2.7)$$

with $$\mathbf{\tau}=-\left(\rho\overline{\mathbf{c}'\mathbf{c}'}-p\mathbf{I}\right) \text{ and } \mathbf{h}=\frac{1}{2}\rho\overline{\mathbf{c}'(\mathbf{c}'\cdot\mathbf{c}')} \qquad (2.8)$$

However, these equations are not closed by the macroscopic quantities themselves because $\mathbf{\tau}$ and $\mathbf{h}$ are still in their microscopic forms. Using the transfer equation for

certain forms of Q, equations for $\boldsymbol{\tau}$ and $\mathbf{h}$ can be obtained. However, new unknown quantities will appear in these equations to describe the existing unknown quantities. Therefore, approximations must be made to close these equations.

2.1.5 Moment Methods and Continuum Equations

In order to close the previous equations, moment methods use assumptions (Grad's approach or the Chapman-Enskog expansion) to truncate higher-order moments.

It is generally assumed that the velocity distribution function may be expressed in the form of a power series as

$$f = f_0\left(1 + a_1(Kn) + a_2(Kn)^2 + \cdots\right) \tag{2.9}$$

where, coefficients $a_i\,(i = 1, 2, \cdots)$ only depend on macroscopic quantities, and Kn is the Knudsen number of a flow. Truncation of the series is made to close the moment equations so that the higher order moments can be calculated using the truncated velocity distribution function.

The zero-order Chapman-Enskog expansion is the local equilibrium distribution:

$$f_0 = \left(\frac{m}{2\pi kT}\right)^{3/2} \exp\left(-\frac{mc'^2}{2kT}\right) \tag{2.10}$$

With this Maxwellian distribution, $\boldsymbol{\tau}$ and $\mathbf{h}$ vanish, and the resulting set of equations leads to the Euler equations. These equations are obtained at the limit of zero Knudsen number. As a result, they can only be used in situations where viscous effects and heat transfer can be neglected.

The first-order expansion has the following distribution,

$$f = f_0\left(1 + q_i^* C_i\left(\tfrac{2}{5}C^2 - 1\right) - \tau_{ij}^* C_i C_j\ \right) \tag{2.11}$$

with
$$C = c/(2kT/m)^{1/2} \tag{2.12}$$

$$q_i^* = -\frac{\kappa}{p}\left(\frac{2m}{kT}\right)^{1/2}\frac{\partial T}{\partial x_i} \tag{2.13}$$

and
$$\tau_{ij}^* = \frac{\mu}{p}\left(\frac{\partial v_i}{\partial x_j} + \frac{\partial v_j}{\partial x_i} - \frac{2}{3}\frac{\partial v_k}{\partial x_k}\delta_{ij}\right) \tag{2.14}$$

where μ and κ are the viscous coefficient and the coefficient of heat conduction, respectively. This distribution function enables $\boldsymbol{\tau}$ and $\mathbf{h}$ to be written as products of the coefficients μ and κ with the velocity and temperature gradients, thus reducing the conservation equations to the Navier-Stokes equations. The Navier-Stokes equations are widely used because flows in our daily life generally involve small Knudsen number.

The second-order expansion leads to the Burnett equations, which is a set of very complicated higher-order continuum equations. The Burnett equations expand the validity of the continuum model to flows that are more rarefied than those for which the Navier-Stokes equations are valid. However, the Burnett equations are very complicated, and many difficulties are encountered when the equations are applied to practical applications (Gad-el-Hak, 1999).

2.2 Evaluation of Typical Numerical Approaches in the Frame of Modeling Micro-Scale Gas Flows

Many numerical approaches have been designed and developed for simulating gas flows. However, not all of them are suitable for modeling micro-scale gas flows. Some of them are too numerically expensive while some are not able to capture the physics of the flow. Hence, it is necessary to evaluate these methods before applying them to model micro-scale gas flows. As it is almost impossible to mention all of them, therefore, only three categories of methods are discussed in this section. These are numerical methods for solving the Boltzmann equation, particle methods, and continuum methods.

2.2.1   Numerical Methods for Solving the Boltzmann Equation

It is very desirable to simulate micro-scale gas flows by directly solving the Boltzmann equation. However, it is a challenge to simulate these flows using the Boltzmann equation based on current computational capabilities. One major problem for such simulations, is that a large number of elements or nodes is required to store the velocity distribution function in the phase space, which is a three-dimensional space (1D

physical space, 1D parallel velocity, and 1D normal velocity) for 1D flows and a six-dimensional space (3D physical space and 3D velocity space) for 3D flows. Another major problem is that calculation of the collision term involves a large number of operations. As a result, direct solutions of the Boltzmann equation have been limited to simple flow geometries for monatomic gases.

The first successful method for directly solving the Boltzmann equation was introduced in a series of papers by Nordsieck, Hicks, and Yen (Bird, 1994). They dealt with one-dimensional steady flow problems, and employed a conventional finite-difference technique for the left hand side of the equation and a Monte Carlo sampling technique for the collision term, namely, the right hand side of the equation. Recently, development of Boltzmann solvers is mainly due to the work of Ohwada et al. (1989, 1993, 1996). Their method was also a finite-difference method, in which the collision integral is computed efficiently and accurately by the numerical kernel method developed by Sone et al. (1989). However, application of this method this far has been limited to one-dimensional flow problems.

2.2.2 Particle Methods

Particle methods are generally numerically expensive. If all the molecules in a flow are modeled in a simulation, then only flows having a very small domain or very rarefied flows (e.g., $n = 1m^{-3}$) can be simulated. The direct simulation Monte Carlo (DSMC) method, however, can simulate moderate 2D rarefied gas flows, or even simple 3D problems, based on current computer resources, because each simulated particle in the DSMC method represents a large number of real molecules which makes a DSMC simulation much more efficient than a molecular dynamics simulation. The DSMC method has been widely used in many fields, such as rarefied atmospheric gas dynamics, materials processing, and vacuum systems. However, it is a challenge to apply the DSMC method for simulating micro-scale gas flows.

First of all, the statistical noise of the DSMC method makes its results difficult to interpret for low-speed micro-scale gas flows unless a huge sampling size is used (micro-scale gas flows are generally low-speed flows). For instance, the velocity scatter of a particle simulated in the DSMC method is $\sqrt{2RT}$ (where R is the gas constant and T is the gas temperature), and so the scatter is about 400 m/s for air at standard temperature. If particles for sampling are statistically independent, the statistical scatter is then about $\sqrt{2RT/N}$ (N is the sample size), which means for air at standard temperature, a sample size of 1.6×10^3 is needed to control the scatter to be within 10 m/s, and a sample size of 1.6×10^7 is needed to control the scatter to be within 0.1 m/s. In addition, particles in the samples are not completely statistically independent which increases the statistical scatter. In order to increase the independency of particles, many time steps are required between two sampling steps. As a result, it is very expensive to obtain a meaningful DSMC result for low speed micro-scale gas flows.

Second of all, it is difficult to implement effective external boundary conditions for the DSMC method. Conventional boundary conditions for the DSMC method, such as free stream conditions and vacuum conditions, do not work for micro-scale gas flows. Instead, one must use inflow and outflow conditions that impose the correct propagation of information across the boundaries. If a large number of particles is used in each computational cell, it is possible to apply an implicit boundary condition for simple flow problems where overall mass balance can be imposed (Liou and Fang, 2000). However, for general flows, it is impossible to balance all effects resulting from the statistical scatter. Therefore, the difficulty to implement an effective boundary condition also limits the application of the DSMC method for micro-scale gas flows.

2.2.3 Continuum Methods

Continuum methods are well developed for solving continuum equations, including the Euler and the Navier-Stokes (N-S) equations. Although these methods are

very efficient, their validity depends on the limitations of the underlying continuum equations. As discussed in Section 2.1, the Euler equations are too limited, whereas the Burnett equations are very complicated. Hence, in the following, the discussion is limited to numerical methods for solving the Navier-Stokes equations.

Micro-scale gas flows are generally in the slip and transitional flow regimes. As a result, numerical methods based on the N-S equations can describe some micro-scale gas flows, or part of a flow when such a method is combined with other valid approaches. However, several factors affect or limit the application of numerical methods based on the N-S equations.

First of all, there is no generally applicable criterion to indicate when breakdown of the N-S equations occurs. The N-S equations are first-order moment equations derived from the Boltzmann equation based on the Knudsen number. As a result, effects of neglected high-order terms must be investigated. In addition, although the Knudsen number is well defined as the ratio of the mean free path of molecules to the smallest characteristic length of the flow, this smallest characteristic length is not well defined. Therefore, there is still a difficulty to determine the applicable scope for the N-S equations.

Second of all, a slip boundary condition is required to extend the application of numerical methods based on the N-S equations. In order to determine the general slip boundary condition, a one-dimensional approximation is always assumed for the Knudsen layer. However, near sharp edges, corners, and other singular points on a body, the Knudsen layer cannot be locally considered to be one-dimensional. Kogan (1973) pointed out that the drag on a plate parallel to a flow cannot be predicted by solving the N-S equations with a general slip boundary to an accuracy of order $1/\text{Re}$. Therefore, it is generally not a good idea to apply numerical approaches based on the N-S equations to flows having a sharp edge, corner, or other singular point on a body.

Thirdly, the convergence of traditional numerical approaches solving the N-S equations is very slow for micro-scale gas flows due to the small Reynolds number. For micro-scale gas flows, viscous diffusion is on the same order as the pressure gradient, and convection is less important; this makes time-marching techniques, e.g., the MacCormack (1969) scheme, difficult to apply. The time step for an explicit MacCormack scheme is very small for low Reynolds number flows having small cell sizes as suggested by Peyret and Taylor (1983) as

$$\Delta t \le \frac{\Delta x^2}{(2\mu/\text{Re})\left(2\gamma/\text{Pr} + \sqrt{2/3}\right) + \left(|u| + |v| + \sqrt{2}a\right)\Delta x} \tag{2.15}$$

Fortunately, the matrix preconditioning technique can accelerate the convergence to the steady state for steady flows (Choi and Merkle, 1993).

Therefore, numerical approaches solving the Navier-Stokes equations can be applied to simulate micro-scale gas flows in the continuum or slip flow regime with careful treatment.

2.3 Direct Simulation Monte Carlo (DSMC) Method

The direct simulation Monte Carlo (DSMC) method is a widely used particle method as an effective numerical technique to simulate rarefied, nonequilibrium gas flows. This method was innovated and mainly developed by Bird (1976; 1994) based on kinetic theories. Many review papers describing the DSMC method can be found in the literature (Bird, 1978, 1998, 2001; Muntz, 1989; Oran et al., 1998; Ivanov and Gimelshein, 1998).

2.3.1 DSMC Overview

The fundamental idea of the DSMC method is to track a large number of statistically representative particles in the computational domain. The motion and interactions of each particle are used to modify particle positions, velocities, and

chemical species. The flow information is then sampled from the microscopic information about the simulated particles.

The primary approximation is to uncouple the molecular motions and intermolecular collisions over small time intervals. Particle motions are modeled deterministically, whereas the collisions are treated statistically. The limitations of the DSMC method are the same as those of classical kinetic theory: the assumption of molecular chaos and the restriction to dilute gases. Hence, the DSMC method can be used to simulate any rarefied gas flow.

The validity of the DSMC method is very difficult to be determined by strict mathematical reasoning, although it has been shown (Nanbu, 1980; Babovsky & Illner, 1989) that the DSMC method is equivalent to solving the Boltzmann equation for a monatomic gas undergoing binary collisions. Bird (1976) shows that the basic probabilistic assumptions used in the DSMC method are common to the Boltzmann equation, as long as the number of simulated particles, the time step and the cell size are kept within reasonable limits. The validity of the DSMC method comes from the following facts (mainly from articles in various proceedings of the International Symposia on Rarefied Gas Dynamics): many DSMC calculations agree well with corresponding experimental data; excellent agreement has been shown for shock computations (Salomons and Mareshak, 1992) and slip lengths (Morris et al., 1992) in the comparisons of DSMC with molecular dynamics; many computational studies have shown that DSMC solutions approach Navier-Stokes solutions in the limit of very low Knudsen number.

2.3.2 Algorithm of the DSMC Method

For the DSMC method, the computational domain is divided into a network of cells, where each cell serves as a separate region for molecular interaction and as a space element for sampling flow information. Therefore, the cell size should be less than the

mean free path or based on the requirements on gradient resolution, but is much larger than the mean molecular spacing. In order to decouple the movement of particles and the interaction between particles, the time step employed in the DSMC method is smaller than the mean collision time of gas molecules. The procedure of a typical DSMC simulation is shown in Figure 2.2.

A DSMC simulation proceeds from a set of prescribed initial conditions. Namely, a large number of particles is generated in the computational domain, with their initial microscopic properties determined by the macroscopic quantities such as density, temperature and velocity, according to equilibrium distributions.

Interactions between particles are modeled for each time step. Collision pairs are randomly selected within each cell. Probabilities of particle collisions are determined by the collision rates obtained from kinetic theory. During each collision, particles exchange momentum and energy, and chemical reactions may also take place. The properties of collided particles are determined statistically while conservation of momentum and energy between collision pairs is enforced. Next, new particles may be generated from the outer boundaries. The number of generated particles is determined by kinetic theory. Then, all particles are moved to a new location following their individual trajectory for a time step, except that new generated particles are moved for a randomly determined fractional time step. Particles are discarded when they leave the computational domain.

For steady flows, once a steady state is established, time averaging is performed in each cell to evaluate the macroscopic mean values of the flow properties. For unsteady flows, ensemble averaging is used by repeating the previous procedures with different random number seeds setting the initial state of the simulated particles.

```
                    ┌─────────┐
                    │  start  │
                    └─────────┘
                         │
         ┌───────────────────────────────┐
         │   Set up cell network and     │
         │  set initial cell information  │
         └───────────────────────────────┘
                         │
         ┌───────────────────────────────┐
         │  Distribute particles into cells │
         │   with their initial information │
         └───────────────────────────────┘
                         │
              ┌────────────────────────┐
              │ Time = Time + time step │
              └────────────────────────┘
                         │
                ┌──────────────────────┐
                │ Select collision pairs │
                └──────────────────────┘
                         │
                ┌──────────────────────┐
                │ Perform binary collisions │
                └──────────────────────┘
                         │
                 ┌─────────────────┐
                 │ Inject new particles │
                 └─────────────────┘
                         │
         ┌───────────────────────────────┐
         │   Move particles and compute   │
         │  interactions with boundaries  │
         └───────────────────────────────┘
                         │
              Time>sample time?
                         │
              Sample flow properties
                         │
              Time>final time?
```

Unsteady flow: repeat until required sample is obtained

No   Time>sample time?

No   Time>final time?

Unsteady flow: average runs
Steady flow: average samples
after established steady flow

Output result

stop

Figure 2.2. DSMC flowchart

2.3.3 MONACO Code Overview

The numerical code used for the DSMC method during the present study is called MONACO (Dietrich and Boyd, 1996). It is a general-purpose code for modeling 2D, axi-symmetric, or 3D rarefied gas flows. The code contains some object-oriented features, and different functionalities are separated for easy maintenance and update. The main body of code MONACO consists of four libraries: kernel, geometry, physical modeling, and utilities. The kernel library organizes different tasks and links all the libraries together. It handles the data structure definition, initialization, file input/output, and parallelization. The geometry library includes grid structure analysis, new particle generation, and particle movement control. The physical modeling library performs the particle collision, sampling, particle-surface interaction, and possible chemical reaction. The utilities library handles the grid pre-processing and data post-processing. Each library is divided into many small modules. New modules can be added to meet special requirements of different applications. The DSMC algorithms are implemented in the C programming language for easy memory management and code manipulation.

The basic unit in MONACO is the computational cell whose memory address is stored in an array. Each cell is treated as an independent entity that has its geometry information, neighboring cell information, and particle information. The geometry information includes the number and the coordinates of the nodes forming the cell. The neighboring cell information specifies the address (cell index) of other cells or the type of boundaries that neighbor the cell. The particle information stores the number of particles in the cell and a linked list for these particles with their microscopic information. Additional information can also be stored for each particle or cell without any coding difficulty. As a result, MONACO is able to handle problems having complicated geometry, is efficient for indexing and cross-referencing particles, and is efficient for parallelization.

2.4 A Numerical Approach for Solving the Navier-Stokes Equations

We describe a numerical technique to solve the Navier-Stokes (N-S) equations because some micro-scale gas flows (or parts of them) can be modeled using the N-S equations. The technique used here, following McCormack and Candler (1989) and Hennighausen (2001), is a finite volume method for solving the compressible Navier-Stokes equations. The fluxes are evaluated with a second-order accurate modified Steger-Warming flux-vector splitting approach. An implicit Gauss-Seidel line-relaxation method can also be used for the time integration to enhance numerical convergence. This approach for solving the Navier-Stokes equations is referred to as the Navier-Stokes solver for the rest of the present thesis.

2.4.1 Finite Volume Formulations for the Navier-Stokes Equations

The Navier-Stokes equations are expressed in conservation form as follows:

$$\frac{\partial \mathbf{U}}{\partial t} + \nabla \cdot \left(\mathbf{F}_o + \mathbf{F}_\mu \right) = 0 \tag{2.16}$$

where

$$\mathbf{U} = \begin{bmatrix} \rho \\ \rho\mathbf{u} \\ e \end{bmatrix}, \mathbf{F}_o = \begin{bmatrix} \rho\mathbf{u} \\ \rho\mathbf{u}\mathbf{u} + p\mathbf{I} \\ (e+p)\mathbf{u} \end{bmatrix}, \mathbf{F}_\mu = \begin{bmatrix} 0 \\ -\boldsymbol{\tau} \\ -\boldsymbol{\tau}\cdot\mathbf{u}+\mathbf{q} \end{bmatrix} \tag{2.17}$$

$$p = (\gamma - 1)\rho\varepsilon, \varepsilon = e/\rho - \mathbf{u}\cdot\mathbf{u}/2 \tag{2.18}$$

$$\tau_{ij} = \mu\left(\frac{\partial u_i}{\partial x_j} + \frac{\partial u_j}{\partial x_i} \right) - \frac{2}{3}\mu\frac{\partial u_k}{\partial x_k}\delta_{ij}, q = -k\nabla\cdot T \tag{2.19}$$

First, the equations are integrated over a small volume Ω, and Gauss' divergence theorem is applied, obtaining:

$$\frac{\partial\langle\mathbf{U}\rangle}{\partial t} + \frac{1}{Vol}\int_{\partial\Omega}\left(\mathbf{F}_o + \mathbf{F}_\mu\right)\cdot d\mathbf{S} = 0 \tag{2.20}$$

where

$$\langle\mathbf{U}\rangle = \frac{1}{Vol}\int_\Omega \mathbf{U}dV \tag{2.21}$$

and *Vol* is the volume of the computational cell and d**S** is an element of $\partial\Omega$, the surface of Ω.

Next, the inviscid flux $\mathbf{F}_0$ is split into components along the characteristic directions of the flow, because the hyperbolic property of this flux allows upwind numerical approximations to be used for the spatial derivatives. Then the equations become

$$\frac{\partial\langle\mathbf{U}\rangle}{\partial t}+\frac{1}{Vol}\int_{\partial\Omega}\left(\mathbf{F}_o^+\left(\Lambda^+\right)+\mathbf{F}_o^-\left(\Lambda^-\right)+\mathbf{F}_\mu\right)\cdot d\mathbf{S}=0 \qquad (2.22)$$

where Λ^+ and Λ^- are the positive and negative parts of the flux eigenvalues.

Finally, the equations are discretized in 2-D for each computational cell (i,j) as follows:

$$\frac{\mathbf{U}_{i,j}^{n+1}-\mathbf{U}_{i,j}^n}{\Delta t}=-\frac{1}{A_{i,j}}\left\{\left[\mathbf{F}_o^+ +\mathbf{F}_o^- +\mathbf{F}_\mu\right]_{i+1/2,j}^n l_{i+1/2,j} -\left[\mathbf{F}_o^+ +\mathbf{F}_o^- +\mathbf{F}_\mu\right]_{i-1/2,j}^n l_{i-1/2,j}\right.$$
$$\left.+\left[\mathbf{F}_o^+ +\mathbf{F}_o^- +\mathbf{F}_\mu\right]_{i,j+1/2}^n l_{i,j+1/2} -\left[\mathbf{F}_o^+ +\mathbf{F}_o^- +\mathbf{F}_\mu\right]_{i,j-1/2}^n l_{i,j-1/2}\right\} \qquad (2.23)$$

where n is the time index, $A_{i,j}$ is the area of cell (i,j), and l is the length of a cell edge. The fluxes $\mathbf{F}_o^+$ and $\mathbf{F}_o^-$ are calculated using upwind differencing, whereas $\mathbf{F}_\mu$ is found using centered differences.

2.4.2 Boundary Conditions

The classical wall condition for fluid dynamics is the no-slip condition. Thus a zero velocity at the wall is prescribed when the isothermal condition is assumed. However, in order to extend the approach for flows in the slip regime, a slip wall model is adopted as follows:

$$u_{gas}-u_{wall}=\frac{2-\sigma_v}{\sigma_v}\frac{1}{\rho\left(2RT_w/\pi\right)^{1/2}}\tau_s +\frac{3}{4}\frac{\Pr(\gamma-1)}{\gamma\rho RT_w}(-q_s) \qquad (2.24)$$

$$T_{gas}-T_{wall}=\frac{2-\sigma_T}{\sigma_T}\frac{2(\gamma-1)}{\gamma+1}\frac{1}{R\rho\left(2RT_w/\pi\right)^{1/2}}\tau_s(-q_n) \qquad (2.25)$$

where σ_v is the tangent momentum accommodation coefficient, σ_T is the thermal accommodation coefficient, q_n,q_s are the normal and tangential heat transfer from the

gas to the wall, T_w is the wall temperature, ρ is the gas density, τ_s is the shear stress component parallel to the wall, R is the gas constant, γ is the ratio of specific heats, P_r is the Prandtl number.

The outer boundary condition for external flows generally involves the free stream condition. However, a characteristic boundary method (Hirsch, 1990) is adopted here because it is impossible to have an infinite computational domain. For an exit boundary, the exit pressure is prescribed as the free stream pressure.

CHAPTER III

THE INFORMATION PRESERVATION METHOD FOR
MODELING MICRO-SCALE GAS FLOWS

For micro-scale gas flows, particle methods are generally accurate but expensive whereas continuum methods are efficient but questionable in terms of physical accuracy. In this chapter, a method called the information preservation method is developed based on a particle method by preserving macroscopic information in microscopic particles, with the intention of reducing the computational cost for simulating micro-scale gas flows and maintaining high accuracy.

3.1 Introduction

The information preservation (IP) method, first proposed by Fan and Shen (1999), has been used to overcome the problem of statistical scatter associated with the direct simulation Monte Carlo (DSMC) method when simulating low-speed, constant density flows. It achieved great success for several unidirectional transitional gas flows (Fan and Shen, 2001), including Couette flow, Poiseuille flow, and the Rayleigh problem. This method was later developed to simulate low-speed microchannel flows (Cai et al., 2000) and to investigate the flows around a NACA0012 airfoil (Fan et al., 2001) using the isothermal assumption by calculating the macroscopic velocity and by solving the density flow field from the continuity equation.

The IP method is developed based on the DSMC method by additionally preserving macroscopic information in simulated particles. In the IP method, all microscopic information, including particle movements and collisions, is handled by the

DSMC method, and the macroscopic information is updated using other algorithms. The flow field is obtained by sampling the preserved macroscopic information instead of the microscopic information, so that the statistical scatter of the flow information can be greatly reduced for low-speed gas flows. However, the principle for updating the macroscopic information has not been thoroughly studied.

In the next section (Section 3.2), the principle is explained, and the IP method is developed to include energy information. Based on this principle, an energy flux model is introduced in Section 3.3, and a collision model is described in Section 3.4, in order to update the preserved macroscopic information. Section 3.5 presents a detailed implementation of the IP method, and Section 3.6 discusses some advantages and disadvantages of the method. Finally, Section 3.7 gives conclusions concerning the development of the IP method.

3.2 Modeling the Preserved Macroscopic Information

Micro-scale gas flows can generally be described by the density, velocity, and temperature at each location. This macroscopic information is then to be preserved for the IP method. Therefore, each particle simulated in the IP method has the following information: particle location, particle microscopic velocity, internal energy, macroscopic density, macroscopic velocity $\mathbf{V}_i$, and macroscopic temperature T_i (it will be shown that it is not necessary to preserve the macroscopic density for particles). The computational cells will also preserve the macroscopic density ρ_c, macroscopic velocity $\mathbf{V}_c$ and macroscopic temperature T_c in order to help update the preserved particle information. Because particle location, particle microscopic velocity, and internal energy are handled by the DSMC method, only the preserved macroscopic information requires modeling, which will be discussed in the following.

The transfer equation:

$$\frac{\partial}{\partial t}\left(n\overline{Q}\right)+\nabla\cdot\left(n\overline{\mathbf{c}Q}\right)=\Delta[Q] \tag{3.1}$$

provides a connection between the microscopic information and the macroscopic information for a flow. Hence, the transfer equation will be considered first with the intention to obtain physical equations for the preserved macroscopic information with the quantity Q set to mass, momentum and translational energy, respectively.

In order to clarify the different velocities associated with a particle i, the microscopic velocity of a particle is denoted by $\mathbf{c}_i$, the preserved macroscopic velocity is expressed as $\mathbf{V}_i$, while the macroscopic velocity of the flow field is written as $\mathbf{c}_0$. These velocities hold the following relationships with scatters $\mathbf{c}'_i$, $\mathbf{c}''_i$ and $\mathbf{c}'''_i$:

$$\mathbf{c}_i = \mathbf{c}_0 + \mathbf{c}'_i \tag{3.2}$$

$$\mathbf{V}_i = \mathbf{c}_0 + \mathbf{c}''_i \tag{3.3}$$

$$\mathbf{c}'''_i = \mathbf{c}'_i - \mathbf{c}''_i \tag{3.4}$$

3.2.1 Preserved Density

The transfer equation for mass is as follows:

$$\frac{\partial}{\partial t}\left(nm\right)+\nabla\cdot\left(nm\overline{\mathbf{c}_i}\right)=0 \tag{3.5a}$$

which can be written as:

$$\frac{\partial}{\partial t}\left(\rho\right)+\nabla\cdot\left(\rho\mathbf{c}_0\right)=0 \tag{3.5b}$$

It is obvious that the density of the flow can be found from the continuum Equation 3.5b, which means it is not necessary to preserve macroscopic density for each simulated particle. However, an IP scheme that preserves the density for simulated particles has also been developed (Sun et al., 2002).

3.2.2 Preserved Velocity

The transfer equation for momentum appears as Equation 3.6, which can be written as Equation 3.9 using the following procedure.

$$\frac{\partial}{\partial t}\left(nm\overline{\mathbf{c}_i}\right)+\nabla\cdot\left(nm\overline{\mathbf{c}_i^2}\right)=0 \tag{3.6}$$

With

$$\overline{\mathbf{c}_i^2}=\overline{\left(\mathbf{V}_i+\mathbf{c}_i'''\right)\mathbf{c}_i}=\overline{\mathbf{c}_i\mathbf{V}_i}+\overline{\mathbf{c}_i'''\left(\mathbf{c}_i'+\mathbf{c}_0\right)}=\overline{\mathbf{c}_i\mathbf{V}_i}+\overline{\mathbf{c}_i'''\mathbf{c}_i'} \tag{3.7}$$

then,

$$\frac{\partial}{\partial t}\left(nm\overline{\mathbf{V}_i}\right)+\nabla\cdot\left(nm\overline{\mathbf{c}_i\mathbf{V}_i}\right)=-\nabla\cdot\left(nm\overline{\mathbf{c}_i'''\mathbf{c}_i'}\right) \tag{3.8}$$

or

$$\frac{\partial}{\partial t}\left(nm\overline{\mathbf{V}_i}\right)+\nabla\cdot\left(nm\overline{\mathbf{c}_i\mathbf{V}_i}\right)=-\nabla p'+\nabla\cdot\boldsymbol{\tau}' \tag{3.9}$$

where,

$$\boldsymbol{\tau}'=-\left(\rho\overline{\mathbf{c}_i'''\mathbf{c}_i'}-p'\mathbf{I}\right) \tag{3.10}$$

and

$$p'=nk\overline{T_i} \tag{3.11}$$

Equation 3.9 is in the form of the transfer equation with $Q=m\mathbf{V}_i$, which can be regarded as the governing equation for the preserved macroscopic velocity of particles.

In Equation 3.9, the first term of the left hand side is the change rate of the momentum. The second term is the change due to the microscopic movement of the particles, which means that the preserved macroscopic velocity is carried by the particles as the preserved macroscopic velocity is not directly coherent with the microscopic velocity. The right hand side of the equation is the collision integral with a pressure term and a viscous term that must be modeled when two particles collide.

3.2.3 Preserved Temperature

The transfer equation for energy is shown as Equation 3.12. We intend to obtain a control equation for the preserved temperature.

$$\frac{\partial}{\partial t}\left(\frac{1}{2}nm\overline{c_i^2}\right)+\nabla\cdot\left(\frac{1}{2}nm\overline{\mathbf{c}_i\cdot c_i^2}\right)=0 \tag{3.12}$$

The macroscopic temperature can be sampled as the following:

$$T = \overline{T_i} + \frac{\overline{V_i^2} - \overline{V_i}^2}{3R} = \overline{T_i} + \frac{\overline{V_i^2} - c_0^2}{3R}$$

(3.13)

then,

$$c_0^2 + 3RT = \overline{V_i^2 + 3RT_i}$$

(3.14)

Hence,

$$\overline{c_i^2} = \overline{c_0^2} + \overline{c_i' c_i'} = c_0^2 + 3RT = \overline{V_i^2 + 3RT_i}$$

(3.15)

Also,

$$\overline{\mathbf{c}_i \cdot c_i^2} = \overline{(\mathbf{c}_0 + \mathbf{c}_i') c_i^2} = \mathbf{c}_0 \overline{V_i^2 + 3RT_i} + \overline{\mathbf{c}_i'(\mathbf{c}_i \cdot \mathbf{c}_i)}$$

(3.16)

So,

$$\frac{\partial}{\partial t}\left(\frac{1}{2}nm\overline{(V_i^2 + 3RT_i)}\right) + \nabla \cdot \left(\frac{1}{2}nm\overline{(V_i^2 + 3RT_i)\mathbf{c}_i}\right) = -\nabla \cdot \left(\frac{1}{2}nm\overline{\mathbf{c}_i'(\mathbf{c}_i \cdot \mathbf{c}_i)}\right)$$

(3.17)

Furthermore,

$$\overline{\mathbf{c}_i'(\mathbf{c}_i \cdot \mathbf{c}_i)} = \overline{\mathbf{c}_i'(\mathbf{c}_i' \cdot \mathbf{c}_i')} + 2\overline{\mathbf{c}_i'(\mathbf{c}_i' \cdot \mathbf{c}_0)}$$

(3.18)

and

$$\nabla \cdot \left(\overline{\mathbf{c}_i'(\mathbf{c}_i' \cdot \mathbf{c}_0)}\right) = \nabla \cdot \left(\overline{\mathbf{c}_i' \mathbf{c}_i'} \cdot \mathbf{c}_0\right)$$

(3.19)

Hence,

$$\nabla \cdot \left(\frac{1}{2}nm\overline{\mathbf{c}_i'(\mathbf{c}_i \cdot \mathbf{c}_i)}\right) = \nabla \cdot \mathbf{h} + \nabla \cdot (p'\mathbf{c}_0) - \nabla \cdot (\mathbf{c}_0 \cdot \boldsymbol{\tau}'')$$

(3.20)

with

$$\rho \overline{\mathbf{c}_i' \mathbf{c}_i'} = p'\mathbf{I} - \boldsymbol{\tau}''$$

(3.21)

and

$$\mathbf{h} = \frac{1}{2}\rho \overline{\mathbf{c}_i'(\mathbf{c}_i' \cdot \mathbf{c}_i')}$$

(3.22)

Therefore,

$$\frac{\partial}{\partial t}\left(\frac{1}{2}nm\overline{(V_i^2 + 3RT_i)}\right) + \nabla \cdot \left(\frac{1}{2}nm\overline{(V_i^2 + 3RT_i)\mathbf{c}_i}\right)$$
$$= -\nabla \cdot \mathbf{h} - \nabla \cdot (p'\overline{\mathbf{V}_i}) + \nabla \cdot (\overline{\mathbf{V}_i} \cdot \boldsymbol{\tau}'')$$

(3.23)

Clearly, Equation 3.23 is also in the form of the transfer equation with

$Q = \frac{1}{2}m\overline{(V_i^2 + 3RT_i)}$. In order to avoid preserving the average of the preserved energy,

Equation 3.23 is approximated as Equation 3.24,

$$\frac{\partial}{\partial t}\left(\frac{1}{2}nm\overline{\left(V_i^2 + 3RT_i\right)}\right) + \nabla \cdot \left(\frac{1}{2}nm\overline{\left(V_i^2 + 3RT_i\right)\mathbf{c}_i}\right)$$
$$= -\nabla \cdot \mathbf{h} - \nabla \cdot \left(p'\overline{\mathbf{V}_i}\right) + \nabla \cdot \left(\overline{\mathbf{V}_i \cdot \tau''}\right) + unknown\ function \tag{3.24}$$

with $Q = \frac{1}{2}m\left(V_i^2 + 3RT_i\right)$.

Equation 3.23 or Equation 3.24 is apparently more complicated than Equation 3.8 or Equation 3.9. Exactly modeling all terms in Equation 3.24 becomes very difficult. Attempts to model the preserved temperature have been made recently (Shen et al., 1999; Sun et al., 1999). However, these results are far from satisfactory.

On the other hand, the change of the preserved energy results from three factors: particle collision, particle movement, and the pressure force effect shown in Equation 3.24. The particle collision effect includes heat transfer and viscous dissipation. Particle movement, however, has different energy transfer from the transfer of the preserved energy (the second term of the left hand side of Equation 3.24) as will be shown in the next section. Hence, this difference should also be included in a control equation. As a result, a physical form for modeling the preserved temperature is then proposed as Equation 3.25.

$$\frac{\partial}{\partial t}\left(\frac{1}{2}nm\overline{\left(V_i^2 + 3RT_i\right)}\right) + \nabla \cdot \left(\frac{1}{2}nm\overline{\left(V_i^2 + 3RT_i\right)\mathbf{c}_i}\right)$$
$$= collision\ effects - \nabla \cdot \left(p'\overline{\mathbf{V}_i}\right) + necessary\ heat\ transfer \tag{3.25}$$

In the next two sections, an energy flux model and a collision model are proposed to model the heat transfer difference and collision effects, respectively. The accuracy of these models is examined in Chapter IV.

3.3 An Energy Flux Model for the Preserved Temperature

The IP method is based on the microscopic movement of the particles simulated by the DSMC method. There is a contradiction between the real flux and the IP

representation for the energy flux across an interface (e.g., a surface of a computational cell), which can be demonstrated by the following example.

$$\overline{\frac{1}{2}mc_i^2} = \frac{3}{2}kT_1 \qquad\qquad \overline{\frac{1}{2}mc_i^2} = \frac{3}{2}kT_2$$
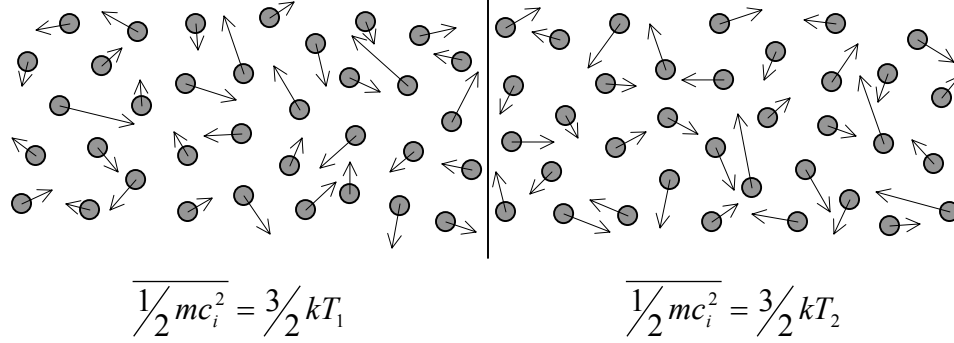
Figure 3.1. Flow between two stationary gases separated by a plate

Consider a flow of two gases separated by a plate as shown in Figure 3.1. The temperature of the gas on the left side of the plate is T_1, whereas the temperature of the gas on the right side of the plate is T_2. Thus the average translational energy of the two groups of particles is $\frac{3}{2}kT_1$ and $\frac{3}{2}kT_2$, and particles preserve the macroscopic temperature at T_1 or T_2, respectively. The two gases will become mixed after the plate is suddenly removed. Kinetic theory shows that the average energy of the particles that move across the interface is $2kT_1$ for the left side and $2kT_2$ for the right side. This occurs because the translational energy flux of the component normal to the interface is twice the flux of the component in the other directions because particles having larger energy can move across the interface from far away (Figure 3.2). However, each particle only carries an energy with $\frac{3}{2}kT_1$ or $\frac{3}{2}kT_2$ as shown in Equation 3.25 for the IP presentation. Therefore, the difference between the real flux and the represented one should be included as in Equation 3.25.

The energy flux model aims to include the difference between the real energy flux and the IP representation. Remember the goal of the IP method is to reduce the statistical scatter; therefore, this model seeks to represent the net energy flux across an interface instead of recovering the microscopic energy for every particle. To do this, each particle

$$\overline{\frac{1}{2}mc_i^2} = 2kT_1 \qquad\qquad\qquad \overline{\frac{1}{2}mc_i^2} = 2kT_2$$
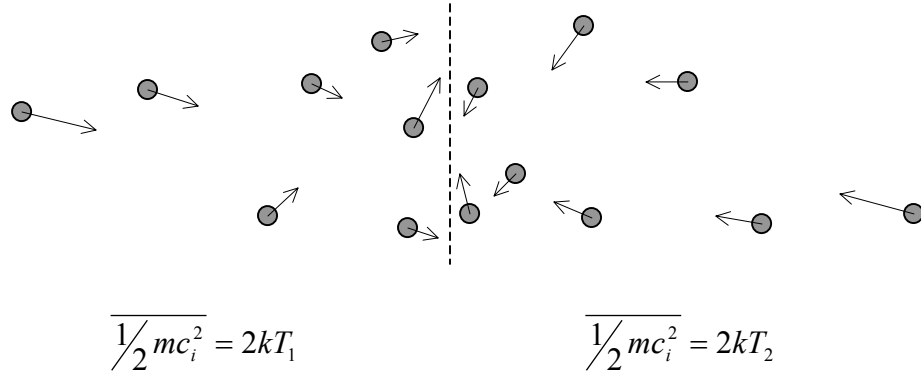
Figure 3.2. Illustration of particles that can move across the interface in a short time

crossing the interface carries an additional energy which is the result of the mentioned difference subtracted by a reference energy. This reference energy helps keep the additional energy to a small level, and the effect of the reference energy is included in Equation (3.25). The additional energy, however, is borrowed from the other particles in the computational cells as the conservation of the total energy should be satisfied. This model can be illustrated by the example of the flow of two gases separated by a plate. Figure 3.3 illustrates the principle of the energy flux model for the example. First, the particles crossing the interface have the average translational energy of $2kT$. Second, in the IP representation, each of those particles has carried an energy of $\frac{3}{2}kT$, which means each particle must carry an additional energy of $\frac{1}{2}kT$. Third, in order to reduce the statistical scatter, each particle only carries an additional energy of $\frac{1}{2}k(T - T_{ref})$, where T_{ref} is a reference temperature. In general, the reference energy cannot be balanced. Therefore, the effect of the net reference energy must be included in Equation (3.25). Furthermore, the final additional energy carried by each particle is borrowed from other particles in the cell, which means other particles need to share this energy to satisfy the conservation of the total energy.

In the above example, the particles crossing the interface have an average translational energy of $2kT$. In general, the average energy is a function of the mean flow velocity $\mathbf{c}_0$ and the angle θ between the flow direction and the normal of the interface as

Real situation: N_1 N_2

$$\overline{\tfrac{1}{2}mc_i^2} = 2kT_1 \qquad \overline{\tfrac{1}{2}mc_i^2} = 2kT_2$$

IP represents: $\tfrac{3}{2}kT_1$ $\tfrac{3}{2}kT_2$

Need additional: $\tfrac{1}{2}kT_1 \xrightarrow{N_1} \xleftarrow{N_2} \tfrac{1}{2}kT_2$

IP represents: $\tfrac{3}{2}kT_1$ $\tfrac{3}{2}kT_2$

Additional: $\tfrac{1}{2}k(T_1 - T_{ref}) \xrightarrow{N_1} \xleftarrow{N_2} \tfrac{1}{2}k(T_2 - T_{ref})$

Plus $\tfrac{1}{2}(N_1 - N_2)kT_{ref} \longrightarrow$
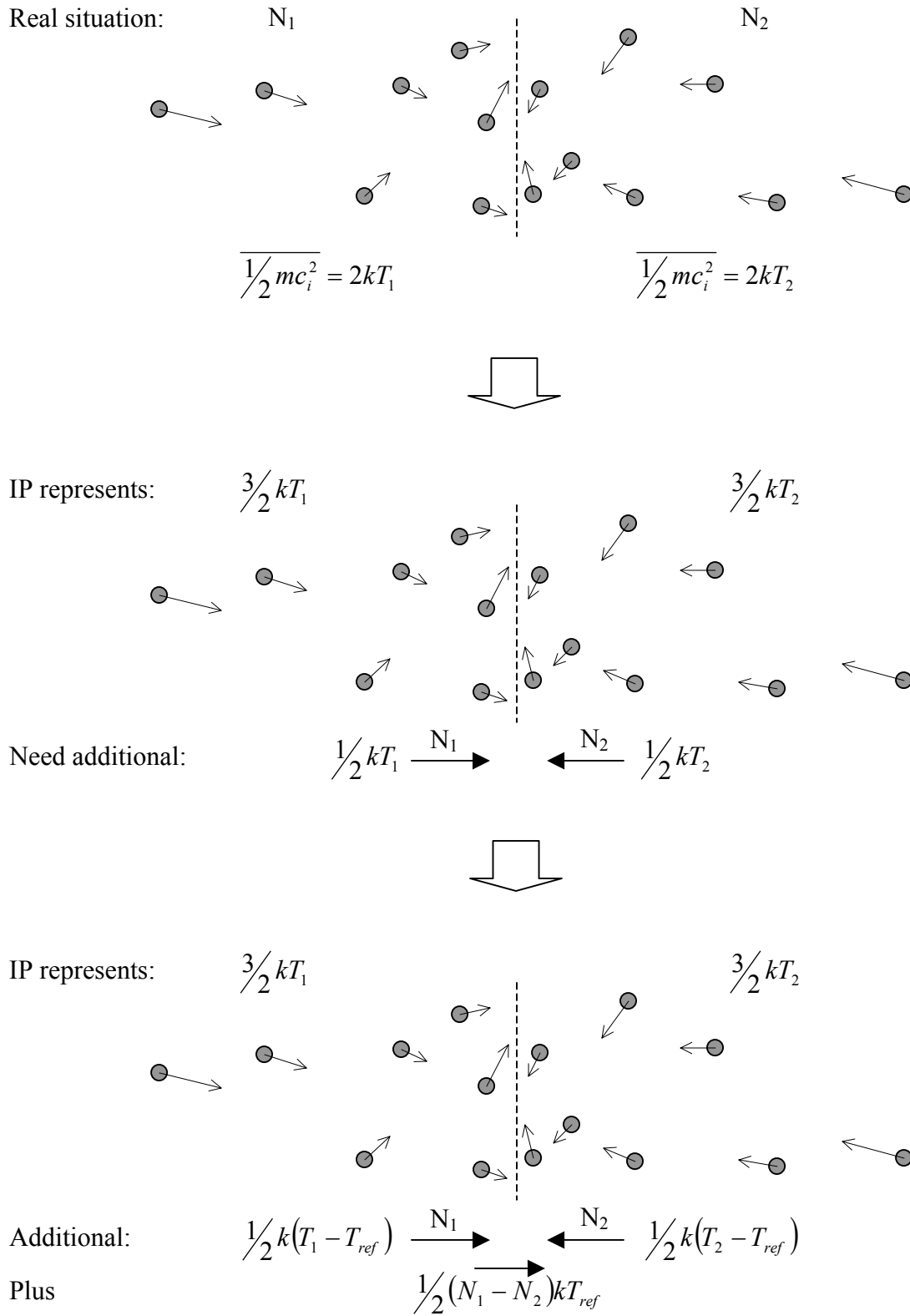
Figure 3.3. Illustration of the principle of the energy flux model

shown in Equation 3.26:

$$\overline{\frac{1}{2}mc_i^2}\Bigg|_{\mathbf{c}_i \cdot \mathbf{n} > 0} = 2kT + \frac{1}{2}mc_0^2 + \frac{\sqrt{\pi}\big/_2\, kT \cdot s(1 + erf(s))}{\exp(-s^2) + \sqrt{\pi}s(1 + erf(s))} \tag{3.26}$$

or,

$$\overline{\frac{1}{2}mc_i^2}\Bigg|_{\mathbf{c}_i \cdot \mathbf{n} > 0} = \frac{3}{2}kT + akT \tag{3.27}$$

with $s = c_0 \cdot \sqrt{\dfrac{m}{2kT}} \cdot \cos\theta$. Then the additional energy will be in the form of $ak(T - T_{ref})$.

If T_{ref} is chosen as the temperature of the interface, the following physical form

for the preserved energy (the combination of the preserved velocity and preserved

temperature) is obtained:

$$\frac{\partial}{\partial t}\left(\frac{1}{2}nm\overline{(V_i^2 + 3RT_i)}\right) + \nabla \cdot \left(\frac{1}{2}nm\overline{(V_i^2 + 3RT_i)\mathbf{c}_i}\right)$$

$$= \begin{array}{c}collision\\effects\end{array} - \nabla \cdot (p'\overline{\mathbf{V}_i}) + \begin{array}{c}reference\ energy\\effect\end{array} + \begin{array}{c}additional\\heat\ transfer\end{array} \tag{3.28}$$

The term called "additional heat transfer" means that each particle i will carry an

additional energy of $ak(T_i - T_{ref})$ when it crosses an interface where a is to be

determined from Equations 3.26 and 3.27. The term of "reference energy effect" can be

expressed as $-\nabla \cdot ((\dot{\mathbf{N}}_1 a_1 - \dot{\mathbf{N}}_2 a_2)kT)$, where $\dot{\mathbf{N}}_i$ is the half number flux across an

interface from side i, and a_i is the coefficient in the additional energy form. The only

unknown term in Equation 3.28 is the "collision effects" term that will be discussed in the

next section.

In the implementation, the IP method preserves an additional variable T_a for

particles to describe the additional energy $ak(T - T_{ref})$ as $\xi kT_a/2$, where ξ is the

number of degrees of freedom. As stated earlier, the additional energy is borrowed from

other particles; therefore a new variable $T_{a,c}$ is used for cells to record the borrowed

energy as $\xi kT_{a,c}/2$. At the end of each time step, the borrowed energy is evenly provided

by all the particles in the cell to maintain the conservation of energy.

3.4 A Collision Model for the Preserved Macroscopic Information

The preserved macroscopic information will change due to molecular collisions because of momentum exchange, internal energy exchange and viscous dissipation. For low-speed, constant density flow systems, Fan and Shen (2001) used the following simple collision model for the preserved macroscopic velocity:

$$V_1'' = V_2'' = (V_1' + V_2')/2 \qquad (3.29)$$

where superscripts $'$ and $''$ denote pre- and post-collision, and subscripts 1 and 2 denote particle 1 and particle 2 in the collision pair. Numerical tests show that this simple collision model cannot correctly simulate the viscosity of the gases. Fan and Shen (2001) adjusted the molecular diameters for the IP method according to experimental data. Thus the molecular diameters for the IP method and for the DSMC method are different. Then the DSMC collisions with the molecular diameter for the IP method may not be correctly modeled, which will affect the results from the IP method.

Hence, the simple collision model needs to be modified. The preserved macroscopic information for two collision particles will not be the same after one particle collision. It will depend on the relative speed of the two particles, the deflection angle in the collision plane and so on. A detailed mechanism for the IP method is then very difficult to obtain. Thus, a phenomenological model for the distribution of the information for the two particles is proposed to include the effect of the deflection angle in the collision plane:

$$\mathbf{V}_1'' = \frac{1 + C_\mu \cdot \cos(\chi)}{2} \mathbf{V}_1' + \frac{1 - C_\mu \cdot \cos(\chi)}{2} \mathbf{V}_2' \qquad (3.30)$$

$$\mathbf{V}_2'' = \frac{1 - C_\mu \cdot \cos(\chi)}{2} \mathbf{V}_1' + \frac{1 + C_\mu \cdot \cos(\chi)}{2} \mathbf{V}_2' \qquad (3.31)$$

$$T_1'' = \frac{1 + C_\kappa \cdot \cos(\chi)}{2} T_1' + \frac{1 - C_\kappa \cdot \cos(\chi)}{2} T_2' + (V_1' - V_2')^2 \left(1 - C_\mu^2 \cos^2 \chi\right) / (4 \cdot \xi \cdot R) \qquad (3.32)$$

$$T_2'' = \frac{1 - C_\kappa \cdot \cos(\chi)}{2} T_1' + \frac{1 + C_\kappa \cdot \cos(\chi)}{2} T_2' + (V_1' - V_2')^2 \left(1 - C_\mu^2 \cos^2 \chi\right) / (4 \cdot \xi \cdot R) \qquad (3.33)$$

with $$\cos(\chi) = \frac{(\mathbf{V}_1' - \mathbf{V}_2') \cdot (\mathbf{V}_1'' - \mathbf{V}_2'')}{|\mathbf{V}_1' - \mathbf{V}'| \cdot |\mathbf{V}_1'' - \mathbf{V}_2''|}$$ (3.34)

where, the values of C_μ and C_κ are assumed and verified by numerical tests to be constants only depending on gas species, and χ is the deflection angle after collision in the collision plane.

Table 3-1 Values of C_μ and C_κ for the VHS molecular model

	He	Ar	N_2	O_2	air
C_μ	-0.15	-0.18	-0.25	-0.21	-0.21
C_κ	1.15	1.28	0.87	0.87	0.87

Table 3-1 lists the values of C_μ and C_κ determined by numerical experiments for five gases (He, Ar, N_2, O_2, and air) with the variable hard sphere (VHS) model (Bird, 1981). In determining these values, low speed Couette flows are used for C_μ and heat transfer flows between two parallel plates are employed for C_κ.

In Figure 3.4, two plates at 273K are separated by 1m, with one at rest and the other with a parallel velocity of 1 m/s. C_μ is determined when the numerical shear stress agrees with the theoretical result when the Knudsen number of the flow is 0.01. The

plate 2: $T_2 = 273$K, $V_{x,2} = 1$ m/s

y = 1 m

gases

Kn=0.01

y = 0 m

plate 1: $T_1 = 273$K, $V_{x,1} = 0$
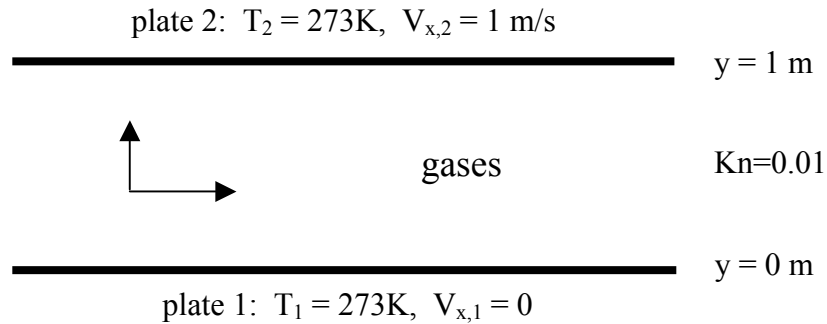
Figure 3.4. Schematic diagram for Couette flows for determining the value of C_μ

Table 3-2 Shear stress distributions (×10⁵kg/m/s²) for five gases in Couette flows

y/L	He	Ar	N$_2$	O$_2$	air
0.1	1.834	2.067	1.616	1.879	1.683
0.2	1.834	2.067	1.617	1.878	1.682
0.3	1.834	2.069	1.617	1.878	1.681
0.4	1.834	2.071	1.618	1.878	1.681
0.5	1.834	2.072	1.621	1.877	1.681
0.6	1.833	2.073	1.620	1.880	1.682
0.7	1.833	2.075	1.618	1.879	1.681
0.8	1.832	2.074	1.615	1.876	1.678
0.9	1.833	2.069	1.616	1.875	1.681
theory	1.824	2.066	1.616	1.873	1.678

numerical shear stress is calculated at cell edges parallel to the plate as

$$\tau_{IP} = \frac{\sum m\left(V_{x,i}^{in} - V_{x,j}^{re}\right)}{\Delta t \cdot \Delta A}$$ **(3.35)**

with the summation over all incoming particles i and all outgoing particles j that cross the edge having an area ΔA during a time Δt. The theoretical result is obtained through $\tau = \mu\, \partial u / \partial y$ with the viscosity coefficient μ found from experimental data (Chapman and Cowling, 1970). Table 3-2 lists the shear stress distributions for the five gases in these Couette flows. The relationship between the viscous coefficient and the gas temperature is illustrated in Figure 3.5. The agreement between the numerical result and theory ($\mu \propto T^{\omega}$ from Chapman and Cowling, 1970) is satisfactory. These data indicate that C_{μ} is a constant.
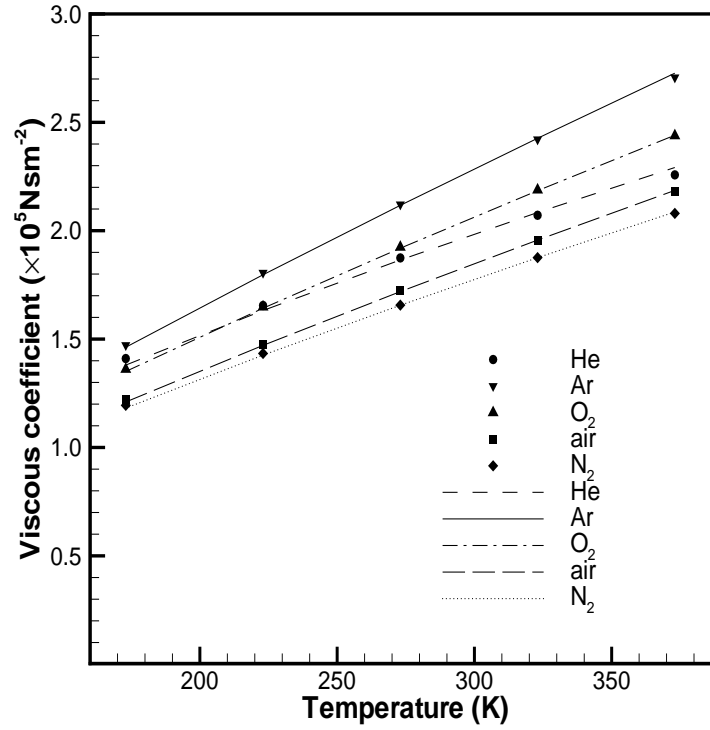
Figure 3.5. Relationship between the viscous coefficient and the temperature for five gases (symbol: IP; line: theory $\mu \propto T^{\omega}$)

Figure 3.6 shows the configuration of the heat flows between two parallel plates for determining C_{κ}. Both plates are at rest, with one at 173K and the other at 373K. The Knudsen number is again 0.01. In this case, it is difficult to obtain an exact theoretical result because the temperature distribution is nonlinear and the flow exhibits some non-equilibrium phenomena. Hence, the average heat flux from the DSMC method is used to determine C_{κ} for the IP method. The heat flux is calculated as follows:

$$q_{DSMC} = \frac{\sum\left(\left(\frac{1}{2}mc_i^2 + E_{rot,i} + E_{vib,i}\right)^{in} - \left(\frac{1}{2}mc_j^2 + E_{rot,j} + E_{vib,j}\right)^{re}\right)}{\Delta t \cdot \Delta A} \qquad (3.36)$$

for the DSMC method, and

$$q_{IP} = \frac{\sum\left(\left(\frac{1}{2}mV_i^2 + \frac{\xi}{2}k(T_i + T_{a,i})\right)^{in} - \left(\frac{1}{2}mV_j^2 + \frac{\xi}{2}k(T_j + T_{a,j})\right)^{re}\right)}{\Delta t \cdot \Delta A} \qquad (3.37)$$

for the IP method. The heat flux distributions in the heat flows are listed in Table 3-3.

plate 2: $T_2 = 373K$, $V_{x,2} = 0$

y = 1 m

gases   Kn=0.01

y = 0 m

plate 1: $T_1 = 173K$, $V_{x,1} = 0$
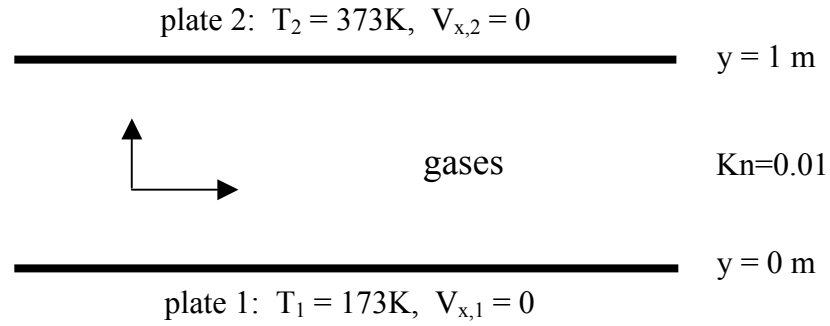
Figure 3.6. Schematic diagram for heat transfer flows between two parallel plates for determining the value of C_κ

Table 3-3 Heat flux distributions (kg/s^3) for five gases in heat transfer flows

y/L	He	Ar	N$_2$	O$_2$	Air
0.1	26.18	3.080	4.333	4.366	4.305
0.2	26.21	3.080	4.330	4.363	4.302
0.3	26.22	3.080	4.334	4.362	4.307
0.4	26.23	3.083	4.332	4.361	4.300
0.5	26.24	3.077	4.333	4.377	4.301
0.6	26.26	3.080	4.342	4.370	4.301
0.7	26.27	3.083	4.337	4.366	4.302
0.8	26.29	3.083	4.337	4.362	4.299
0.9	26.29	3.084	4.337	4.360	4.314
DSMC	26.27	3.083	4.322	4.357	4.310

3.5 Implementation of the Information Preservation Method

In this section, the general procedure of the information preservation (IP) method is described, and a detailed implementation of the method is presented.

3.5.1 General Procedure of the IP Method

In general, the information preservation method preserves macroscopic information on individual particles simulated in the DSMC method, and updates the preserved information during several steps including particle movement and particle collision, and obtains flow field information by sampling the preserved information. This procedure is illustrated in Figure 3.7.

In the IP method, each particle has the following information: particle location, particle microscopic velocity, internal energy, macroscopic velocity $\mathbf{V}_i$, macroscopic temperature T_i and additional temperature $T_{a,i}$, along with the following information for each computational cell: the macroscopic density ρ_c, macroscopic velocity $\mathbf{V}_c$, macroscopic temperature T_c and additional cell temperature $T_{a,c}$. All this information is initialized by the ambient condition while the additional temperature is set to zero. Next, all particles update preserved information based on the following two equations:

$$\frac{\partial}{\partial t}\left(\rho_c \overline{\mathbf{V}_i}\right) + \nabla \cdot \left(\rho_c \overline{\mathbf{c}_i \mathbf{V}_i}\right) = \nabla \cdot \boldsymbol{\tau}' - \nabla p' \tag{3.38}$$

$$\frac{\partial}{\partial t}\left(\frac{1}{2}\rho\overline{\left(V_i^2 + \xi RT_i\right)}\right) + \nabla \cdot \left(\frac{1}{2}\rho\overline{\left(V_i^2 + \xi RT_i\right)\mathbf{c}_i}\right)$$
$$= \begin{array}{c} collision \\ effects \end{array} - \nabla \cdot \left(p'\mathbf{V}_c\right) + \begin{array}{c} reference\ energy \\ effect \end{array} + \begin{array}{c} additional \\ heat\ transfer \end{array} \tag{3.39}$$

First, the preserved macroscopic velocity and preserved temperature update their values according to Equations 3.30-3.34 when particle collisions occur. This means the first term on the right hand side of Equation 3.38 and Equation 3.39 is included. Second, particles move around according to their microscopic velocity, which corresponds to the second term on the left hand side of the equations. When a particle crosses an interface (an internal cell edge or a boundary), the particle carries an additional energy of

start

Set up cell network and
set initial cell information

Distribute particles into cells
with their initial information

Time = Time + time step

Select collision pairs

Perform binary collisions

Inject new particles

Move particles and compute
interactions with boundaries

Unsteady flow:
repeat until
required sample
is obtained

Calculate other effects (e.g., pressure)

Calculate preserved cell information

No ← Time>sample time?

Sample flow properties

No ← Time>final time?

Unsteady flow: average runs
Steady flow: average samples
after established steady flow

Output result

stop

Figure 3.7. DSMC-IP flowchart

$ak(T_i - T_{ref})$ while the additional cell temperature records this "borrowing", which is the fourth term on the right hand side of Equation 3.39. Third, each particle updates its information using the rest of the terms as shown in Equation 3.40 and Equation 3.41,

$$\frac{\partial}{\partial t}(\rho_c \mathbf{V}_i) = -\nabla p' \qquad (3.40)$$

$$\frac{\partial}{\partial t}\left(\frac{1}{2}\rho(V_i^2 + \xi RT_i)\right) = -\nabla \cdot (p'\mathbf{V}_c) + \textit{reference energy effect} \qquad (3.41)$$

with $$p' = \rho_c RT_c \qquad (3.42)$$

where R is the specific gas constant. In this step, the "borrowed" additional energy is evenly subtracted from all particles in the cell. Fourth, each cell updates its preserved cell information:

$$\frac{\partial}{\partial t}(\rho_c) + \nabla \cdot (\rho_c \mathbf{V}_c) = 0 \qquad (3.43)$$

$$\mathbf{V}_c = \overline{\mathbf{V}_i} \qquad (3.44)$$

$$T_c = \overline{T_i} \qquad (3.45)$$

$$T_{a,c} = 0 \qquad (3.46)$$

After particles and cells update their preserved information, the cell information is sampled if needed before the next time step begins. Then, after the required time steps are finished, the preserved cell information is processed to obtain the flow field information. The details are discussed in the next section.

3.5.2 Detailed Implementation of the IP Method

For micro-scale gas flows, the velocity is generally small and rarefaction often occurs only around solid objects. Therefore, when a particle crosses an interface, the additional energy can be approximated as $\frac{1}{2}k(T_i - T_{ref})$. Then the reference energy effect becomes zero. In our 2D parallel IP code that is based on a parallel optimized DSMC code named "MONACO" (Dietrich and Boyd, 1996), macroscopic velocity

components $V_{x,i}$, $V_{y,i}$ and temperatures T_i, $T_{a,i}$ are preserved for each simulated particle i. Macroscopic velocity components $V_{x,c}$, $V_{y,c}$, temperatures T_c, $T_{a,c}$ and density ρ_c are preserved for each computational cell.

The general implementation of the IP procedures (based on the DSMC procedures) can be summarized as follows (see also Figure 3.7):

(1) **Initialization**

The information for all particles and cells is initialized by the ambient conditions after the computational domain is set up, while $T_{a,i}$ and $T_{a,c}$ are set to zero.

For each time step, one collision sub-step, one movement sub-step and one modification sub-step are executed to update the information preserved in particles followed by the update of the information preserved in the cells.

(2) **Particle collision sub-step**

Particles are selected randomly to make pairs, and binary collisions are performed for a subset of these pairs based on the usual DSMC procedures. The preserved macroscopic information is updated according to Equations 3.30-3.34.

(3) **Particle movement sub-step**

Particles are moved at their microscopic velocity as in the DSMC method. The preserved information of particles may change when particles interact with interfaces. Possible particle-interface interactions are:

3a) Particles migrate from one cell to another

When particle i moves from cell k to another cell, momentum and energy transfer occur, and additional energy transfer is required as stated in Section 3.3. The preserved additional energy for the particle and for the cell are adjusted as follows:

$$T'_{a,i} = \left(T_i - T_{ref}\right)/\xi \tag{3.47}$$

$$T'_{a,c,k} = T_{a,c,k} + T_{a,i} - T'_{a,i} \tag{3.48}$$

where, T_{ref} is the interface temperature interpolated from the preserved cell temperatures of neighboring cells.

3b) Particles leave or enter the computational domain

If a particle leaves the computational domain, the preserved information of the particle is lost along with the particle itself. Similar to the DSMC method, new particles may enter into the computational domain, and these particles are assigned information according to the boundary condition with $T_{a,i} = 0$.

3c) Particles reflect from a symmetric boundary

When a particle reaches a symmetric boundary, it is reflected. The normal velocity component is reversed in direction, and the parallel velocity component remains unchanged.

3d) Particles reflect from a wall

The preserved information of particles collided with a wall is set in accordance with the collective behavior of a large number of real molecules. Namely, if it is a specular reflection, only the normal velocity component is reversed. However, if it is a diffuse reflection, the preserved macroscopic velocity and temperature of the reflected particles are set to the velocity and the temperature of the wall. Also, the preserved additional temperature is changed.

For specular reflection:

$$T'_{a,i} = -T_{a,i} \tag{3.49}$$

$$T'_{a,c,k} = T_{a,c,k} + T_{a,i} - T'_{a,i} \tag{3.50}$$

For diffuse reflection:

$$T''_{a,i} = \left(T_i - T_{ref}\right)/\xi \tag{3.51}$$

$$T'_{a,c,k} = T_{a,c,k} + T_{a,i} - T''_{a,i} \tag{3.52}$$

$$T'_{a,i} = \left(T_w - T_{ref}\right)/\xi \tag{3.53}$$

Here, $T''_{a,i}$ denotes the additional temperature of the particle when it is "absorbed" by the wall. $T_{ref} = \sqrt{T_i \cdot T_w}$ is the constant gas temperature of collisionless flow between two plates with one at T_i and the other at T_w (Gombosi, 1994).

After the collisions and movements of particles are considered, the additional energy preserved by the cell k is shared across all N_p particles in the cell:

$$T'_i = T_i + T_{a,c,k}/N_p \tag{3.54}$$

$$T'_{a,c,k} = 0 \tag{3.55}$$

(4) **Modification sub-step**

The preserved information of particles is modified by Equations 3.40 and 3.41 (We have assumed the reference energy effect is zero). These two equations are solved using a finite volume method as:

$$\mathbf{V}_i^{t+\Delta t} - \mathbf{V}_i^t = -\frac{\Delta t \cdot Vol}{N_p W_p m} \frac{1}{A} \oint_{cell} p'\mathbf{n}dl \tag{3.56}$$

$$\left(\frac{V_i \cdot V_i}{2} + \frac{\xi \cdot R \cdot T_i}{2}\right)^{t+\Delta t} - \left(\frac{V_i \cdot V_i}{2} + \frac{\xi \cdot R \cdot T_i}{2}\right)^t = -\frac{\Delta t \cdot Vol}{N_p W_p m} \frac{1}{A} \oint_{cell} (p'\mathbf{V}_c \cdot \mathbf{n})dl \tag{3.57}$$

In the previous equations, A is the area of the cell, Vol is the volume of the cell, dl is the edge element of the cell, $\mathbf{n}$ is the unit vector normal to the cell edge, and W_p is the number of gas molecules represented by one particle. The integrals are evaluated over all cell edges. The cell information on cell edges is linearly interpolated using the information of the neighboring cells. The density ρ_c is replaced by the ratio of the real mass of the total represented molecules in the cell to the volume of the cell such that the statistical effects for this sub-step due to the number fluctuation of particles in a cell can be avoided. For example, Equation 3.56 can be reorganized as follows:

$$\frac{\sum_{i=1}^{N_p} mW_p\left(\mathbf{V}_i^{t+\Delta t} - \mathbf{V}_i^t\right)}{\Delta t \cdot Vol} = -\frac{1}{A} \oint_{cell} p'\mathbf{n}dl \tag{3.58}$$

It is clear that the number fluctuation of particles in a cell does not affect the total pressure effects for all the particles in the cell.

(5) **Update preserved cell information**

After the preserved information of particles is updated, the preserved information for cells is updated by averaging the information of all N_p particles in each cell.

$$\mathbf{V}'_c = \sum_{i=1}^{N_p} \left(\frac{\mathbf{V}_i}{N_p} \right) \tag{3.59}$$

$$T'_c = \sum_{i=1}^{N_p} \left(\frac{T_i + T_{a,i}}{N_p} \right) \tag{3.60}$$

$$\rho'_c - \rho_c = -\frac{\Delta t}{A} \oint_{cell} (\rho_c \mathbf{V}_c \cdot \mathbf{n}) dl \tag{3.61}$$

(6) **Sample flow properties**

The flow properties are obtained by using time or ensemble averaging of the preserved information. The flow velocity $\mathbf{V}_f$, flow temperature T_f and flow density ρ_f are calculated as follows:

$$\mathbf{V}_f = \sum_{t=1}^{N_{step}} \left(\frac{\mathbf{V}_{c,t}}{N_{step}} \right) \tag{3.62}$$

$$T_f = \sum_{t=1}^{N_{step}} \left(\frac{T_{c,t}}{N_{step}} + \frac{1}{N_{step} \cdot \xi \cdot R} \left(\sum_{i=1}^{N_{p,t}} \frac{\mathbf{V}_{i,t} \cdot \mathbf{V}_{i,t}}{N_{p,t}} - \left(\sum_{i=1}^{N_{p,t}} \frac{\mathbf{V}_{i,t}}{N_{p,t}} \right) \cdot \left(\sum_{i=1}^{N_{p,t}} \frac{\mathbf{V}_{i,t}}{N_{p,t}} \right) \right) \right) \tag{3.63}$$

$$\rho_f = \sum_{t=1}^{N_{step}} \left(\frac{\rho_{c,t}}{N_{step}} \right) \tag{3.64}$$

The expressions for the pressure p_w and shear stress τ_w on the wall, and heat flux q_w to the wall are as follows:

$$p_w = p_c + \frac{\sum_{i=1}^{N_s} m\left(V_{n,i}^{re} - V_{n,i}^{in} \right)}{t_s \cdot \Delta A} \tag{3.65}$$

$$\tau_w = \frac{\sum_{i=1}^{N_s} m\left(V_{\tau,i}^{in} - V_{\tau,i}^{re} \right)}{t_s \cdot \Delta A} \tag{3.66}$$

$$q_w = \frac{\sum_{i=1}^{N_s} \left(\frac{1}{2} mV_i^2 + \frac{\xi}{2} kT_i \right)^{in} - \sum_{i=1}^{N_s} \left(\frac{1}{2} mV_i^2 + \frac{\xi}{2} kT_i \right)^{re}}{t_s \cdot \Delta A} \tag{3.67}$$

where N_s is the total number of molecules hitting the wall element during t_s, ΔA is the area of the wall element, p_c is the pressure in the neighboring cell, subscript n denotes the normal velocity component and subscript τ denotes the tangential velocity component, superscripts in and re denote the values before and after striking the wall element, respectively.

For steady flows, steps (2)-(5) are repeated until the flow reaches a steady state. Then steps (2)-(5) are further repeated to obtain the desired sampling size, and the step (6) is used to obtain the final results. For unsteady flows, steps (1)-(6) are repeated to reach the desired sample size, using ensemble averaging.

3.6 Advantages and Disadvantages of the Information Preservation Method

The IP method preserves the information of the flow, which contains much less statistical scatter compared with the DSMC method for low-speed flows. Therefore it is possible to simulate complicated low-speed rarefied gas flows using the IP method. Furthermore, the instantly available preserved cell information has other advantages, including that boundary conditions can be easily applied so that coupling the DSMC method and a continuum approach becomes easier. However, models used in the IP method need to be verified and the IP method requires more computer memory.

3.6.1 Computational Cost of the IP Method

The computational cost of the IP method has two aspects: memory cost and time cost. Compared with the DSMC method, the IP method requires more computer memory but generally takes much less time to obtain a solution for a low-speed flow simulation.

For either the DSMC method or the IP method, the cells and particles require a great deal of memory to store their information, whereas other information and operations cost relatively little memory. Suppose the number of particles in each

computational cell is constant (a weight scheme can achieve this), the total memory cost

for a DSMC or IP simulation can then be approximated as follows:

$$M_t = N_{cell} \cdot \left(M_{cell} + N_p \cdot M_{particle}\right) \tag{3.68}$$

where N_{cell} is the number of cells, N_p is the average number of particles in a cell, M_{cell}

is the memory cost of the cell information and $M_{particle}$ is the memory cost of the particle

information.

Based on a 2D MONACO code, a particle uses about 7 float units (x, y, c_x, c_y,

c_z, E_{rot} and E_{vib}) for DSMC and 11 float units (add V_x, V_y, T, T_a) for IP. A cell uses

more than 40 float units for DSMC and uses an additional 11 for IP. Therefore, the IP

method uses at most 57% (4/7=0.57) more memory than the DSMC method does.

The DSMC method or the IP method also spends considerable time for each time

step as can be seen from the DSMC-IP flow chart. If a steady flow is considered, the

computational time can be expressed as follows:

$$T_t = \left(N_{steady} + N_{sample}\right) \cdot N_{cell} \cdot T_{cell} \tag{3.69}$$

where N_{steady} is the number of time steps to reach a steady condition, N_{sample} is the

number of time steps for a specified sample size, and T_{cell} is the average time spent on a

cell for one time step.

Based on the flow chart, T_{cell} consists of the following parts: T_{coll} for selecting

collision pairs and performing collisions where the IP method spends extra but negligible

time compared with the DSMC method, T_{move} for generating new particles and moving

all particles where the effect of the IP method is also small and negligible, T_{IP} for the IP

method to update the particle information and to calculate cell information, and T_{sample} for

sampling the flow properties where the IP method spends about 20% extra time than the

DSMC method. Overall, an IP step requires a little less than twice the time that a DSMC

step requires because of the time T_{IP} and the extra memory that the IP method occupies.

However, for low-speed gas flows, a DSMC simulation requires a very large N_{sample}

compared to N_{steady}, whereas an IP simulation has a much smaller N_{sample}. Details about the sample size are to be discussed in the next section. Generally, an IP simulation requires much less time than a DSMC simulation to obtain a satisfactory solution for micro-scale gas flows.

3.6.2 Statistical Scatter of the IP Method

The statistical scatter of the DSMC method arises directly from the thermal movement of particles whereas the thermal movement of particles causes scatter only at the macroscopic information level for the IP method. Fan and Shen (2001) have shown that an IP simulation reduces the sampling size required for a regular DSMC simulation of low-speed flows by four orders of magnitude. This provides a tremendous gain in computational time, which can lead to effective use of the IP method for microfluidics and MEMS simulations.

The statistical scatter of the IP and DSMC methods can be illustrated quite well by several Couette flows. Figure 3.8 shows a schematic diagram of the flow. Table 3-4 lists the scatter of the velocity in the middle between the two plates. These data were obtained by averaging 100 samples that are shown in Figures 3.9-3.13. The results show that the scatter from the DSMC method is independent of the flow velocity, and is at levels of about 11m/s for a sample size of 1000 particles, 6 m/s for a sample size of 10,000 particles and 3 m/s for a sample size of 100,000 particles. These values are larger than the scatter predicted by $\sqrt{\dfrac{2RT}{N}}$ from statistical theories for a completely independent sample process. The IP simulations, however, exhibit a different behavior. Specifically, the scatter from the IP method is smaller and is proportional to the flow velocity. Another phenomenon is that the Knudsen number of the flow affects the IP scatter; however, IP scatter can be decreased by increasing the sample size by one or two orders of magnitude. For a flow with $V_{\pm} = \pm 1$m/s and Kn = 0.01, the IP scatter is less than 0.01m/s with a sample size of 1000 particles whereas the DSMC scatter is more than 10

plate 2: $T_2 = 273K$, V_+

y = 1 m

y

x

Argon gas

Kn

y = 0 m

plate 1: $T_1 = 273K$, V_-
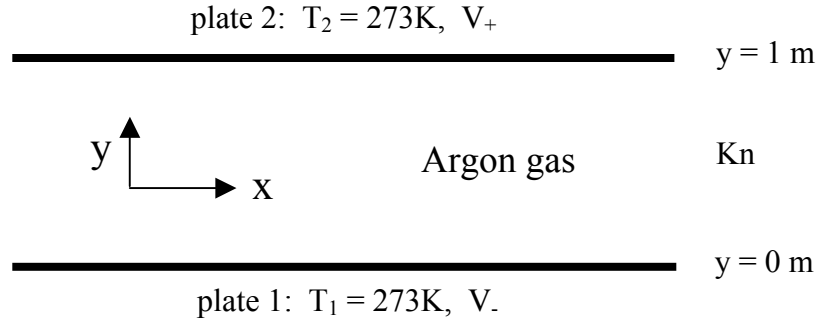
Figure 3.8. Schematic diagram for Couette flows for evaluating statistical scatter

**Table 3-4 Statistical scatter associated with the IP method
and the DSMC method obtained from Couette flows**

Flow condition	Sample size (particles/cell)	Statistical Scatter (m/s)	
		IP method	DSMC method
$V_\pm = \pm100$m/s Kn = 0.01	1000	0.6631	11.74
	10000	0.5864	6.284
	100000	0.2572	3.075
$V_\pm = \pm100$m/s Kn = 0.1	1000	1.052	11.21
	10000	0.5704	5.067
	100000	0.1892	2.122
$V_\pm = \pm100$m/s Kn = 1.0	1000	2.787	10.85
	10000	1.032	6.013
	100000	0.3845	1.832
$V_\pm = \pm1$m/s Kn = 0.01	1000	0.006448	11.35
	10000	0.006916	5.820
	100000	0.002422	3.750
$V_\pm = \pm0.01$m/s Kn = 0.01	1000	0.000046	10.33
	10000	0.000065	6.208
	100000	0.000023	3.433

V$_\pm$ = ±100m/s, Kn = 0.01, sample size = 1,000 particles per cell

V$_\pm$ = ±100m/s, Kn = 0.01, sample size = 10,000 particles per cell

V$_\pm$ = ±100m/s, Kn = 0.01, sample size = 100,000 particles per cell
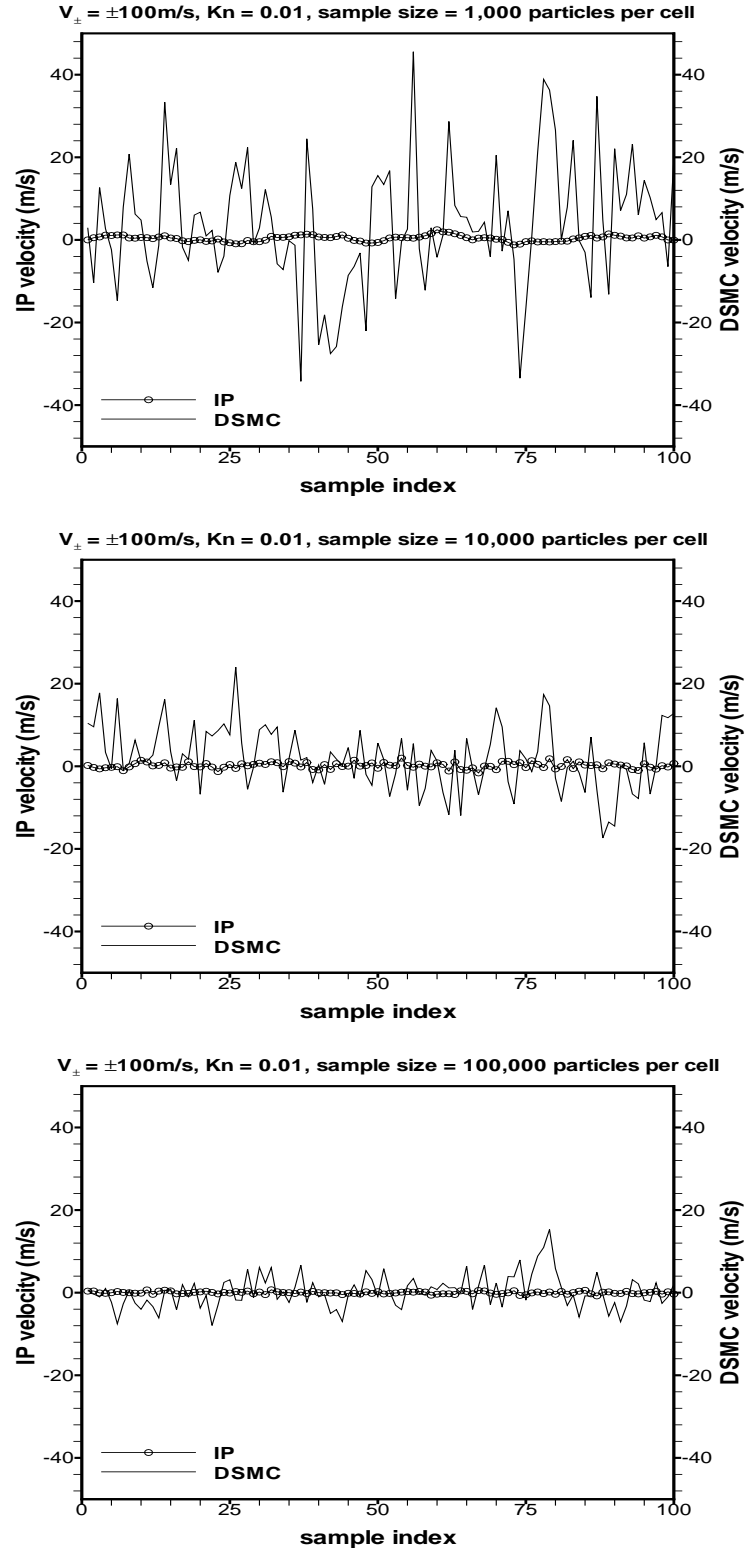
Figure 3.9. Statistical scatter obtained from simulating Couette flows when V$_\pm$ = ±100m/s and Kn = 0.01

V$_\pm$ = ±100m/s, Kn = 0.1, sample size = 1,000 particles per cell

V$_\pm$ = ±100m/s, Kn = 0.1, sample size = 10,000 particles per cell

V$_\pm$ = ±100m/s, Kn = 0.1, sample size = 100,000 particles per cell
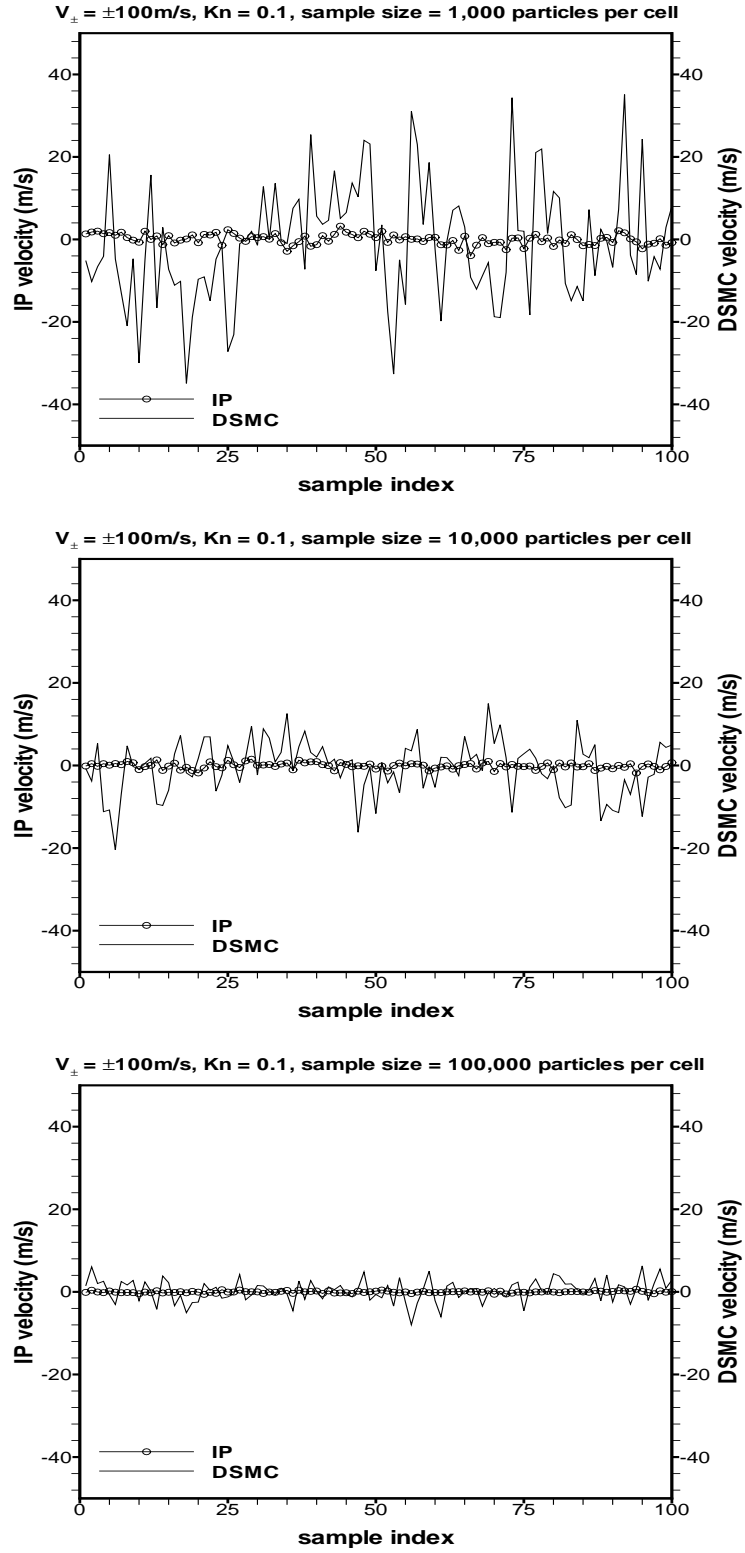
Figure 3.10. Statistical scatter from simulating Couette flows when V$_\pm$ = ±100m/s and Kn = 0.1

V± = ±100m/s, Kn = 1.0, sample size = 1,000 particles per cell

V± = ±100m/s, Kn = 1.0, sample size = 10,000 particles per cell

V± = ±100m/s, Kn = 1.0, sample size = 100,000 particles per cell
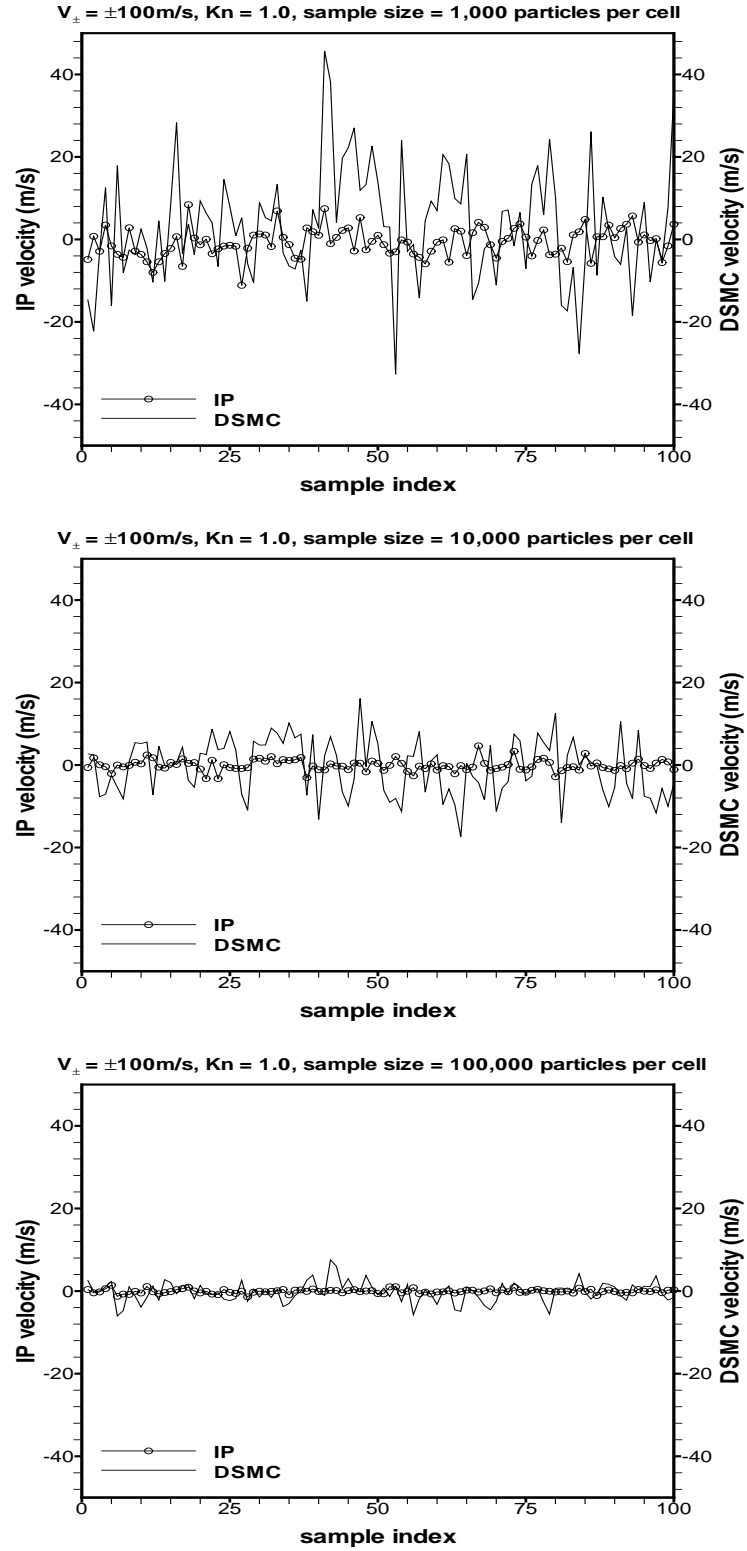
Figure 3.11. Statistical scatter from simulating Couette flows
when V± = ±100m/s and Kn = 1.0

V$_{\pm}$ = ±1m/s, Kn = 0.01, sample size = 1,000 particles per cell

V$_{\pm}$ = ±1m/s, Kn = 0.01, sample size = 10,000 particles per cell

V$_{\pm}$ = ±1m/s, Kn = 0.01, sample size = 100,000 particles per cell
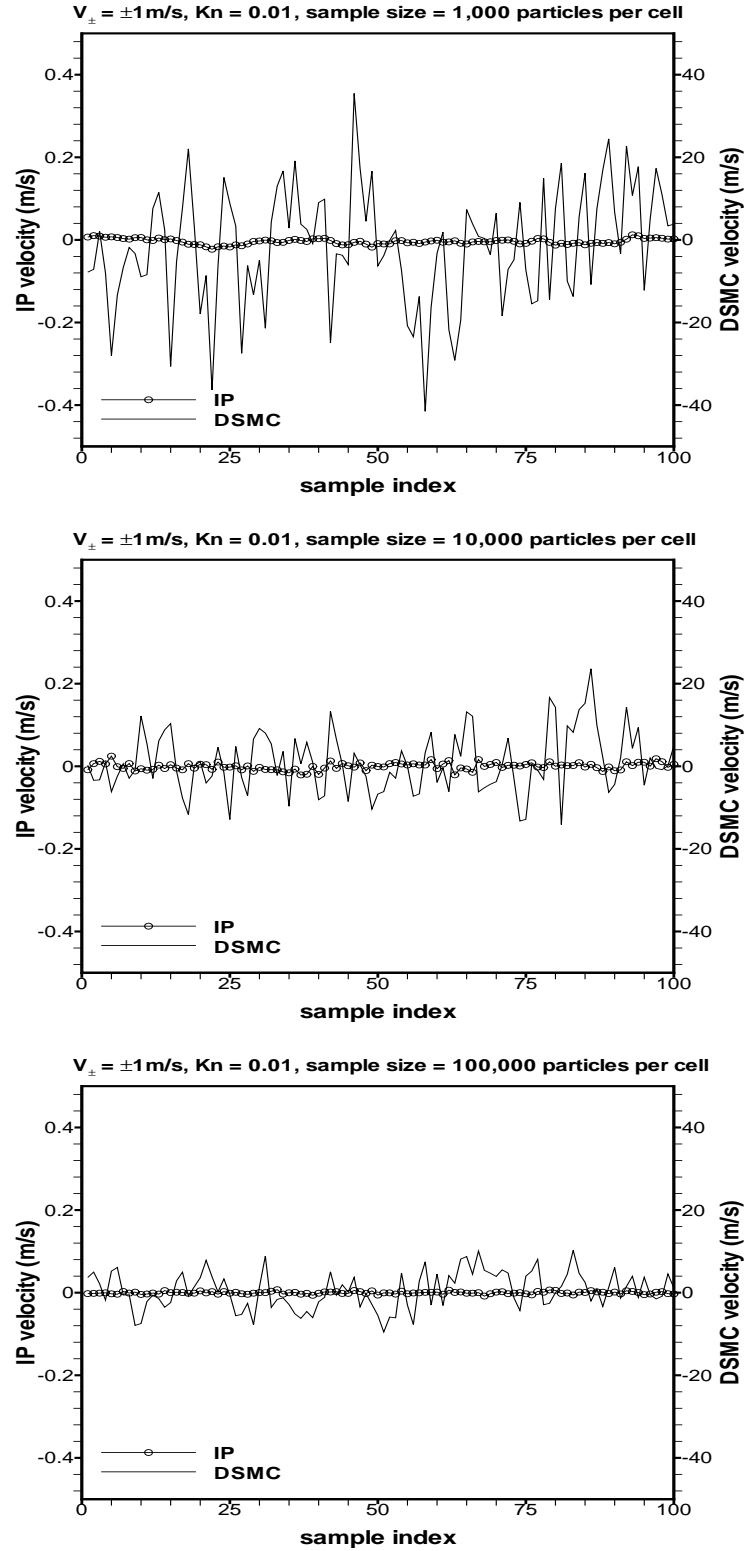
Figure 3.12. Statistical scatter from simulating Couette flows when V$_{\pm}$ = ±1m/s and Kn = 0.01

V$_\pm$ = ±0.001m/s, Kn = 0.01, sample size = 1,000 particles per cell

V$_\pm$ = ±0.001m/s, Kn = 0.01, sample size = 10,000 particles per cell

V$_\pm$ = ±0.001m/s, Kn = 0.01, sample size = 100,000 particles per cell

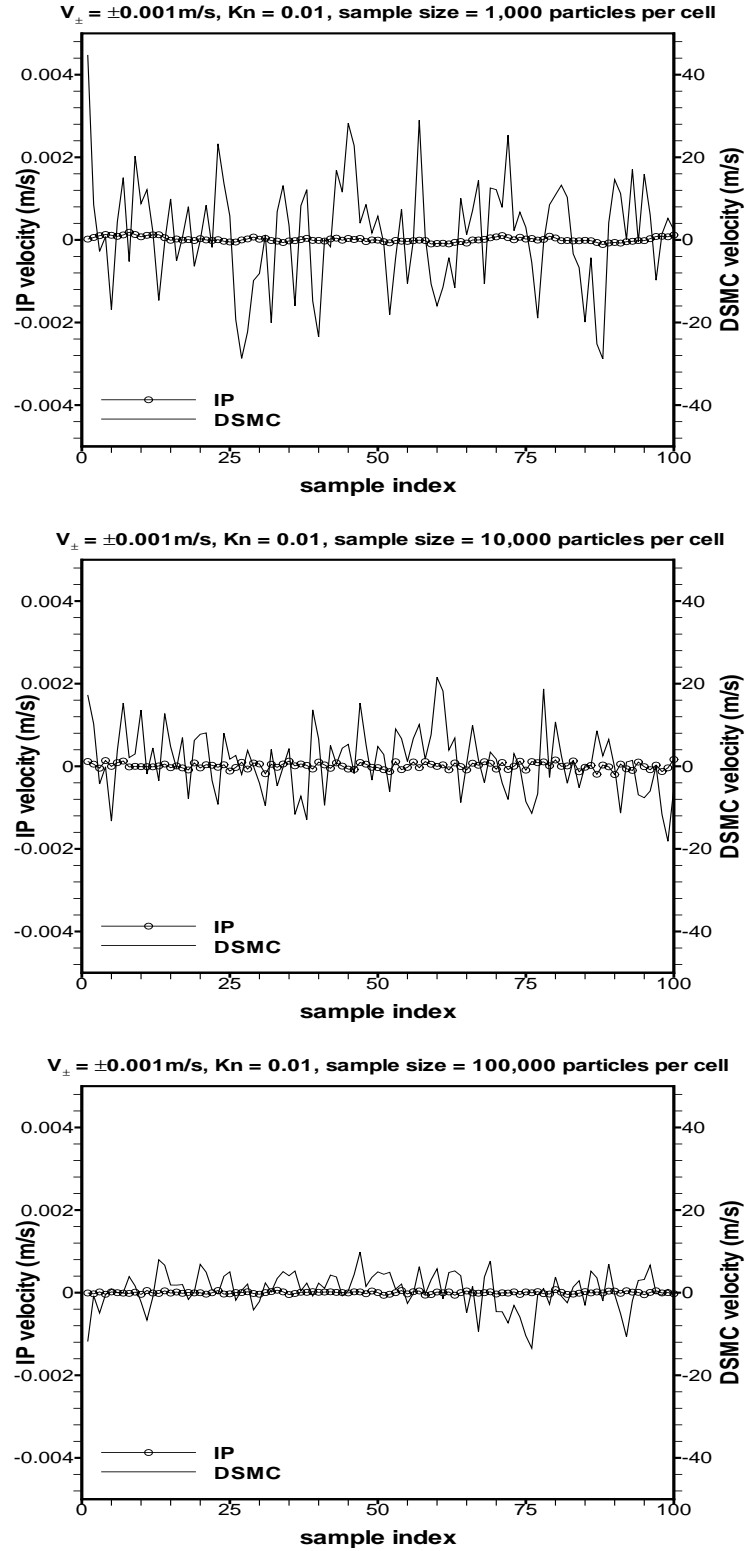**Figure 3.13. Statistical scatter from simulating Couette flows when V$_\pm$ = ±0.01m/s and Kn = 0.01**

 m/s for the same conditions. In order to obtain a scatter less than 0.01 m/s, the DSMC simulation requires a huge sample size.

Comparison of sample size required by an IP or DSMC simulation can also be illustrated using Couette flows (Figure 3.8). For a flow with $V_\pm = \pm100$m/s and Kn = 1.0, the velocity distributions are shown in Figure 3.14 for the results obtained using the IP and DSMC methods. Clearly, the IP method only requires a sample size of 10^4 particles per cell to have a statistical scatter (about 1m/s) that requires the DSMC method to sample 10^6 particles per cell. For low-speed flows, the IP method can still predict a clear flow field with a sample size about 10^4 particles per cell, whereas the DSMC method may or may not be able to predict a meaningful result even with a large sample size. Such an example is illustrated in Figure 3.15 for a Couette flow with $V_\pm = \pm1.0$m/s and Kn = 1.0. The results show that the IP method predicts very satisfactory velocity distributions with a sample size of 10^4 particles per cell, whereas the DSMC method predicts results having a statistical scatter of about 0.2m/s even with a sample size of 10^8 particles per cell. As a result, it is very difficult or even impossible to simulate low-speed flows using the DSMC method. Therefore, the IP method is very helpful for simulating low-speed rarefied gas flows.

V± = 100m/s, Kn = 1.0

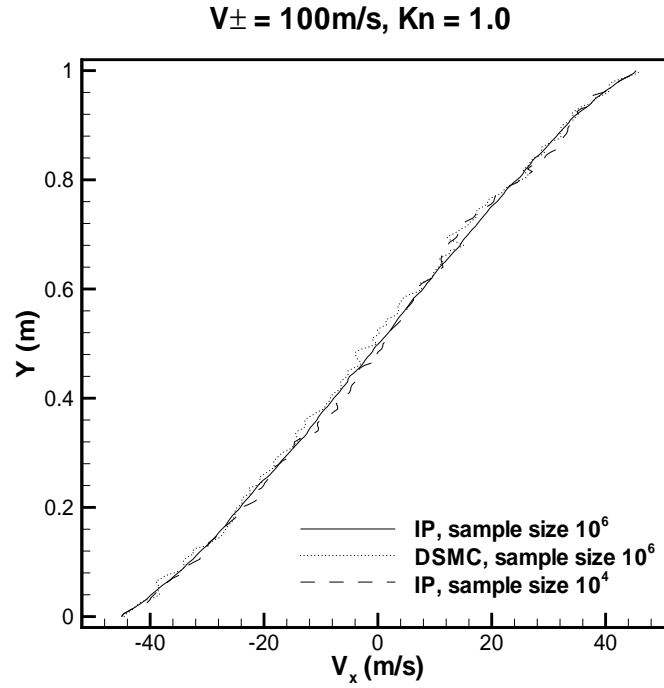**Figure 3.14. DSMC method requires a larger sample size compared with IP method when simulating Couette flows having $V_\pm = \pm100$m/s and Kn = 1.0**
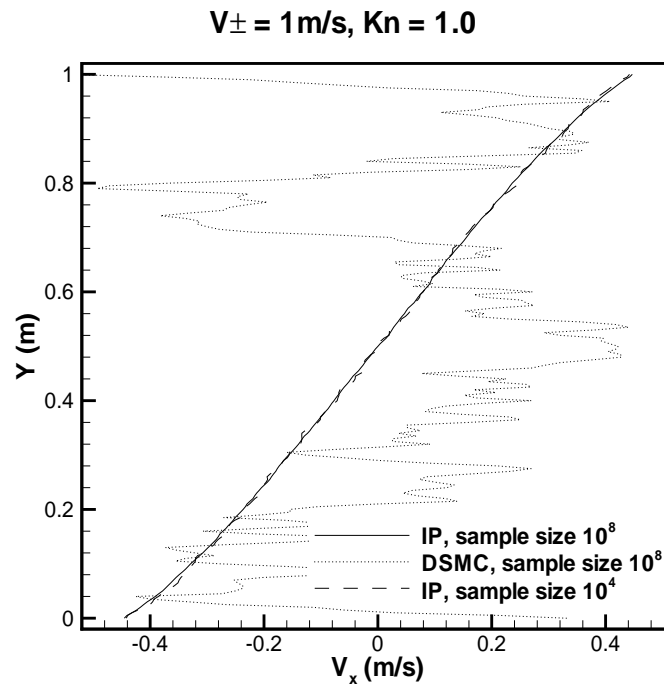
V± = 1m/s, Kn = 1.0

Figure 3.15. DSMC method is impossible to predict Couette flows having $V_\pm = \pm1.0$m/s and Kn = 1.0, whereas IP method is helpful

3.6.3 Advantages of the IP Method

The main advantage of the IP method comes from the small statistical scatter for simulating low-speed rarefied gas flows when compared to the DSMC method. The IP method provides a promising tool for simulating micro-scale gas flows where continuum approaches are generally invalid and the DSMC method is extremely numerically expensive.

Another advantage of the IP method is that the macroscopic values of the flow field are available at any time because the cell information is sampled for each time step. Hence, complicated boundary conditions, including the characteristic line boundary condition, can be applied in the IP method, especially for subsonic flows where the far field boundary condition can not be easily implemented by the DSMC method. Any IP simulation contains the DSMC results; therefore the DSMC method can use the IP result to implement effective boundary conditions, which improves the effectiveness of the DSMC method.

One more advantage of the IP method is that it can easily exhibit the development of a flow, which means it is quite easy to determine whether a simulation has reached a steady state or not. Such an example is illustrated in Figure 3.16 that displays the pressure history at several locations along a flat plate having thickness ratio of 5% and is placed at a 10-deg angle of attack in an otherwise uniform air stream. A similar DSMC simulation, however, has a pressure scatter of the same order of magnitude as the mean value, so that it is difficult to determine whether a flow reaches the steady state.

3.6.4 Disadvantages of the IP Method

The IP method, on the other hand, has several disadvantages compared to the DSMC method. However, the IP method can be further developed in the near future, so that these associated disadvantages may disappear.

The IP method is a relatively new method. The principle of the method merits further study and more physically accurate models may be developed. Another disadvantage of the IP method is that it has stability difficulties in some instances. The stability problem arises because the random movement of particles can cause instabilities for the preserved cell information. However, using smaller time steps or more simulated particles can solve this problem.
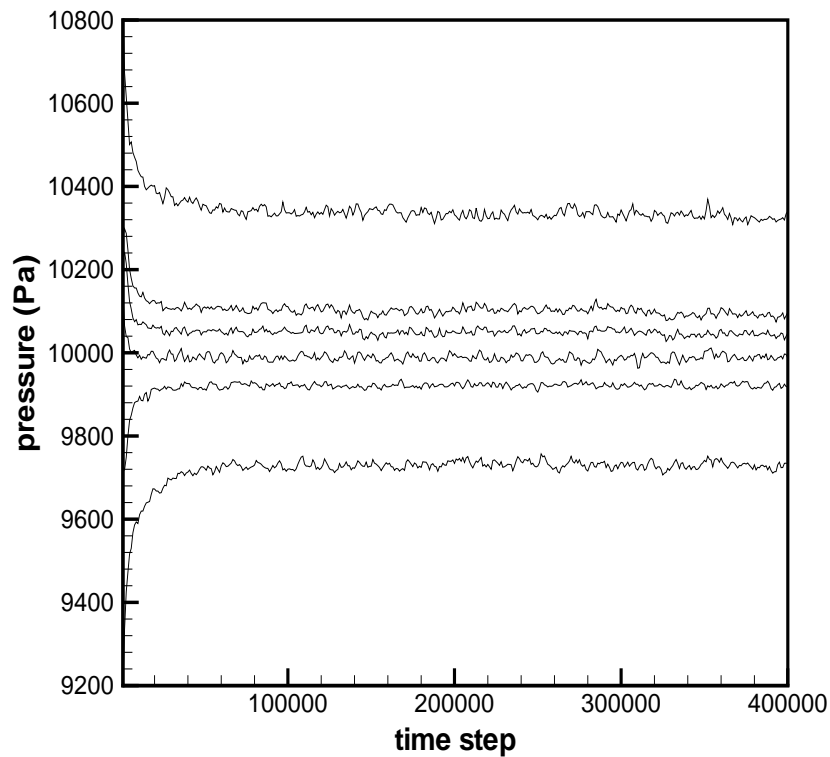
Figure. 3.16. Pressure history at several locations along a flat plate having thickness ratio of 5% under a flow with a 10-deg angle of attack

3.7 Conclusions

In this chapter, the information preservation (IP) method is developed for simulating general low-speed rarefied gas flows. The method updates and samples macroscopic information that is preserved in simulated particles whose microscopic information is followed in the DSMC method. The principle of the IP method is explained and models are introduced in describing the preserved information. It is shown that the IP method exhibits small statistical scatter for low-speed flows and has significant advantages compared to the DSMC method. The validity of the method will be examined in the next chapter.

CHAPTER IV
VALIDATION OF THE INFORMATION PRESERVATION METHOD

In the previous chapter, the information preservation (IP) method exhibited its ability to reduce the statistical scatter associated with particle methods when simulating gas flows. In this chapter, the validity of the IP method is investigated for simulating micro-scale gas flows.

A general approach for validating a new method is to apply the method to several benchmark problems and compare its results with existing experimental data or results obtained by previously validated methods. Unfortunately, there are few experimental data or simulation results in the literature for micro-scale gas flows. Hence, we have to consider rarefied gas flows for which the direct simulation Monte Carlo (DSMC) method can be applied with reasonable computational cost. The IP method is then evaluated by comparing the results from the IP method and those from the DSMC method for the selected test flows. Such test examples, however, will not adversely affect the evaluation of the IP method for simulating micro-scale gas flows because the selected rarefied gas flows and general micro-scale gas flows have similar underlying physics.

In this chapter, four different flow problems are chosen to assess the IP scheme. In the first example, heat transfer between two plates at different temperatures (thermal Couette flow), the IP method is examined for its ability to simulate flows having a large temperature variation. In the second example, the IP method simulates a high-speed Couette flow. The balance between the energy dissipation and the thermal conductivity of the flow is investigated at different Knudsen numbers. In the third example, a general Rayleigh problem is studied, which reveals a limitation of the IP method for simulating

unsteady flows. In the final example, flow over a NACA0012 airfoil, the IP method

shows an application for simulating general two-dimensional problems. At the end of this

chapter, a brief conclusion is given about the validity of the IP method for simulating

micro-scale gas flows.

4.1 Thermal Couette Flows

It is important to investigate the ability of the present IP scheme to simulate flows

having temperature variations because previous studies have shown that the IP method is

capable of simulating isothermal flows. One such flow is a heat transfer flow between

two plates at different temperatures that is called thermal Couette flow in this thesis. This

flow is one of the most fundamental problems in rarefied gas dynamics. Studies by

Teagen and Springer (1968) and Ohwada (1996) have shown that the thermal Couette

flow cannot be solved by approximate approaches, including moment methods. The

DSMC method, however, predicts the same results as those obtained by solving the

Boltzmann equation using an accurate finite difference method (Kosuge et al., 2001).

plate 2: α_2, $T_2 = 373K$, $V_{x,2} = 0$

$y = 1$ m

y

argon gas

x

$y = 0$ m

plate 1: α_1, $T_1 = 173K$, $V_{x,1} = 0$

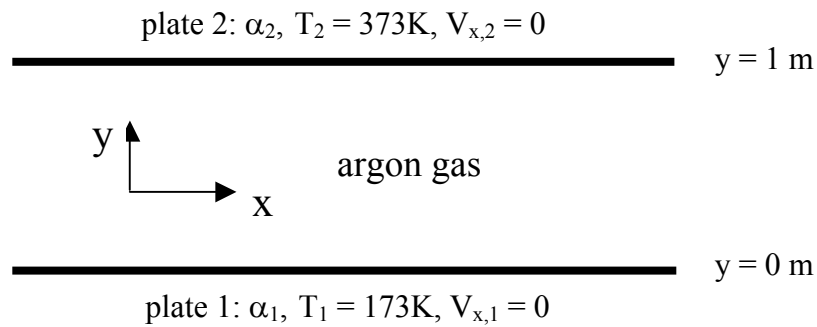**Figure 4.1. Schematic diagram for thermal Couette flows**

A schematic diagram of the thermal Couette flow is illustrated in Figure 4.1. The

two plates at rest are 1m apart, with one at 173K and the other at 373K. Between the two

plates is an argon gas whose density is selected such that the Knudsen number (Kn) of the

flows at 273K ranges from 0.01 to 100. The computational domain between the two

plates is divided into 200 computational cells with a cell spacing of less than one mean free path of the gas for all simulated cases. The time step is 2.5×10^{-6} second, which is much less than the mean collision time for all cases. Therefore, the cell spacing and the time step satisfy the requirements for a DSMC simulation. With the previous physical and numerical specification, a DSMC simulation needs a sample size of about 100,000 particles per cell to obtain a meaningful result, whereas an IP simulation only requires a sample size of 1,000 particles per cell for the case with Kn=0.01 and a sample size of at most 10,000 particles per cell for the case with Kn=100. However, for the results given in this section, a much larger sample size of 20,000,000 particles per cell is used after the simulations run for 100,000 time steps to ensure that the steady state is reached for both methods. This large sample size is used because it is better to obtain smoother results to validate the IP method and because a single simulation code is used for which both results are obtained at the same time.

The temperature profiles obtained from the IP and DSMC methods are illustrated in Figure 4.2 for flows having different Knudsen numbers when the thermal accommodation coefficient for both plates is 1.0. Excellent agreement is obtained between the IP and DSMC results for Knudsen numbers of 0.01, 0.1, 1.0 and 100. When the Knudsen number is 10, a small difference between the two results is observed. This difference is relatively small, however, for such a strongly non-equilibrium flow. The results illustrated in Figure 4.2 also show that the temperature jump at both gas-plate surfaces increases as the Knudsen number of the flow increases. This results in a decreasing gradient of the gas temperature with increasing Knudsen number.

The heat fluxes obtained from both methods are illustrated in Figure 4.3. Again, very good agreement between the two methods is obtained. These results show that the heat flux decreases when the Knudsen number increases (the sign of the heat flux indicates the flux direction). However, if the heat flux (q) is nondimensionalized as shown in Equation 4.1, and is normalized by the heat flux (Equation 4.2) obtained from

**Figure 4.2. DSMC method and IP method predict similar temperature profiles
for the thermal Couette flows at different Knudsen numbers
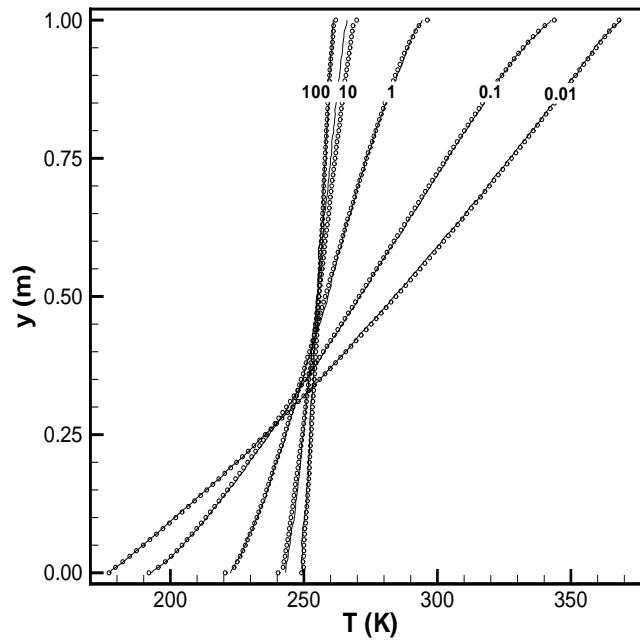(Kn = 0.01, 0.1, 1, 10, 100 as labeled in the plot; circle: IP, line: DSMC)**
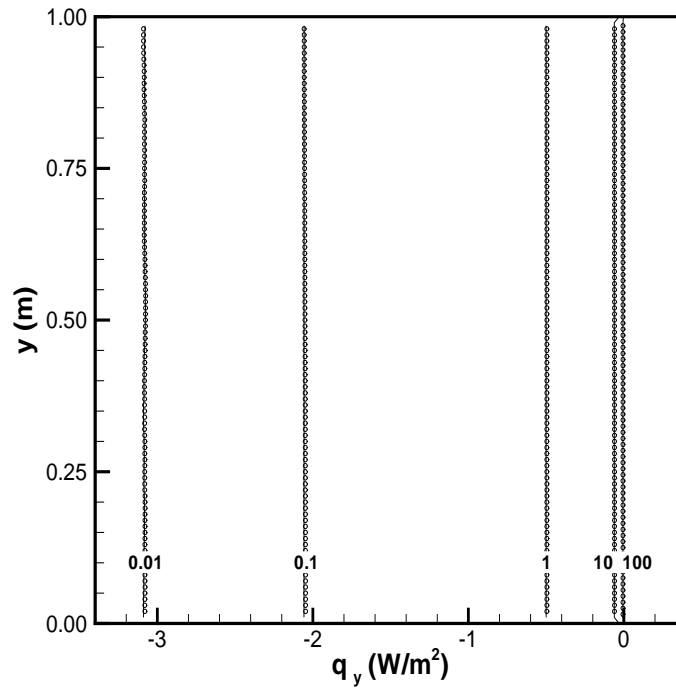

**Figure 4.3. DSMC method and IP method predict similar heat flux profiles
for the thermal Couette flows at different Knudsen numbers
(Kn = 0.01, 0.1, 1, 10, 100 as labeled in the plot; circle: IP, line: DSMC)**

free-molecular theory (Gombosi, 1994), the normalized heat flux Q/Q_{FM} exhibits a different behavior: the heat transfer increases when the Knudsen number of the flow increases as shown in Figure 4.4.

$$Q = \frac{q}{\sqrt{2} \cdot \rho_0 (RT_0)^{3/2}}, \qquad (4.1)$$

$$Q_{FM} = \frac{-2}{\sqrt{\pi}} \cdot \frac{\sqrt{T_1 T_2} \left(\sqrt{T_2} - \sqrt{T_1} \right)}{T_0^{3/2}} \qquad (4.2)$$

where ρ_0 is the average density of the flow, and $T_0 = (T_1 + T_2)/2$ is the average temperature of the two plates.
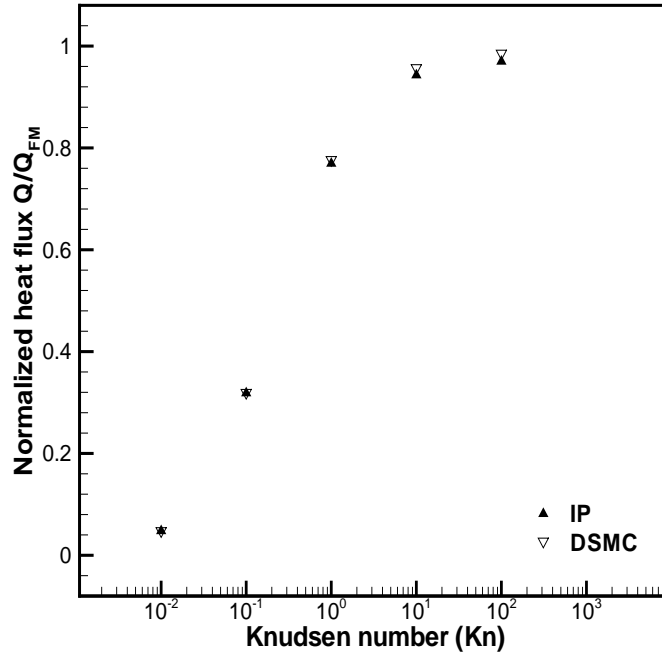
Figure 4.4. Normalized heat flux as a function of the Knudsen number for the thermal Couette flows

The IP method is also examined for its ability to deal with different wall conditions. For this purpose, two flow conditions are considered with Knudsen numbers of 0.01 and 1.0. For a Knudsen number of 0.01, the thermal accommodation coefficient for both plates is set to 1.0, 0.8, 0.6, 0.4, and 0.2 in turn. When the Knudsen number is 1.0, several combinations of values for the thermal accommodation coefficient of the

plates are used to further investigate the effects of the wall condition. As shown in Figures 4.5 and 4.6, the agreement between the IP results and the DSMC results is very good. The figures also show that the thermal accommodation coefficient plays an important role for both methods. A small coefficient generally results in a large temperature jump and a small temperature gradient because few gas molecules accommodate to the plate condition. Therefore, the effects of the thermal accommodation coefficient must be considered when modeling micro-scale gas flows as experiments, e.g., Arkilic (1997), have shown that the thermal accommodation coefficient is around 0.8 for some gases in contact with a prime silicon crystal.
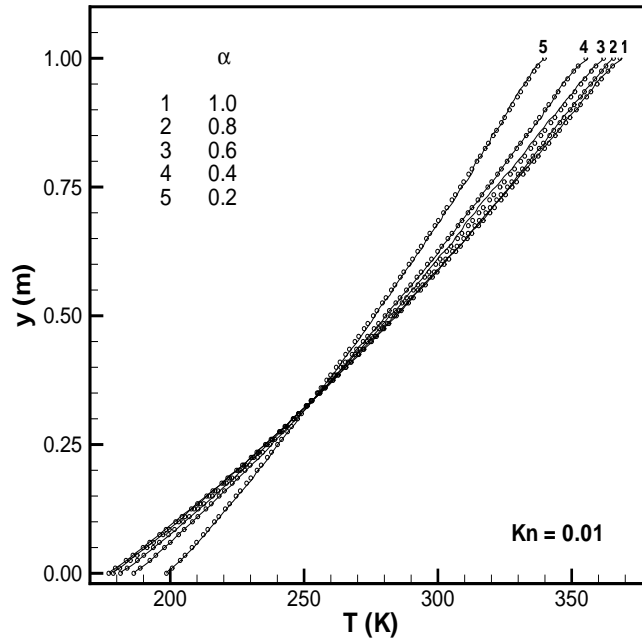

Figure 4.5. DSMC method and IP method predict similar temperature profiles for the thermal Couette flows under different wall conditions when Kn=0.01 (α = 1.0, 0.8, 0.6, 0.4, 0.2 for both plates; circle: IP, line: DSMC)
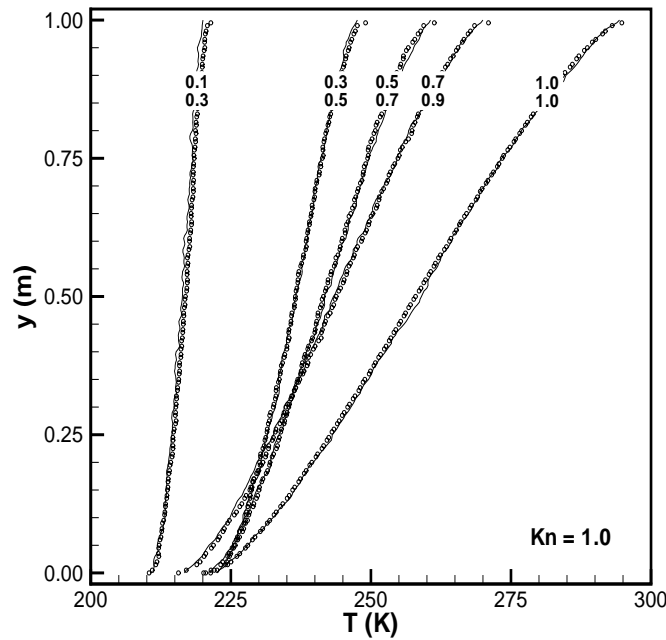
**Figure 4.6. DSMC method and IP method predict similar temperature profiles
for the thermal Couette flows under different wall conditions when Kn=1.0
(α_1 = 1.0, 0.9, 0.7, 0.5, 0.3 for the plate at y = 0m, and α_2 = 1.0, 0.7, 0.5, 0.3, 0.1
for the plate at y = 1m; circle: IP, line: DSMC)**

4.2 High-Speed Couette Flows

The previous example has shown that the IP method is able to simulate rarefied
heat transfer flows. In this section, the IP method is applied to flows where both the
viscosity and the thermal conductivity are important. A good example for this kind of
flow is a high-speed Couette flow. In such a flow, the energy dissipation of the flow
causes the gas temperature to have a significant increase, which requires the thermal
conductivity and the energy dissipation to be balanced in order to reach a steady state
condition.

The schematic diagram of the Couette flows is illustrated in Figure 4.7. The two
parallel plates are 1m apart with one at rest and the other moving with a velocity of
300m/s. The temperature of both plates is 273K, and the gas between the two plates is
argon. A similar case (Kn=0.00925) can be found in Bird (1994) where a detailed

analysis is provided. In the current simulation, the IP method is examined for simulating

Couette flows ranging from the near-continuum regime to the free-molecular regime,

with the same numerical specifications as in the previous example.

plate 2: $\alpha_2 = 1.0$, $T_2 = 273K$, $V_{x,2} = 300m/s$

y = 1 m

y

argon gas

x

y = 0 m

plate 1: $\alpha_1 = 1.0$, $T_1 = 273K$, $V_{x,1} = 0$
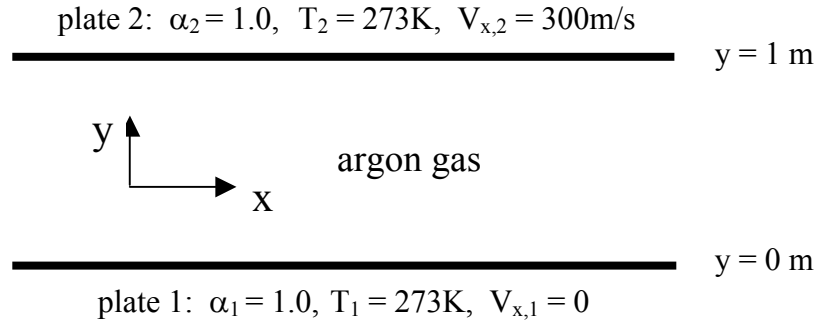
Figure 4.7. Schematic diagram for the high-speed Couette flows

The velocity profiles obtained from the IP and DSMC methods are shown in

Figure 4.8 for flows having different Knudsen numbers. Clearly, the agreement between

the IP results and the DSMC results is excellent. Figure 4.8 also shows the velocity

distribution is anti-symmetric, and that the slip velocity on both surfaces increases when
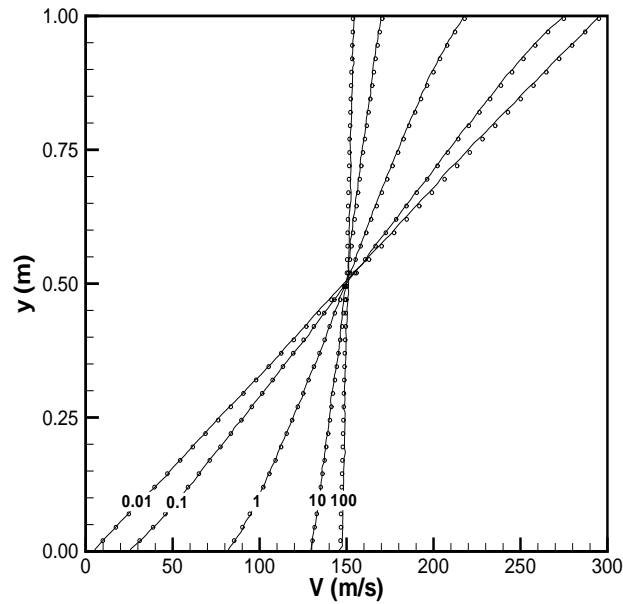
**Figure 4.8. DSMC method and IP method predict similar velocity profiles
for the Couette flows at different Knudsen numbers
(Kn = 0.01, 0.1, 1, 10, 100 as labeled in the plot; circle: IP, line: DSMC)**

the Knudsen number of the flow increases. The temperature profiles of the flows are illustrated in Figure 4.9. Again, the agreement between the IP and DSMC results is very good except that the DSMC results exhibit some statistical scatter. It is found that the gas temperature increases when the Knudsen number of the flow increases because the energy dissipation increases.

Figure 4.9. DSMC method and IP method predict similar temperature profiles for the Couette flows at different Knudsen numbers (Kn = 0.01, 0.1, 1, 10, 100 as labeled in the plot; circle: IP, line: DSMC)

The shear stress distributions between the plates for the condition of Figure 4.9 are plotted in Figure 4.10. Good agreement is obtained between the results obtained from the IP and DSMC methods although there is a small difference of 2% between the IP results and the DSMC results. However, this difference is not surprising, because the constant C_μ in the IP collision model is determined when the IP shear stress obtained from a Couette flow having Kn=0.01 agrees with the value evaluated from the continuum theory. A similar difference is also found by Bird (1994): the shear stress ($0.00624 Nm^{-2}$) obtained using the DSMC method for the case with Kn= 0.00925 is a little smaller than the expected value ($0.00639 Nm^{-2}$) evaluated from the continuum theory. This difference

occurs because the continuum theory cannot exactly describe a flow having Kn=0.01 because a slip velocity about 3.1m/s is observed for this flow condition. Thus, the IP method may use the DSMC result to adjust the value of the constant C_μ; however, such an adjustment is not necessary for practical applications because this difference is negligible.
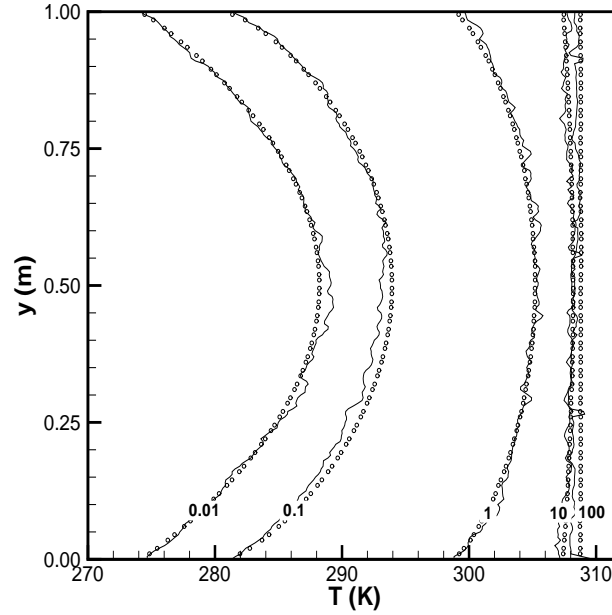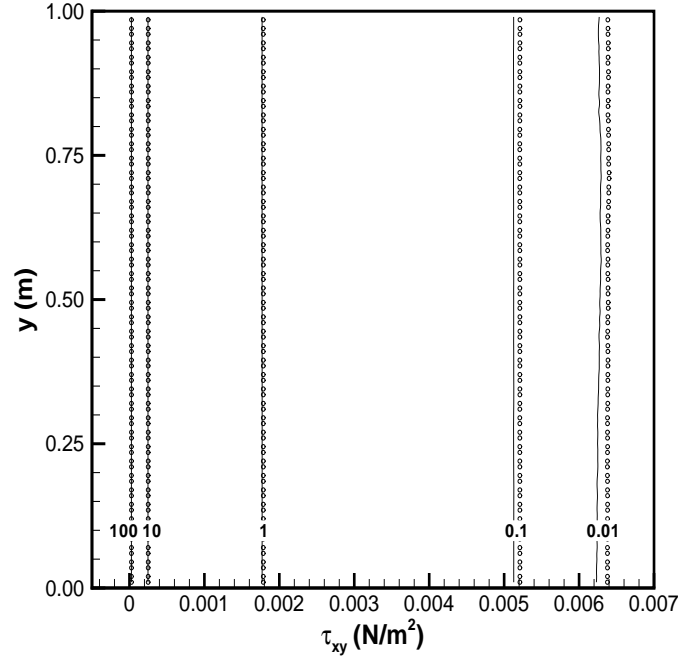

**Figure 4.10. DSMC method and IP method predict similar shear stress profile
for the Couette flows at different Knudsen numbers
(Kn = 0.01, 0.1, 1, 10, 100 as labeled in the plot; circle: IP, line: DSMC)**

4.3 Rayleigh Flows

The previous two examples show that the IP method can simulate steady gas flows across a wide range of Knudsen number. It is also interesting to assess the validity of the IP method for simulating unsteady flows. One typical unsteady flow is a Rayleigh flow.

A Rayleigh flow is an unsteady flow in which a plate below a gas at rest suddenly acquires a constant parallel velocity and a constant temperature. In Figure 4.11, the argon

gas is at rest at time t=0 with a temperature of 273K. When t>0, the plate moves with a constant velocity of 10m/s and has a constant temperature of 373K. The plate will then continue to heat the gas and will also transfer its momentum to the gas. Therefore, the gas starts to move and the flow becomes unsteady.

Outer boundary

- -

y

x

argon gas, T= 273 K, $V_x = 0$

y = 0 m

plate 1: $\alpha = 1.0$, $T_1 = 373K$, $V_x = 10m/s$

Figure 4.11. Schematic diagram for Rayleigh flows

There is an analytical solution (Bird, 1976) to the Rayleigh flow problem for times much less than the mean collision time τ_0 ($\tau_0 = \lambda/v_m$, where v_m is the mean molecular speed having a value of $v_m = \sqrt{8RT/\pi}$):

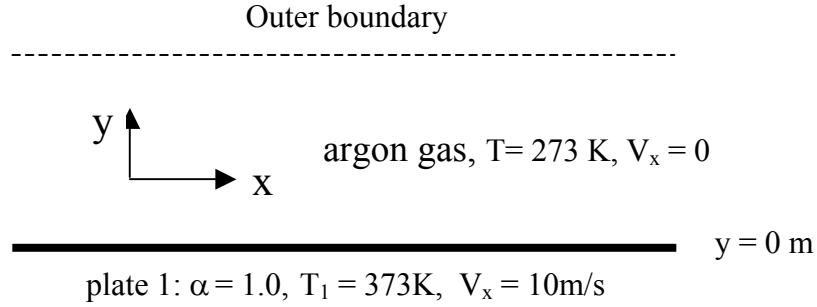$$\frac{n}{n_\infty} = \frac{1}{2}\left[\left\{1+erf\left(\frac{\beta_\infty y}{t}\right)\right\}+\left(\frac{T_\infty}{T_w}\right)^{\frac{1}{2}}erfc\left(\frac{\beta_w y}{t}\right)\right] \qquad (4.3)$$

$$V_x = \frac{1}{2}V_{x,w}\left(\frac{T_\infty}{T_w}\right)^{\frac{1}{2}}erfc\left(\frac{\beta_w y}{t}\right)\bigg/\left(\frac{n}{n_\infty}\right) \qquad (4.4)$$

$$V_y = \frac{1}{2\pi^{\frac{1}{2}}\beta_\infty}\left\{\exp\left(-\frac{\beta_w^2 y^2}{t^2}\right)-\exp\left(-\frac{\beta_\infty^2 y^2}{t^2}\right)\right\}\bigg/\left(\frac{n}{n_\infty}\right) \qquad (4.5)$$

$$T = T_\infty\left[1+\frac{1}{2}erfc\left(\frac{\beta_w y}{t}\right)\left(\frac{T_\infty}{T_w}\right)^{\frac{1}{2}}\left(\frac{T_w}{T_\infty}-1\right)\bigg/\left(\frac{n}{n_\infty}\right)\right]+\frac{y}{t}\frac{V_y}{3R}+\frac{V_{x,w}\cdot V_x}{3R}-\frac{1}{3R}\left(V_x^2+V_y^2\right) \;(4.6)$$

where $\beta = (2RT)^{\frac{1}{2}}$, $\beta_w = (2RT_w)^{\frac{1}{2}}$, $erf(\ )$ and $erfc(\ )$ are the error and the complementary error functions, respectively.

The previous equations, however, can only describe flows when the molecular collisions can be neglected. Thus, a numerical method is required to simulate the flow

when the time is larger than the mean collision time. For the current numerical

simulations, the initial density of the argon gas is varied so that the unsteady flow is

limited in the current computational domain for a specific time. The computational

domain as shown in Figure 4.11 is divided into 200 computational cells. The cell spacing

is generally less than one mean free path of the gas, and otherwise the sub-cell technique

(Bird, 1994) is used. The time step is 7.0×10^{-7} second that is much less than the mean

collision time for all cases. A total sample size of 5,000,000 particles per cell is used in

order to obtain a meaningful DSMC result for all the cases.

The simulated results at $t=0.01 \tau_0$ are illustrated in Figure 4.12 for the IP and

DSMC methods along with the analytical solution. Clearly, the DSMC results agree well

with the analytic solution, whereas the IP method fails to predict the correct results

except for the parallel velocity distribution. This is because all particles in the IP

implementation carry the same energy when they reflect from the plate. However, when

molecules leave the plate, those molecules having larger thermal velocities carry more
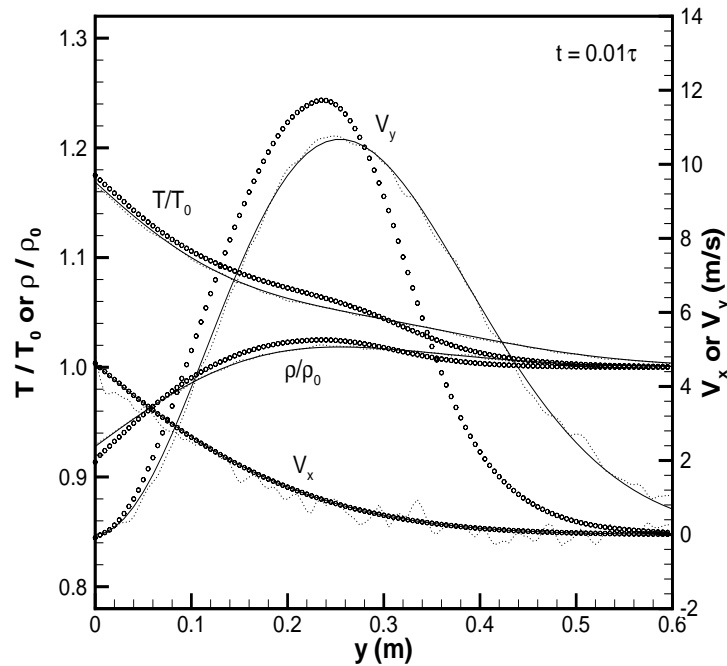
Figure 4.12. Profiles for the Rayleigh flow at t=0.01 τ_0 with λ_0=26.6m
(circle: IP, dot line: DSMC, solid line: collisionless flow theory)

energy; as a result, the energy transferred from the plate can be carried farther into the gas. Therefore, for the region far from the plate (y>0.3m), the temperature predicted by the IP method is smaller than the analytic result, whereas it is larger than the analytical result for the near plate region (y<0.3m). The density profile and normal velocity profile are affected by the wrong temperature profile in the IP method, whereas the parallel velocity profile is correct because the IP implementation only affects the energy transport.

The previous situation is improved as time increases, see Figures 4.13-4.16. When the time t=10τ_0, the particles undergo 10 collisions on average. Thus the effect of random movements of the particles reflected from the plate is decreased due to collisions. Thus, the implementation of the IP method tends to be correct when there are enough collisions. Figure 4.16 shows that the agreement between the IP results and the DSMC results is very good when the time t=100τ_0. Therefore, the energy flux model in the IP method works fine for this flow when the time is not too small.
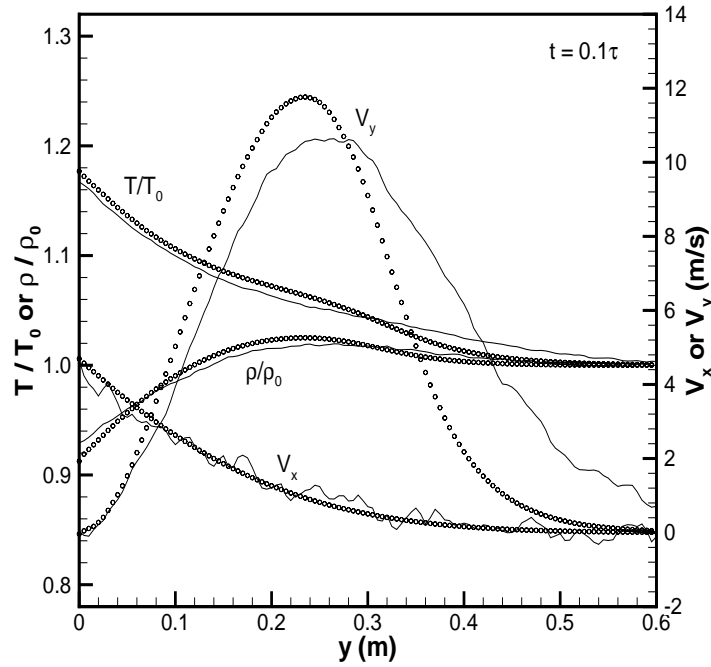
Figure 4.13. Profiles for the Rayleigh flow at t=0.1τ_0 with λ_0=2.26m (circle: IP, line: DSMC)
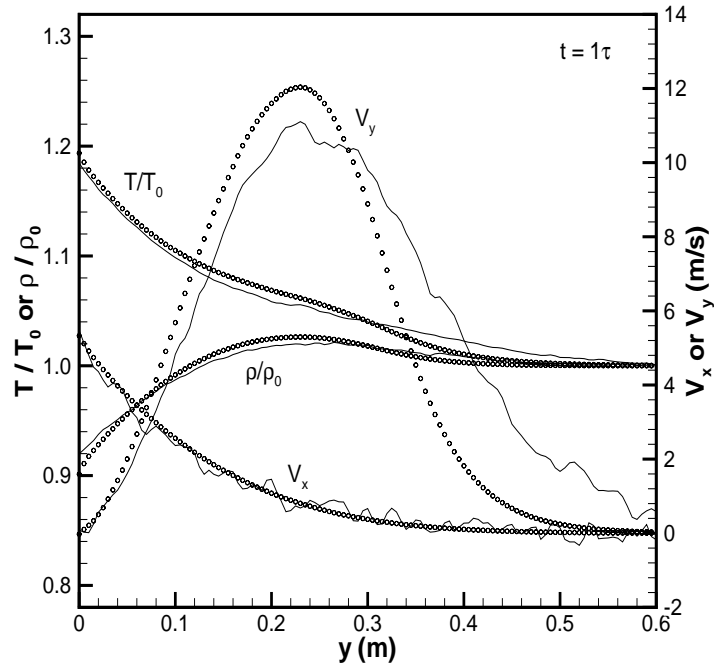
Figure 4.14. Profiles for the Rayleigh flow at t=1 τ_0 with λ_0=0.226m (circle: IP, line: DSMC)
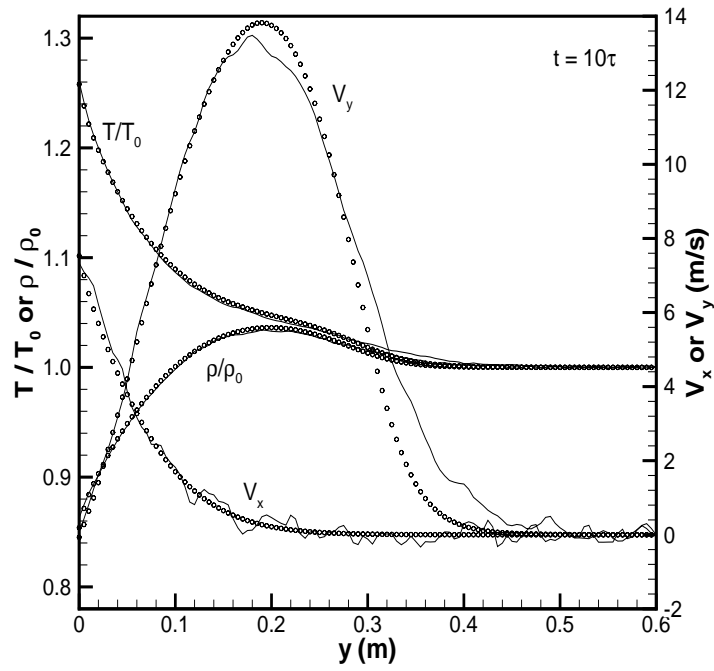
Figure 4.15. Profiles for the Rayleigh flow at t=10 τ_0 with λ_0=0.0226m (circle: IP, line: DSMC)
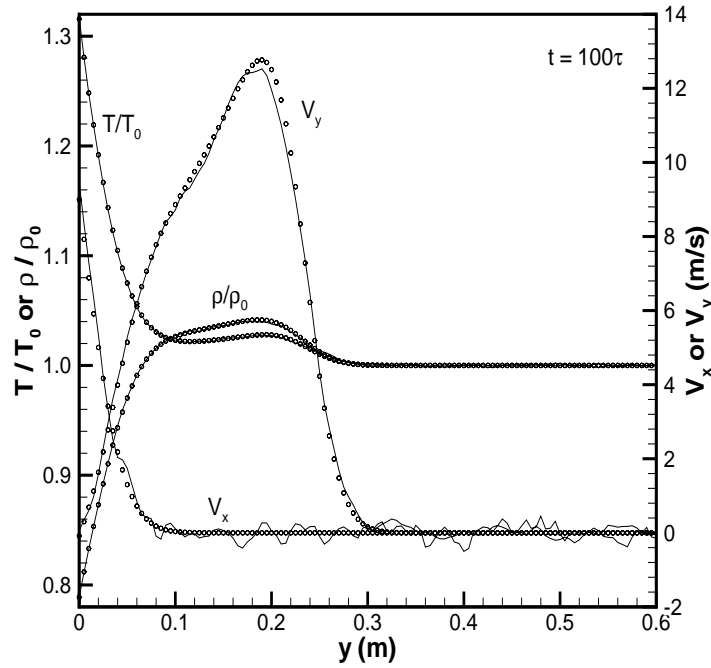
Figure 4.16. Profiles for the Rayleigh flow at t=100τ_0 with λ_0=0.00226m (circle: IP, line: DSMC)

4.4 Flow Over a NACA0012 Airfoil

One-dimensional flows are selected as test examples because of their well defined properties. However, the IP method is not limited to 1D flows. In this section, an air flow around a NACA0012 airfoil having a chord length of 0.04m is considered. The detailed flow condition is summarized in Table 4-1, where Re_∞ and Kn_∞ are based on the chord length. Again, the selected flow velocity is not very small so that reasonable DSMC results can be obtained. Some experimental data and a Navier-Stokes solution of the flow for these conditions can be found in Fan et al. (2001).

Table 4-1 Free stream conditions for flow over a NACA0012 airfoil

Ma_∞	Re_∞	Kn_∞	L_{chord} (m)	ρ_∞ (kg/m^3)	U_∞ (m/s)	T_∞ (K)	T_w (K)
0.8	73	0.014	0.04	1.116×10^{-4}	257	257	290

The computational domain is illustrated in Figure 4.17, which exploits the symmetry of the problem. The whole domain is divided into 9,120 non-uniform structured cells that are clustered near the airfoil. On average, about 50 particles are located in each cell. Free-stream flow conditions are applied at all the boundaries except for the symmetric line of the airfoil and the downstream boundary where a gradient boundary condition is adopted, because the computational domain is much larger than the airfoil. The time step is set to 5×10^{-8}s, which is smaller than the mean collision time of the particles. In order to reach the steady state, 30,000 iterations are executed before sampling the flow field.
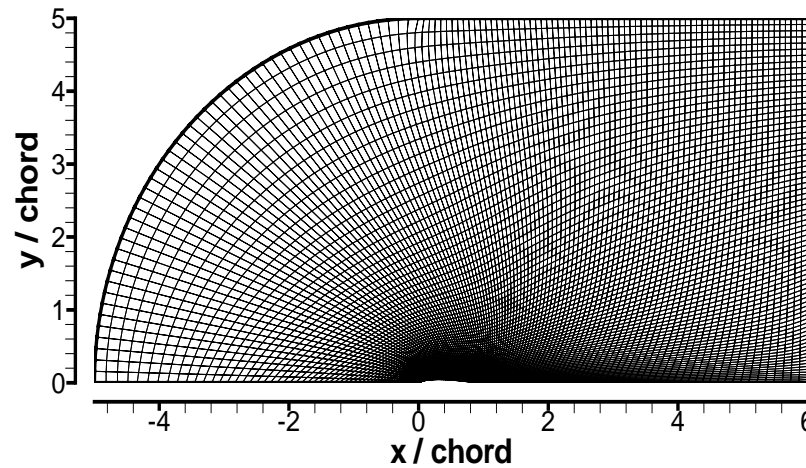
Figure 4.17. Computational grids for flow over a NACA0012 airfoil

The density contours, non-dimensionalized by the free stream density, are illustrated in Figures 4.18 and 4.19 for the DSMC and IP methods, respectively. The total sample size used for the DSMC and IP results is about 450,000 particles per cell. However, the contours in the DSMC results are still not smooth due to statistical scatter. The simulated density distributions exhibit the same basic features for both methods and the agreement between the density fields around the airfoil for the two methods is excellent.
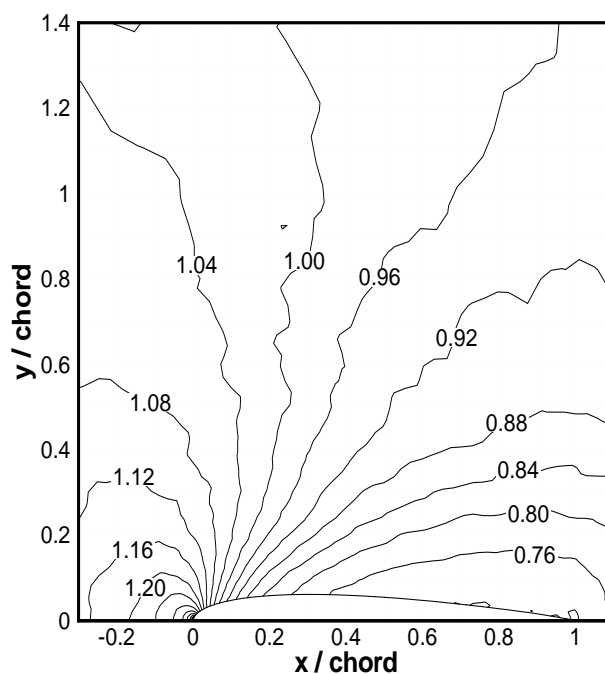
**Figure 4.18. Density flow field (ρ/ρ_∞) obtained using the DSMC method
for flow over a NACA0012 airfoil**
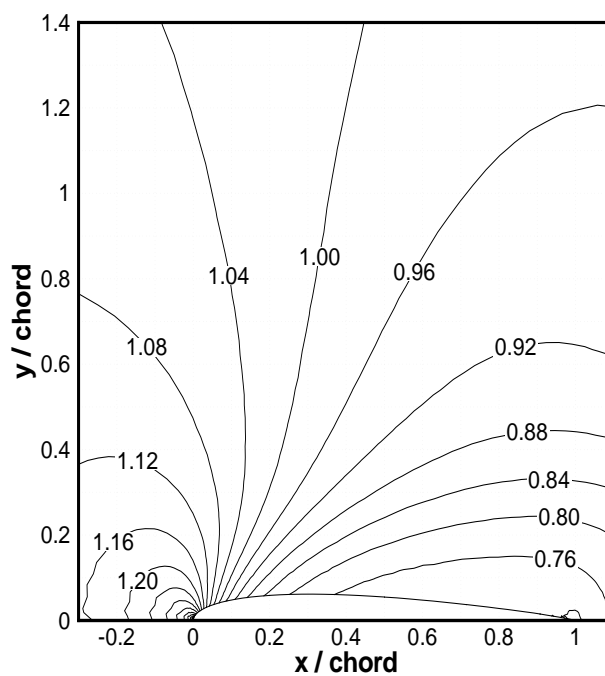
**Figure 4.19. Density flow field (ρ/ρ_∞) obtained using the IP method
for flow over a NACA0012 airfoil**

It is also important to examine the surface properties of the airfoil obtained using the DSMC and IP methods. Figure 4.20 shows the slip velocity distributions obtained using both methods. Here, the slip velocity is the flow velocity of the air attached to the wall. Figures 4.21 and 4.22 show the pressure distributions and the shear stress distributions on the airfoil surface obtained using the two methods. Once again, very good agreement is obtained between the results using the IP and DSMC methods for the results illustrated on these plots.

It would be very interesting to compare the temperature profiles from the DSMC and IP methods to check the validity of the energy transfer model in the IP method for this flow with large bulk velocity. However, a huge sample size is needed to obtain a smooth temperature profile for the DSMC method. Although a comparison of the temperature is not available for this problem, the good agreement of other properties computed by the IP and DSMC methods suggests that the energy transfer model can be accepted for flows having a large bulk velocity.
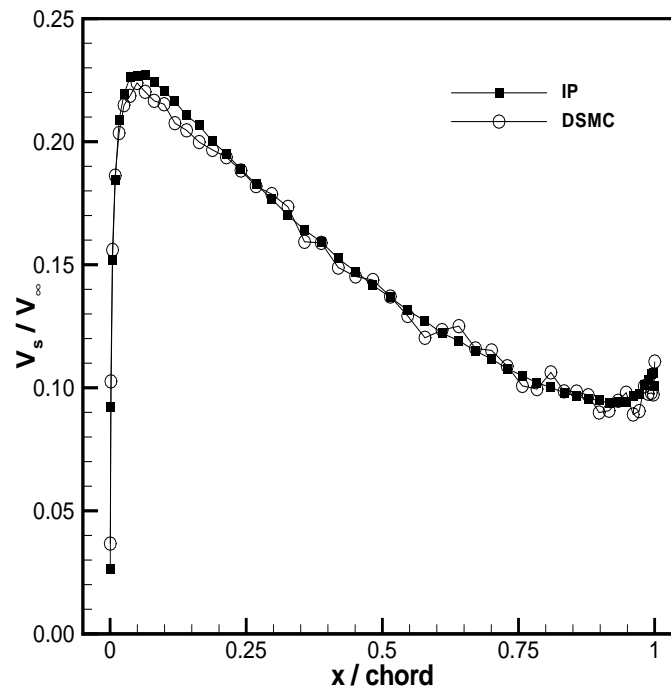
**Figure 4.20. DSMC method and IP method predict similar
slip velocity distributions for flow over a NACA0012 airfoil**
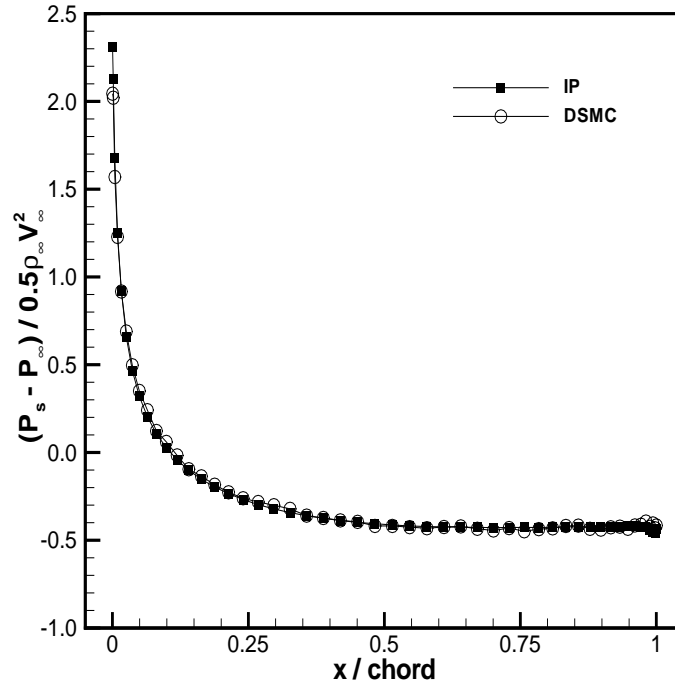
Figure 4.21. DSMC method and IP method predict similar surface pressure distributions for flow over a NACA0012 airfoil
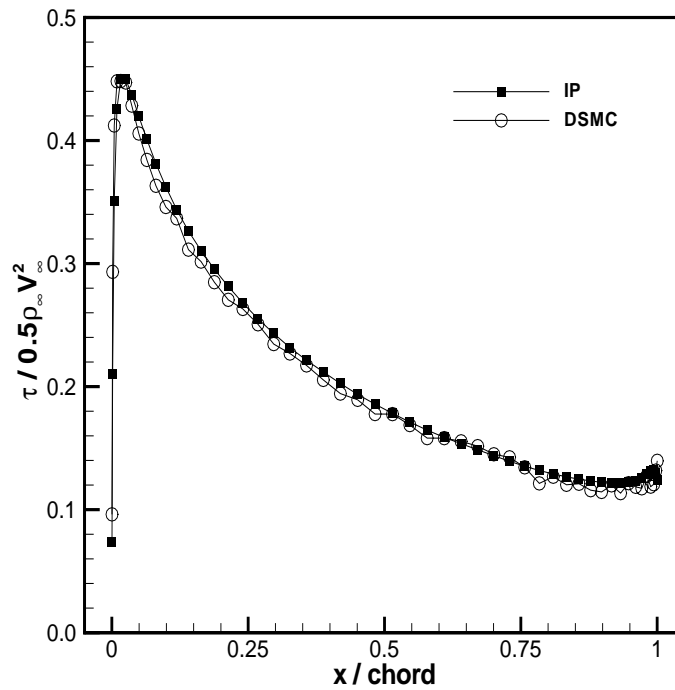
Figure 4.22. DSMC method and IP method predict similar shear stress distributions for flow over a NACA0012 airfoil

4.5 Conclusions

The IP method was proposed to simulate micro-scale gas flows. Being a particle method, the IP method cannot be rigorously proved mathematically. The validity of the method was tested and verified using several typical rarefied gas flows.

The thermal Couette flows showed that the IP method was able to predict the thermal conductivity of the flow and give the correct temperature distribution for a wide flow regime and with different wall conditions. The Couette flows showed the ability of the IP method to simulate flows where both thermal conductivity and viscosity are important. The example of a transonic gas flow over a NACA0012 airfoil also showed that the IP method performed well for general 2D steady flows. The Rayleigh flows, however, showed that the proposed IP implementation was good for unsteady flows only when each particle underwent enough collisions, which means that the IP method is also good for low frequency unsteady flows. Hence, it is concluded that the IP method can be applied to general steady flows and to low frequency unsteady flows.

Specifically, the current implementation of the IP method is suitable to simulate general micro-scale gas flows for several reasons. First, micro-scale gas flows exhibit rarefied phenomena that require a kinetic scheme. Second, the low gas-speed in micro-scale gas flows means the approximation made in the evaluation of the additional energy is acceptable. Third, few micro-scale gas flows are reported for a time less than several mean collision times, which means that it is not necessary for the IP method to preserve all detailed information about microscopic molecules. Therefore, the current implementation of the IP method can simulate micro-scale gas flows with high accuracy.

CHAPTER V

DEVELOPMENT OF A HYBRID CONTINUUM/PARTICLE APPROACH FOR MODELING MICRO-SCALE GAS FLOWS

Micro-scale gas flows are usually subsonic; therefore, there are regions of these flows where the continuum equations are valid. In particular, simulating an external flow involves a computational domain that is much larger than the micro-scale system itself; then most of the computational domain can be described by the continuum equations. Therefore, it is desired to use continuum approaches to simulate the flow in regions where continuum equations are valid, and to adopt kinetic approaches for other regions, because continuum solvers are much more numerically efficient than kinetic approaches (including the information preservation (IP) method). Hence, an effective approach for simulating micro-scale gas flows is a hybrid approach by combining the physical accuracy of a kinetic method and the numerical efficiency of a continuum solver.

Obviously, the IP method is a good choice as the kinetic method for a hybrid approach because the IP method exhibits small statistical scatter and has the macroscopic information available at any time, which can avoid many difficulties encountered when the DSMC method is used. The continuum method in a hybrid approach can be an algorithm that solves the Euler equations, the Navier-Stokes equations, or the Burnett equations. However, the Euler equations are only valid for regions where the viscosity and the thermal conductivity of the flow can be neglected. The Burnett equations, on the other hand, are not easy to use and are relatively expensive to solve. Hence, an approach solving the Navier-Stokes equations is often used as the continuum solver in a hybrid code.

In this chapter, a hybrid approach is developed by coupling the IP method and the continuum solver that is described in Chapter II. Details about coupling the IP method and the Navier-Stokes solver are described in Section 5.1. The determination of the continuum/particle interface is presented in Section 5.2. An implementation of the hybrid approach is described in Section 5.3. Then the hybrid approach is validated in Section 5.4 with its numerical performance shown in Section 5.5. Finally, a brief conclusion about the development of the hybrid approach is presented in Section 5.6.

5.1 The Coupling Between the IP Method and the Navier-Stokes Solver

One key issue of a hybrid approach is how to pass information from one solver to the other. Generally, the particle solver (the IP method in the present hybrid approach) and the continuum solver are coupled with an interface that acts as a boundary for both solvers. Specifically, the particle solver needs the interface to generate particles based on information from the continuum solver, whereas the continuum solver needs fluxes through the interface that requires information from the particle solver.

For general hybrid approaches, the boundary condition for the continuum solver is very difficult or expensive to obtain due to the large statistical scatter associated with the particle solver. However, the IP method preserves the macroscopic information in cells with very small statistical scatter. Comparison of the statistical scatter obtained using the IP method and the DSMC method is illustrated in Figure 5.1 by showing the density profile along a straight line from a low-speed gas flow over a flat plate. Therefore the continuum solver can directly use the macroscopic information preserved in the IP cells to evaluate the fluxes through the interface. Then the interface is totally internal to the continuum solver.

On the other side, the interface provides particles for the particle solver. In many hybrid approaches, the number of generated particles and their microscopic information
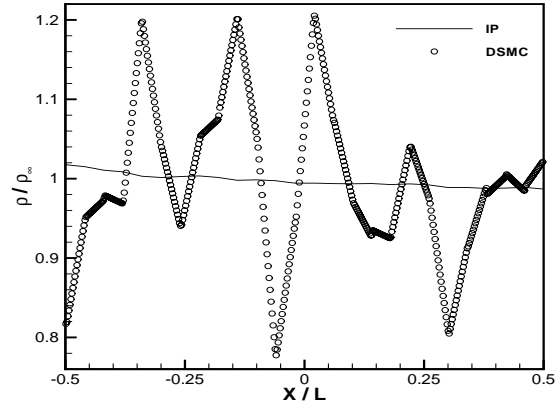
(a) A sample size of 20 particles per cell with 1 time step
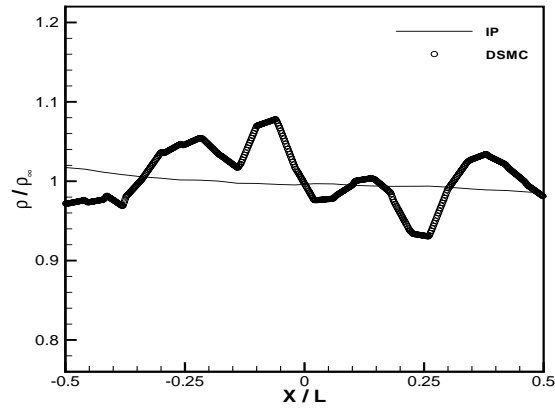
(b) A sample size of 20,000 particles per cell with 1,000 time steps
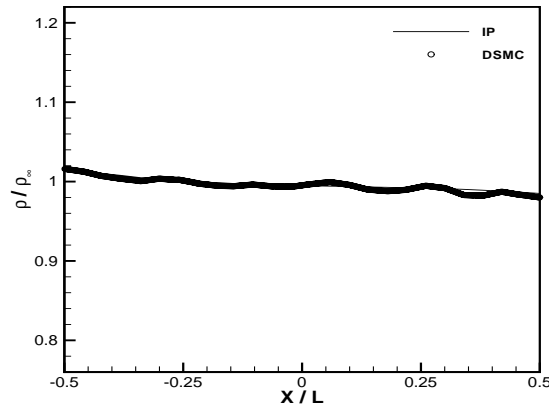
(c) A sample size of 20,000,000 particles per cell with 1,000,000 time steps

Figure 5.1. Density profiles obtained using the IP method and the DSMC method along a straight line from a low-speed gas flow over a flat plate

are determined from half fluxes based on the macroscopic properties at the interface. However, it is only valid for equilibrium flows to sample the velocity for particles from a Maxwellian distribution. In order to have a larger continuum domain, it was suggested by Hash and Hassan (1997) to sample the velocity of particles from a Chapman-Enskog distribution (Equations 5.1-5.4). Furthermore, ideas were reported by Garcia et al. (1999) for generating particles based on the macroscopic values on the interface and their gradients on the nearby continuum cells. In the present hybrid approach, two different strategies are used to generate particles through the interface from the continuum domain.

$$f(\mathbf{C}) = f_0(\mathbf{C})\Gamma(\mathbf{C}), \ \mathbf{C} = \mathbf{c}/(2kT/m)^{1/2} \tag{5.1}$$

$$f_0(\mathbf{C}) = \frac{1}{\pi^{3/2}} e^{-C^2} \tag{5.2}$$

$$\Gamma(\mathbf{C}) = 1 + \left(\mathbf{q}^* \cdot \mathbf{C}\right)\left(\tfrac{2}{5} C^2 - 1\right) - \mathbf{\tau}^* : (\mathbf{CC}) \tag{5.3}$$

$$\mathbf{q}^* = -\frac{\kappa}{p}\left(\frac{2m}{kT}\right)^{1/2} \nabla T, \ \tau_{ij}^* = \frac{\mu}{p}\left(\frac{\partial V_i}{\partial x_j} + \frac{\partial V_j}{\partial x_i} - \frac{2}{3}\frac{\partial V_k}{\partial x_k}\delta_{ij}\right) \tag{5.4}$$

In the first strategy, a condition similar to the Marshak condition (Hash and Hassan, 1996) is used: the full fluxes crossing the interface based on the local macroscopic values are set to be the sum of the counted half fluxes from the IP side and the half fluxes from the continuum side that are to be determined. Details of this condition are shown in Equations 5.5-5.7, where f is the full flux, e is the internal energy, and subscripts $_p$ and $_c$ represent the IP side and the continuum side, respectively.

These equations determine the number of generated particles and the macroscopic information for these particles, whereas the microscopic information for the particles is sampled from the Chapman-Enskog distribution based on the local macroscopic values (Garcia et al., 1998). Because particles cannot be generated as a fractional number, the number of generated particles is rounded to the nearest integer in the present implementation. The difference of the half fluxes due to this rounding process is stored

and is added to the next time step ensuring that the half fluxes from the continuum side are implemented correctly.

$$N_c + N_p = \frac{f_\rho \cdot A \cdot dt}{m} \tag{5.5}$$

$$N_c \mathbf{V}_c + \sum_{j=1}^{N_p} \mathbf{V}_{p,j} = \frac{(\mathbf{f}_{\rho v} - p\mathbf{n}) \cdot A \cdot dt}{m} \tag{5.6}$$

$$N_c (e + 0.5V^2)_c + \sum_{j=1}^{N_p} (e + 0.5V^2)_{p,j} = \frac{(f_{\rho(e+0.5V^2)} - p\mathbf{V} \cdot \mathbf{n}) \cdot A \cdot dt}{m} \tag{5.7}$$

This strategy has been tested for several flows. It turns out that the coupling process works well when the number of simulated particles in each cell is not too small (more than 50 for 1-D flows and more than 200 for 2-D flows). However, the code may crash when there are not enough particles in cells. This occurs because the macroscopic information of generated particles may have large fluctuations due to the rounding of the number and to the fluctuation of the number of particles leaving the particle domain. Therefore, this strategy should be reserved for flows when it is possible to use a large number of particles.

A second strategy is then developed to avoid directly generating particles on the interface. Near the interface, buffer and reservoir cells are used in the continuum domain as illustrated in Figure 5.2. These buffer and reservoir cells are also treated as particle cells except that the macroscopic information about the cells is provided by the continuum solver. Hence, the interface becomes the internal cell edge for the IP treatment. Specifically, the reservoir cells are used to generate particles that can enter the IP domain, which avoids directly generating particles on the interface. The buffer cells, however, are used to improve the quality of the particles that enter the IP domain. The algorithm for this strategy is as follows:

1) In the initialization step, particles are generated for the buffer cells according to the Chapman-Enskog distribution based on the local macroscopic information.

NS cells   IP cells

reservoir   buffer
cells   cells
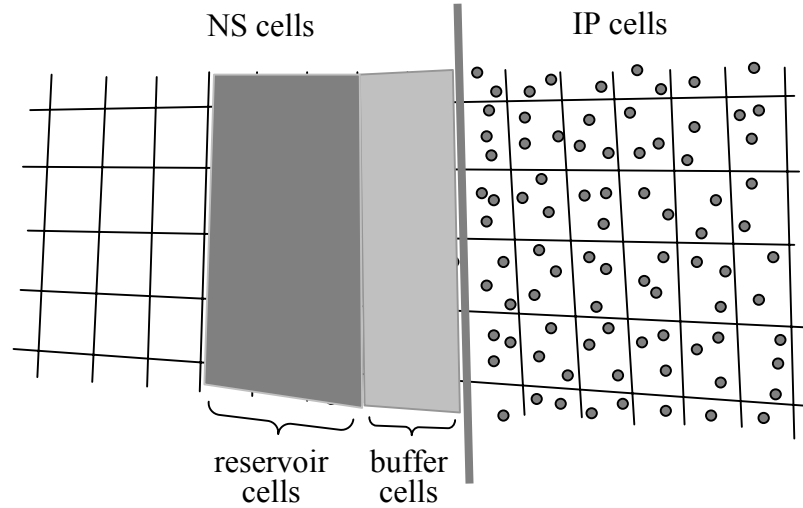
**Figure 5.2. Illustration of the interface and cell structures
for the hybrid continuum/particle approach**

2) During each time step, new particles are generated for the reservoir cells
according to the Chapman-Enskog distribution.

3) Particles in the buffer cells and reservoir cells are selected for collisions and
motion using general IP procedures. A particle is removed when it enters a non-particle
cell.

4) After the collision and movement sub-steps, all particles in the reservoir cells
are removed.

5) Steps 2-4 are repeated until the simulation is finished.

With the previous algorithm, using more buffer cells will improve the interface
properties, but will increase the computational cost. Hence, only one or several levels of
buffer cells are used. The number of reservoir cells is also determined such that only a
negligible number of particles will enter a buffer cell from a continuum cell during one
time step. Generally, two or more levels of reservoir cells are required. This second
strategy works very well, as will be shown in Section 5.4.

5.2 Determination of the Continuum/Particle Interface

Another key issue of a hybrid approach is where to divide the whole computational domain into particle and continuum domains. There are two criteria to determine the continuum/particle interface. The first one is that both solvers must be valid to simulate the flow around the interface, and the second one is that the continuum domain should be as large as possible in order to achieve the maximum efficiency benefit from a hybrid approach. It turns out that the interface should be placed in locations where the continuum equations tend to break down since the IP method is valid for the whole computational domain. Hence, a continuum breakdown parameter should be adopted to determine the interface location.

In principle, a continuum breakdown parameter can be derived from the relationship between the Boltzmann equation and the Navier-Stokes (N-S) equations. The Navier-Stokes equations approximate the Boltzmann equation under near-equilibrium conditions. Hence, any approximation made to derive the N-S equations can be used to derive a continuum breakdown parameter, such as the Knudsen number. A general procedure deriving the N-S equations is to use the Chapman-Enskog theory (Bird, 1994). It turns out that the N-S equations are not valid when the nonlinear terms in the Chapman-Enskog expansion become important. Physically, the continuum equations break down when the velocity distribution function deviates from its equilibrium state by a sufficient degree. However, there is no theory that indicates how large the nonlinear terms in the expansion should be, or how far the function should deviate from equilibrium for the N-S equations to be invalid. Therefore, research is still needed to find an effective continuum breakdown parameter.

In the literature, several continuum breakdown parameters have been proposed, including Bird's parameter P (Bird, 1970), the gradient-length local Knudsen number Kn_{GLL} (Boyd et al., 1995), Tiwari's criterion $\|\phi\|$ (Tiwari, 1998), and the parameter B

(Garcia et al., 1999). These four parameters are illustrated in Equations 5.8-5.11, along with their initial notations. However, only the parameter P and the parameter Kn_{GLL} have been extensively investigated for simulating expanding jet flows and for simulating hypersonic compressible flows, respectively. Therefore, the validity of these parameters for micro-scale gas flows is not clear although all these parameters represent some kind of combination of the coefficients in the first order Chapman-Enskog expansion. Even if a parameter is acceptable for a certain type of flow, the cutoff value for the parameter is also difficult to determine. Some researchers investigate the cutoff value by computing the breakdown parameter when differences between a continuum solution and a kinetic result are larger than 5% whereas some simply take a small number as the cutoff value. Generally, the cutoff value can only be determined by numerical tests, which means the cutoff value depends on tolerance chosen for the difference between the hybrid solution and the kinetic result. It is also possible that the cutoff value is problem-dependent because flow problems vary in their physical behavior. Therefore, a conservative cutoff value is often used in applications of a hybrid approach.

$$P = \frac{U}{\rho v} \left| \frac{d\rho}{ds} \right| \tag{5.8}$$

$$Kn_{GLL} = \frac{\lambda}{Q} \left| \frac{dQ}{dl} \right| \tag{5.9}$$

$$\|\phi\| = \frac{1}{\rho RT} \left[\frac{2}{5} \frac{|q|^2}{RT} + \frac{1}{2} \|\tau\|_E^2 \right]^{1/2} \tag{5.10}$$

$$B = \max \left\{ \left| \tau_{ij}^* \right|, \left| q_{ij}^* \right| \right\} \tag{5.11}$$

In the present implementation of the hybrid approach, the breakdown parameter B is selected to be the particle/continuum interface indicator because this parameter includes all the coefficients of the first-order Chapman-Enskog expansion. However, other parameters can be implemented in the code without any difficulty. The effects of

the cutoff value of the continuum breakdown parameter are illustrated in Section 5.4 by an example.

The continuum/particle interface is physically determined by the continuum breakdown parameter. Hence, the interface keeps on adjusting its location as the simulated flow develops with time. For this purpose, a mapping technique is used to help relocate the interface. A similar technique can be found in the work by Roveda et al. (1998).

In the mapping technique, each computational cell is assigned a three-digit number to represent the type of a cell, which can be an IP cell, a reservoir cell, a buffer cell, or a continuum cell other than buffer or reservoir cell. The number is in the form of "a+10b+100c". Here, "a" indicates whether the cell is in the continuum domain (0) or the IP domain (1). "b" shows whether the cell is adaptive (0) or not (1), which means that cells can be forced to be of a fixed type. "c" is used to indicate the levels of buffer cells or reservoir cells, or to indicate the IP cells neighboring the interface. Figure 5.3 shows a simple map that illustrates the cell types and the interface.

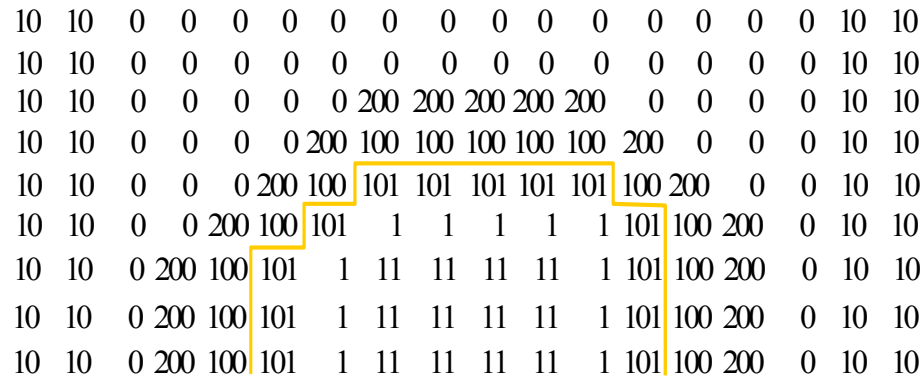| 10	10	0	0	0	0	0	0	0	0	0	0	0	0	0	0	10	10
10	10	0	0	0	0	0	0	0	0	0	0	0	0	0	0	10	10
10	10	0	0	0	0	0	200	200	200	200	200	0	0	0	0	10	10
10	10	0	0	0	0	200	100	100	100	100	100	200	0	0	0	10	10
10	10	0	0	0	200	100	101	101	101	101	101	100	200	0	0	10	10
10	10	0	0	200	100	101	1	1	1	1	1	101	100	200	0	10	10
10	10	0	200	100	101	1	11	11	11	11	1	101	100	200	0	10	10
10	10	0	200	100	101	1	11	11	11	11	1	101	100	200	0	10	10
10	10	0	200	100	101	1	11	11	11	11	1	101	100	200	0	10	10

Figure 5.3. An illustrative map showing the cell types and the interface

The algorithm for setting the cell type is as follows.

1) Sweep all computational cells to determine "a" by comparing the cutoff value of the continuum breakdown parameter to its local value. If the local value is smaller than

the cutoff value, the cell is determined as a continuum cell (a = 0). Otherwise, it is an IP cell (a = 1). Generally, "b" does not change after it is initialized.

2) Set "c" to 1 for all cells neighboring the interface.

3) Set "c" to i+1 for the continuum cells neighboring buffer cells or reservoir cells whose "c" is i (i>0) until all the buffer cells and reservoir cells are marked.

5.3 Implementation of the Hybrid Approach

In the present hybrid approach, both the IP method and the Navier-Stokes solver are implemented in the MONACO system with one structured or unstructured grid. Because each computational cell can be handled by either solver, each cell has the information for both solvers, including the cell type, the continuum breakdown parameter, the density, the velocity, the temperature, the fluxes at each cell edge, and the particle information. For each cell, a solver is chosen by the cell type that is determined by the continuum breakdown parameter. If the continuum solver is chosen, then the macroscopic information is evaluated based on the fluxes through each cell edge. Otherwise, the macroscopic information is updated using the particle information.

The algorithm of the current implementation with our second strategy for generating particles through the interface is presented here:

1) All necessary information for the simulation is initialized. Namely, the computational cells are defined and the cell type is initialized as desired. The macroscopic information about the cell is set according to the ambient condition. Then particles are distributed for the IP cells, the buffer cells, and the reservoir cells.

During each time step, the following operations are executed.

2) All particles collide and move similar to the usual IP code. When a particle reaches an open boundary or a continuum cell other than a buffer cell or a reservoir cell, it is removed. New particles are injected at the open boundary, but no particles are generated from the continuum cell side.

3) The macroscopic values of all cells are re-evaluated. All continuum cells including the buffer cells and the reservoir cells update their values according to the Navier-Stokes solver, whereas all IP cells sample the macroscopic information from the preserved information of the particles contained in the cell.

4) Remove all particles in the reservoir cells because particles are to be re-generated.

5) Calculate the continuum breakdown parameter for every cell and use the interface mapping algorithm to set the new cell type for each cell. Then generate particles according to the Chapman-Enskog distribution for particle cells (including the buffer cells and the reservoir cells) if they do not have a particle, and remove particles from the continuum cells (excluding the buffer cells and the reservoir cells) that are occupied by particles. In many cases, it is not necessary to adjust the interface at every time step. Hence, a frequency for adapting the interface can also be implemented in the code.

5.4 Validation of the Hybrid Approach

The proposed hybrid approach has been applied to several flow simulations. In this section, a Couette flow is simulated using the hybrid approach with the first strategy of generating particles for the IP solver from the continuum side, which shows the validity of the approach. Another example of a flow over a flat plate is used to show the ability of the hybrid approach using the second strategy of generating particles and to reveal the effects of the cutoff value of the continuum breakdown parameter B.

5.4.1 A Couette Flow

The Couette flow is well defined and is often used to evaluate a numerical approach (Hash and Hassan, 1996). In the present simulation, this flow is used to assess the first strategy of generating particles through the interface for the hybrid continuum / particle approach. It is also used to evaluate the validity of general continuum breakdown parameters.

In the Couette flow, one of two parallel plates has a velocity of 300m/s whereas the other is at rest. The temperature of both plates is kept at 273K, and full momentum and thermal accommodation is assumed for both plates. The distance between the two plates and the nominal density of the flow are compatible so that the body-length global Knudsen number of the flow is 0.01, 0.03, or 0.1. In all three cases (Kn_{BLG}=0.01, 0.03, and 0.1), 200 computational cells are used with a cell size that is less than the mean free path of the argon gas. The particle/continuum interface is fixed in all three cases so that 70% of the cells are calculated by the Navier-Stokes solver (see Figure 5.4). It is found that roughly 50 particles for a particle cell is sufficient to obtain a satisfactory solution when Kn_{BLG}=0.01, whereas more than 500 particles are required to avoid the crash of the code when Kn_{BLG}=0.1.

The results obtained using the hybrid approach are illustrated in Figure 5.4, where these results are compared with the full IP results. When Kn_{BLG}=0.01, excellent agreement between the two results is obtained, which shows the consistency of the hybrid approach and the full IP method. When Kn_{BLG}=0.03, the smooth results obtained using the hybrid approach demonstrate that the interface is still working well. However, the slight difference in the temperature profile between the two results in the continuum domain indicates that the continuum equations are beginning to fail. When Kn_{BLG}=0.1, the distorted profiles obtained using the hybrid approach around the interface indicates that the Navier-Stokes equations are not valid there, which also means it is impossible for continuum equations with slip models to predict the flow under this condition.

Next, the general continuum breakdown parameters are evaluated for this Couette flow. The parameter P, which was proposed for predicting expanding flows, fails for this flow because the mass density does not change along the streamline. Some other parameters are shown with their profiles calculated from the full IP results in Figure 5.5. These results show that the gradient-length local Knudsen number also fails because this parameter is mainly zero (excluding the scatter) around the centerline of the Couette
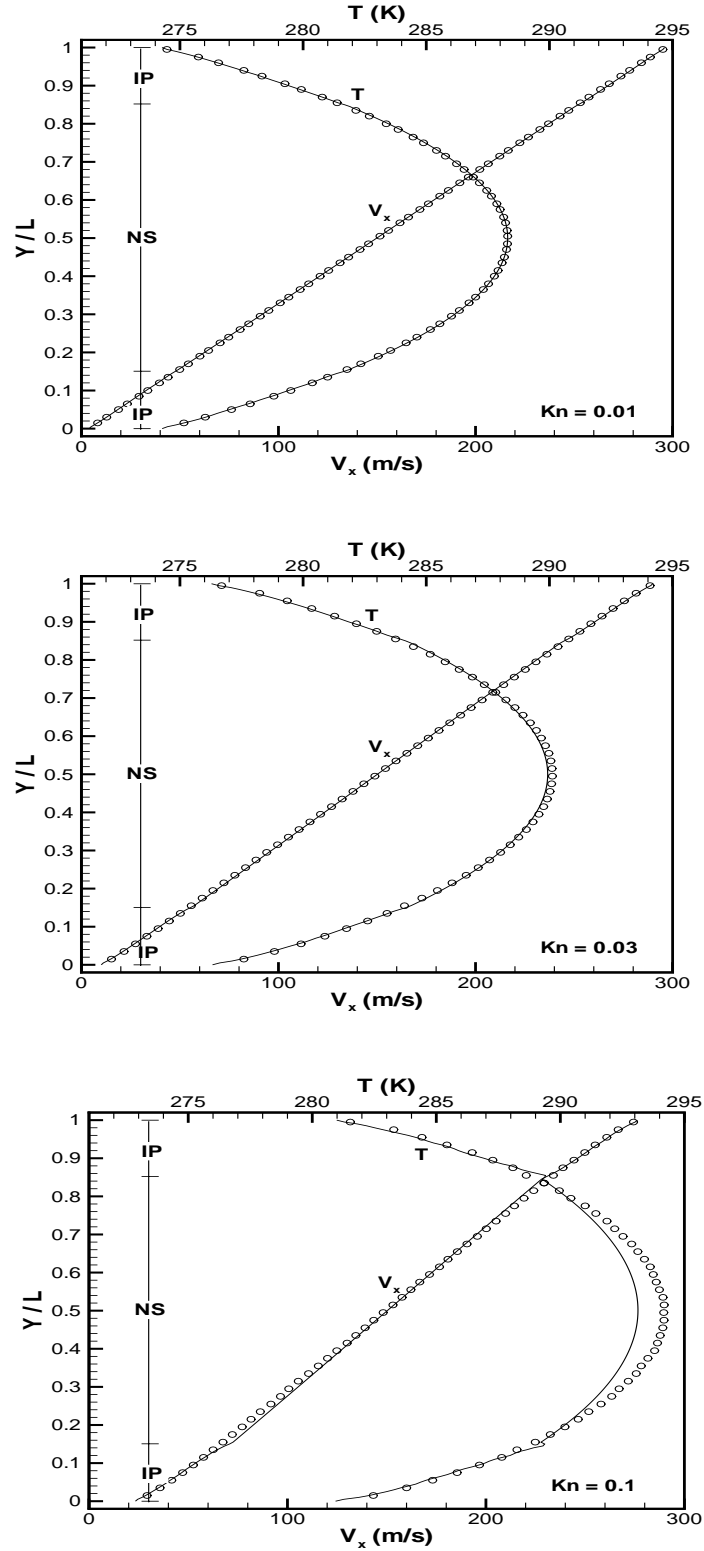
Figure 5.4. Comparison of the velocity and temperature distributions obtained using the IP code (circle) and the hybrid code (line)
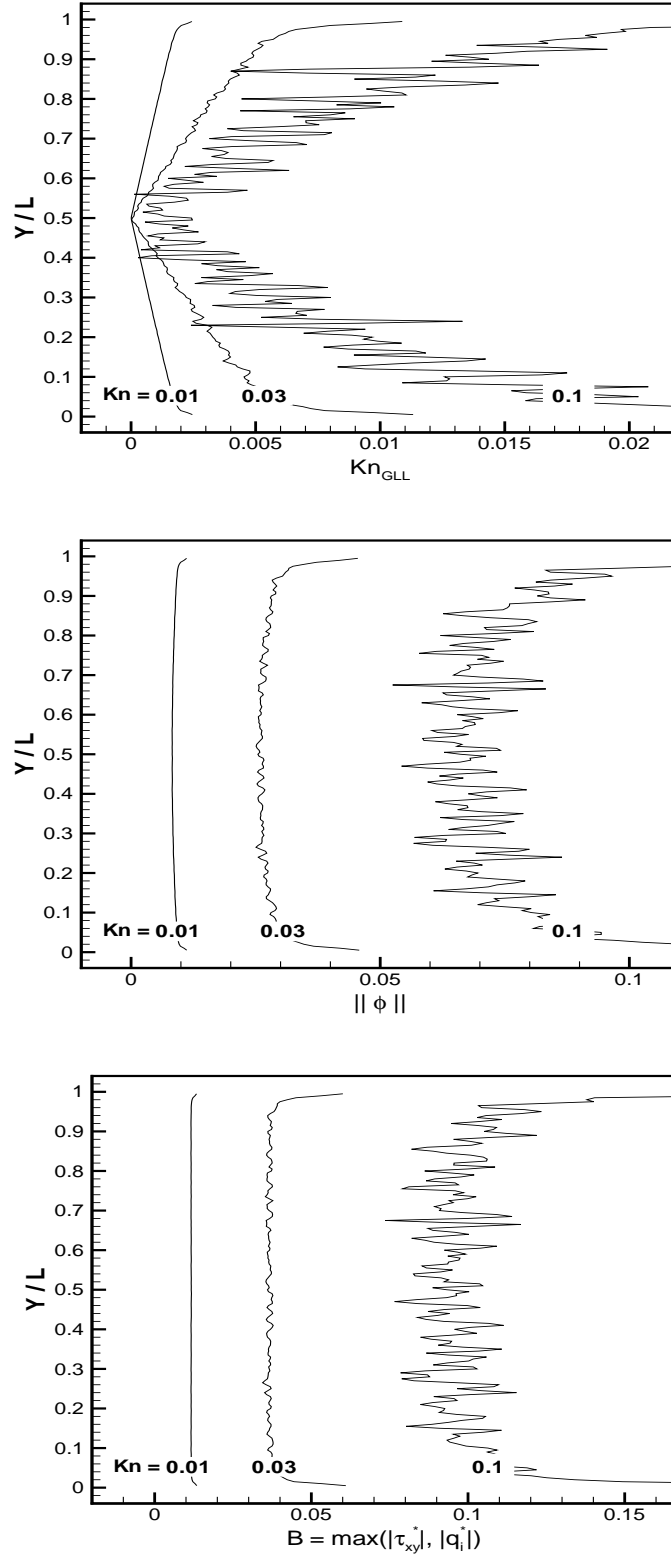
Figure 5.5. Profiles of the continuum breakdown parameters
Kn_{GLL}, $\|\phi\|$ and B for the Couette flows for various Kn_{BLG}

flow. However, the parameter $\|\phi\|$ and the parameter B display similar reasonable behavior. Their values increase when the flow becomes more rarefied. It can be concluded that the cutoff value of these two parameters is on the order of 0.03 for this flow, based on the results illustrated in Figure 5.4. However, the cutoff value may vary for different flows.

5.4.2 Flows over a Flat Plate

For subsonic external micro scale gas flows, a hybrid approach is no doubt the best choice for simulations because most of the computational domain can be described by the continuum equations. In this section, an airflow over a flat plate is simulated using the hybrid approach with the first strategy of generating particles for the particle solver.

The length of the plate is 20 microns and it has a fixed temperature of 295K. The free stream has a Mach number of 0.2, a temperature of 295K, and a density of roughly 1.32 kg/m^3. Thus, the Reynolds number of the flow is about 10, and the body-length global Knudsen number is roughly 0.024. In the simulation, full thermal accommodation is assumed for the plate and the VHS molecular model is used. A computational domain is set up having 60 microns in the upstream region, 130 microns in the downstream region and a full span of 120 microns. Characteristic boundary conditions are adopted for the external boundaries. On average, about 20 particles are used for each particle cell, and the time step is less than the mean collision time of the molecules.

With the previous specifications, we simulate the flow using the hybrid approach with different continuum/particle domain configurations. If the entire computational domain is simulated by the IP solver, then the full IP solver is recovered from the hybrid approach. Similarly, the full Navier-Stokes solver is used when the whole flow is computed by the continuum solver. Figure 5.6 shows a comparison of typical results obtained with different domain configurations. For the general hybrid result in this figure, the cutoff value of the parameter B is set to 0.005, and the dashed line indicates the

continuum/particle interface. The overall agreement among these results is good because the flow is in the slip regime. However, some differences are shown in Figure 5.7 for the surface properties. The slip velocity is the flow velocity of the air attached to the plate. In Figure 5.7, the cutoff value of the parameter B is 0.002 for the results with "hybrid 1", 0.005 for the results with "hybrid 2", and 0.01 for the results with "hybrid 3"; and only one level of buffer cells and two levels of reservoir cells are used. This shows that the surface pressure profiles are very close for all results illustrated except the result from hybrid 3. It is also found that the shear stress and the slip velocity on the surface decrease when the IP domain shrinks. The Navier-Stokes solver, however, predicts larger shear stresses and slip velocities near both ends of the plate, which may indicate the breakdown of the continuum equations in these regions.

The implementation of the interface is also investigated. First, the effect of the number of particles in each particle cell is considered. It is found that there is no obvious changes of overall flow field and the surface properties when the number of particles per cell is increased from 20 to 50, which means that small statistical scatter of the preserved macroscopic information does not cause problems for the N-S solver to use information from the IP domain. Second, the effect of buffer and reservoir cells is investigated. Figure 5.8 shows a comparison of the results obtained with different sets of buffer cells and reservoir cells for the hybrid 3 case. In Figure 5.8, the number of levels for the buffer cells and the number of levels for the reservoir cells are: one and two for "interface 1", two and three for "interface 2", three and three for "interface 3", and four and three for "interface 4". Clearly, the results become better when more buffer cells and reservoir cells are used, which means the quality of particles entering the IP domain from the continuum domain increases when more buffer cells and reservoir cells are used. It also means that it is not good enough to generate particles in the reservoir cells based on the flow information of a single cell. Particles from a different part of a cell may have different information.
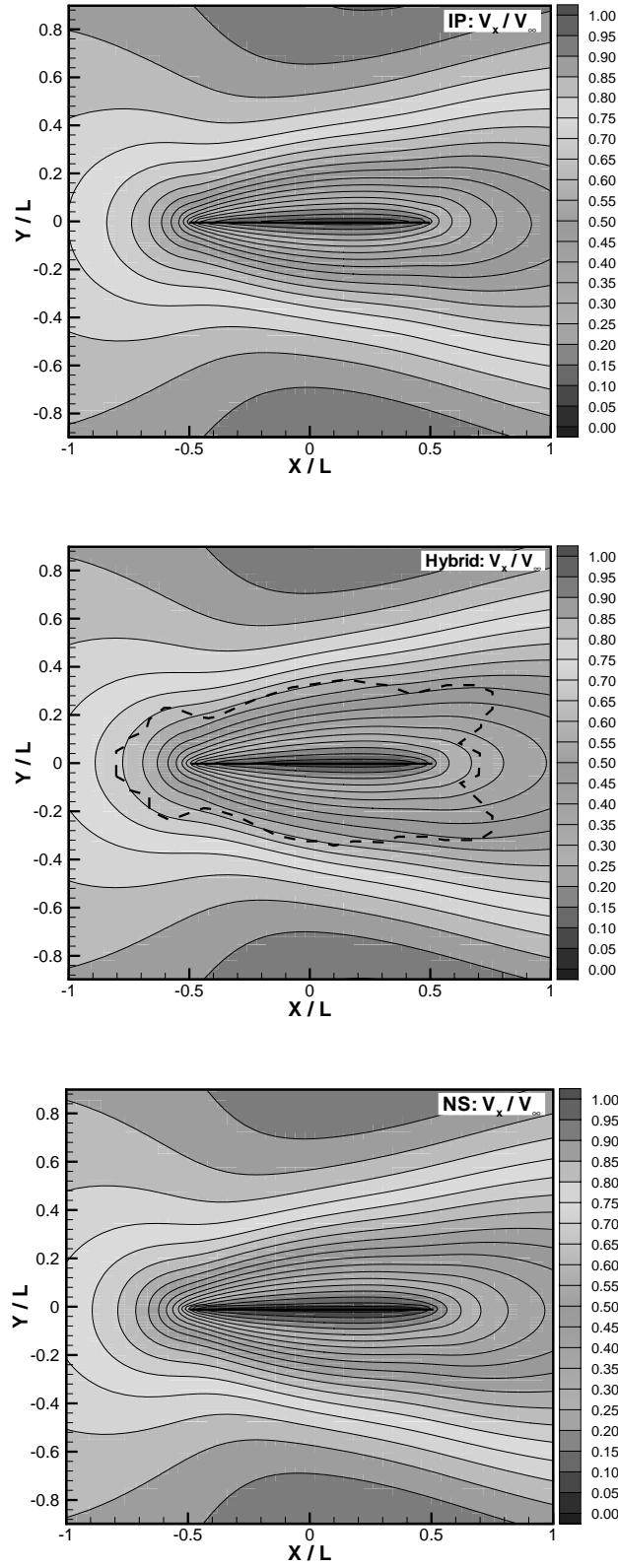
Figure 5.6. Comparison of velocity contours from simulations using the full IP, the hybrid, and the full NS configurations
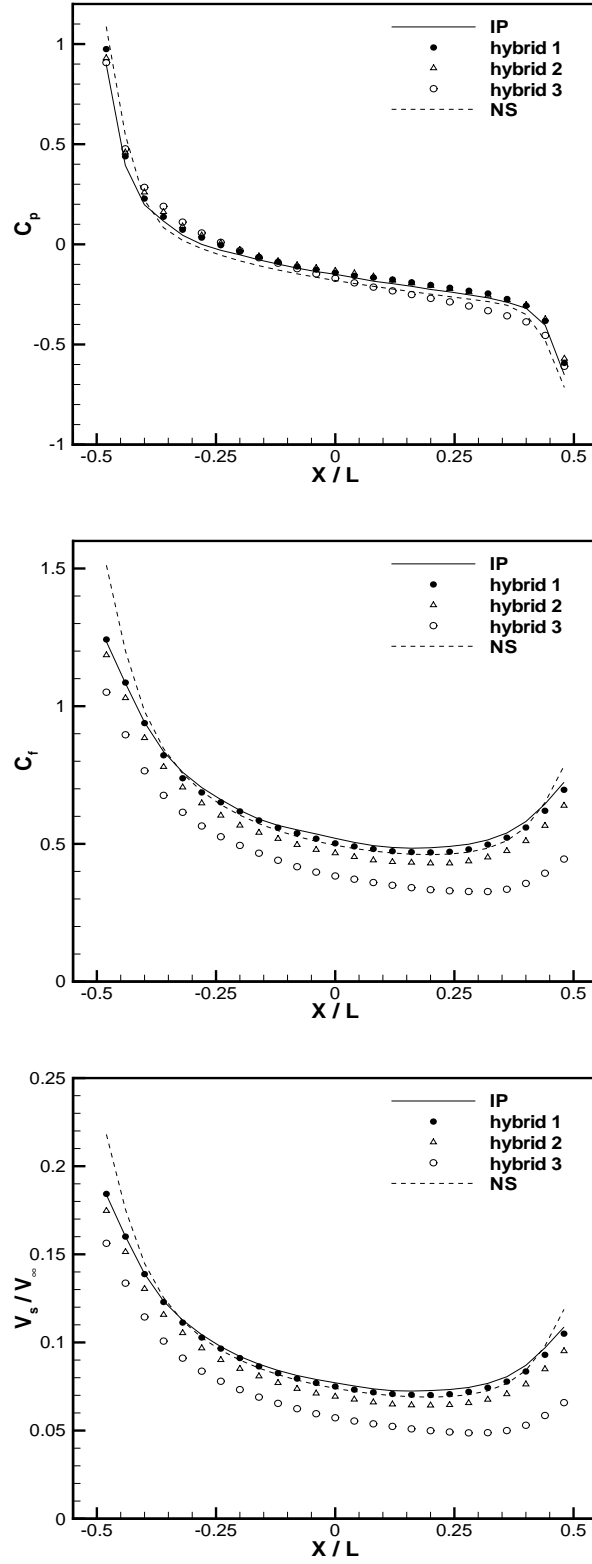
Figure 5.7. Comparison of surface properties from simulations with the full IP, the hybrid, and the full NS configurations
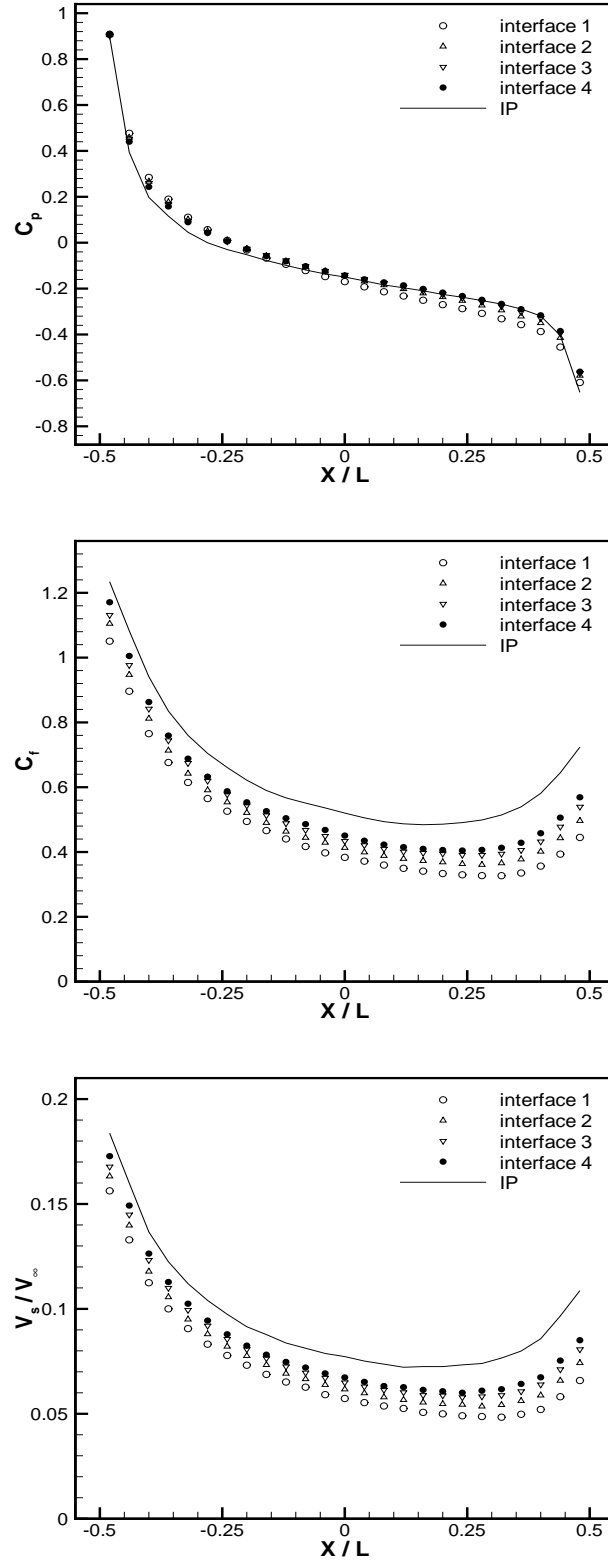
Figure 5.8. Comparison of surface properties from simulations with the full IP and the hybrid 3 domain with different buffer cells and reservoir cells

It seems that 0.002 is an acceptable cutoff value for the continuum breakdown parameter B for the flows over a flat plate using the current hybrid scheme, illustrated in Figures 5.6-5.8. However, this value for the parameter B is much smaller than the value required for the Couette flow. One possible reason for the change of the cutoff value is that this value depends on the flow problem. If it is assumed that continuum equations begin to break down at locations ten mean free paths away from the plate (regarding the plate as a disturbance source), then the gradient of flow information around these locations is smaller for a 2D flow problem than for a 1D flow problem. Similarly, the value of B is also smaller for a 2D problem than for a 1D problem because B is dependent on gradients of flow information (see Equation 5.11 and Equation 5.4). Another reason for the small cutoff value of B is that the implementation of the continuum/particle interface does not provide satisfactory particles for the particle solver. The cutoff value of B should be increased when a better implementation is adopted.

5.5 Numerical Performance

The objective of a hybrid approach is to reduce the computational cost of a numerical simulation by combining the physical accuracy of kinetic methods and the numerical efficiency of continuum solvers. Therefore, a basic requirement for a hybrid approach is to require less computational cost than a kinetic approach when simulating a flow.

The computational cost of a hybrid approach consists of three parts: the cost spent on the particle cells, the cost spent on the continuum cells, and the cost spent on the interface. First, the cost for the particle cells is proportional to the number of particle cells, and depends on the number of simulated particles in each cell. The present results show that the time for a particle cell in the hybrid approach is almost the same as the time for a cell in the IP approach, because the additional variables associated with the hybrid cell only cost more computer memory. Second, the cost for the continuum cells is

proportional to the number of continuum cells. The cost spent on one continuum cell is only about one sixth of the time spent on a particle cell in which about 20 particles are simulated. This is the reason why more continuum cells are preferred as long as they are valid. It should be mentioned that the N-S solver implemented in the MONACO system is less numerically efficient but more powerful than a similar solver implemented in the Fortran language, because the current approach is based on the cell structure which helps solve complicated geometry problems. Third, the cost spent on the interface is more complicated. It depends on the number of buffer cells and the number of reservoir cells. It is found that the time spent on one buffer cell is very close to the time spent on a general particle cell, whereas a reservoir cell requires about two and a half times the time spent on a general particle cell. This is because a large amount of time is spent on redistribution of the particles for the reservoir cells. The average time t_{real} spent on one time step is listed in Table 5-1 for the case of flow over a flat plate for several hybrid configurations when the hybrid code runs on a Pentium 4 personal computer. In Table 5-

Table 5-1 Average time spent on one time step on a Pentium 4 PC

Configuration		N_{IP}	N_{NS}	N_{buf}	N_{res}	t_{est} (ms)	t_{real} (ms)
Full NS			18750			54.7	54.6
Full IP		18750				328	327
Hybrid 1		3840	14910	267	545	139	137
Hybrid 2		1454	17296	148	308	92.0	92.2
Hybrid 3	Interface 1	540	18210	74	160	70.9	71.4
	Interface 2	540	18210	152	258	76.5	77.0
	Interface 3	540	18210	234	270	78.5	78.3
	Interface 4	540	18210	320	282	80.5	80.2

1, we also list the estimated time t_{est} which is evaluated based on Equation 5.12, where N_{IP} is the number of IP cells, N_{NS} is the number of N-S cells, N_{buf} is the number of buffer cells, N_{res} is the number of reservoir cells, and $t_{IP} = 17.5 \mu s$ is the time spent on one IP cell.

$$t_{est} = \left(N_{IP} + N_{NS}/6 + N_{buf} + 2.5N_{res}\right) t_{IP} \tag{5.12}$$

Clearly, the numerical performance of the hybrid approach depends on the ratio of the particle cell number to the continuum cell number and on the percentage of the buffer cells and the reservoir cells. Thus, it is better to apply the hybrid approach to flows in which most of the flow domain can be described by continuum equations.

5.6 Conclusions

In this chapter, general issues related to development of a hybrid continuum / particle approach were explained, and a hybrid approach was developed by combining the IP method and a continuum solver.

There are two critical factors that affect the development of an effective hybrid continuum/particle approach. One is the information exchange between the two coupled approaches. The other is the continuum breakdown parameter and its cutoff value. The present results showed that the information exchange scheme is very important to the performance of a hybrid approach because it affects the cutoff value for a continuum breakdown parameter. The numerical performance of the hybrid approach becomes better when more of the computational domain of a flow can be set as the continuum domain.

The hybrid approach can be applied to simulate general external micro-scale gas flows because these flows have a very large computational domain that can be described by continuum equations. The hybrid approach can also be applied to simulate general steady rarefied gas flow to speed up reaching a steady state for the simulation. Such application is considered in the next chapter.

CHAPTER VI

NUMERICAL SIMULATION OF AIR FLOWS
OVER MICRO-SCALE AIRFOILS

In this chapter, we simulate gas flows over micro-scale flat plates having zero and 5% thickness. The fluid mechanics of flows over a zero-thickness micro-scale flat plate is studied in Section 6.1. The drag on the plate is analyzed in Section 6.2. The fluid mechanics of flows over a micro-scale airfoil (a flat plate having a thickness ratio of 5%) is studied in Section 6.3. The aerodynamic characteristics of the micro-scale airfoil is investigated in Section 6.4. Finally, some conclusions about the simulations of micro-scale gas flows are given in Section 6.5.

6.1 Fluid Mechanics of Air Flows over a Zero-Thickness Micro-Scale Flat Plate

The problem of flow past a two-dimensional flat plate aligned with the free-stream is one of fundamental interest because it generates a wide range of basic flow phenomena. It has been shown that the flow can be described by the laminar boundary layer equations at a moderate Reynolds number ($\mathrm{Re_L} \sim 10^4$), whereas turbulent equations are required when the flow Reynolds number is larger than 10^6. Furthermore, when the Reynolds number of the flow becomes small ($\mathrm{Re_L} < 100$), the flow properties also depend on the Mach number of the flow. Especially, the nature of the flow changes from the continuum flow regime to the free-molecular flow regime when the Reynolds number of the flow becomes smaller for a fixed velocity and plate size.

Flows over a flat plate have been investigated experimentally by Schaaf and Sherman (1954) in the range of $3.4 \times 10^1 < \mathrm{Re} < 2.02 \times 10^3$ for $2.5 < M < 3.8$ and

$3 < \mathrm{Re} < 5 \times 10^2$ for M about 0.2 and 0.6. They measured the drag on the plate for experiments conducted in a low-density wind tunnel, and the results agree with the theoretical result obtained by solving a Rayleigh problem with a slip boundary condition for an incompressible flow (Schaaf, 1950). However, the measured drag does not agree well with the theoretical result obtained by Mirels (1951) although Mirels adopted a similar procedure for compressible flows which is the case for the experiments. Therefore, it is a coincidence for the agreement between the experiment and Schaaf's theory (1950). Because approximations are generally made in theories, e.g., Mirels (1951) and Liu (1959), for gas flows with low Reynolds number, analytic methods can only predict flows qualitatively. In this section, the hybrid continuum/particle approach is applied to simulate gas flows over a micro-scale flat plate at Reynolds numbers less than 100.

Consider air flows past a flat plate having a finite length of 30μm. The flow conditions are as follows: the velocity of the free stream is roughly 69 m/s with a Mach number of 0.2; the temperatures of the free stream and the plate are both 295K; the density of the free stream is determined from the flow Reynolds number based on the plate length. We use several large computational domains to simulate these flows. Figure 6.1 shows half of a typical computational grid where the computational cells are clustered near to the plate. The computational domain is enlarged when the flow Reynolds number decreases so that the flow along the computational boundaries is in or near an equilibrium state. The outer boundary condition is implemented using the characteristic line method. The flow is simulated using the continuum/particle approach based on the following procedure. At first, the continuum solver is applied to all computational cells. After a certain time, the information preservation (IP) method takes over for the domain near the flat plate. Later, the entire computational domain is simulated by the IP method. Finally, the flow is sampled after the skin friction on the plate reaches a constant value. Therefore, the hybrid approach is only used to reduce the computational cost when the

flow reaches the steady state, whereas the IP method is applied to the whole computational domain for the final simulation.
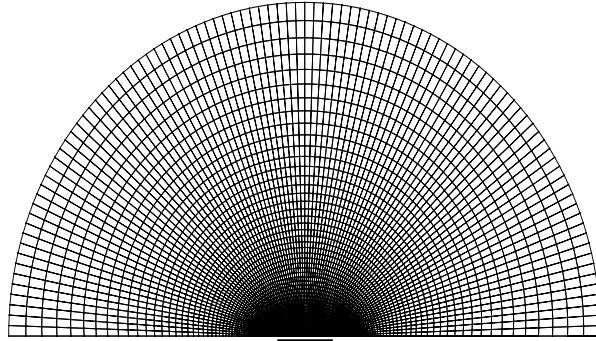

Figure 6.1. Half of a typical computational grid for flows over a flat plate

With the previous specification, we investigate gas flows over the flat plate. Numerical simulations show that the flows exhibit several rarefied phenomena, including velocity slip, compressibility, viscous heating, and temperature jump.

6.1.1 Velocity Slip

Velocity slip means that the air adjacent to a solid boundary has a finite velocity relative to the boundary. Kinetic theory shows the flow velocity of the air adjacent to a wall is the average velocity of all molecules hitting or leaving the wall. If the wall is assumed to be fully momentum-accommodated, then the average velocity of the leaving molecules is equal to the velocity of the wall. However, the velocity of incident molecules is related to the flow velocity where the molecule is recently collided, which means the average velocity of the hitting molecules is generally not the same as the velocity of the wall. Hence, a velocity slip is a common phenomenon for rarefied gas flows. When the characteristic length of a flow is much larger than one mean free path of gas molecules, the slip velocity is relatively small, and the velocity slip effect can be neglected. Otherwise, the velocity slip effect must be considered in both theoretical analysis and numerical simulations.

The slip velocity along the flat plate is shown in Figure 6.2 for several low Reynolds number flows. This slip velocity is obtained as the average of the tangential component of the preserved macroscopic velocity of particles hitting and leaving the plate. The figure shows that the slip velocity increases when the Reynolds number decreases, which means the velocity slip becomes important for low Reynolds number flows. It also shows the slip velocity is not monotonically distributed along the flat plate because both ends of the plate act as stagnation points.
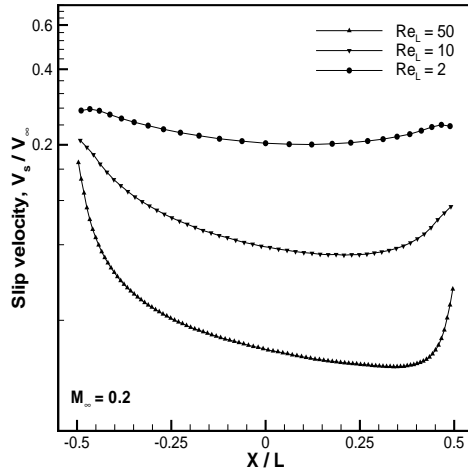

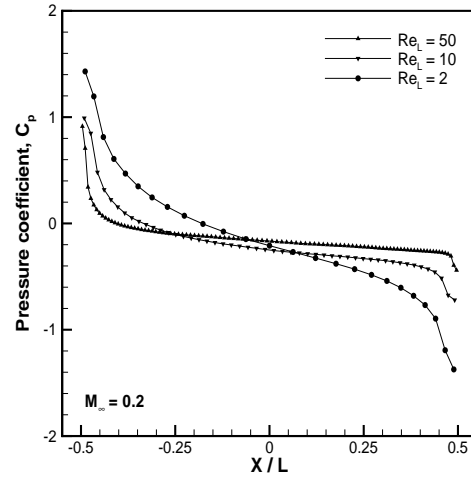**Figure 6.2. Reynolds number effect on slip velocity distributions**

Figure 6.3. Reynolds number effect on pressure coefficient distributions

6.1.2 Compressibility

The compressibility of micro-scale gas flows means that the variation of the density or the pressure of the flow increases when the flow Reynolds number decreases. Figure 6.3 shows the pressure coefficient distributions along the plate for several Reynolds number flows. Clearly, the pressure of the gas around the leading edge is higher than the free stream pressure, and the pressure around the trailing edge is lower than the free stream pressure. The intensity of this behavior increases as the flow Reynolds number decreases, whereas the pressure gradient around both ends of the plate decreases.

6.1.3 Viscous Heating

Viscous heating, or viscous dissipation, is a phenomenon in which a gas is heated due to the work done by viscous stresses of a flow. A Couette flow is a good example to show the rarefied effect on the viscous heating (Chapter IV, Section 4.3). For a gas flow over a flat plate, the viscous heating can be illustrated by showing the heat transfer from the gas to the plate because other terms in the energy equation are relatively unimportant. Distributions of Stanton number along the plate are shown in Figure 6.4. It shows that the Stanton number increases as the flow Reynolds number decreases.
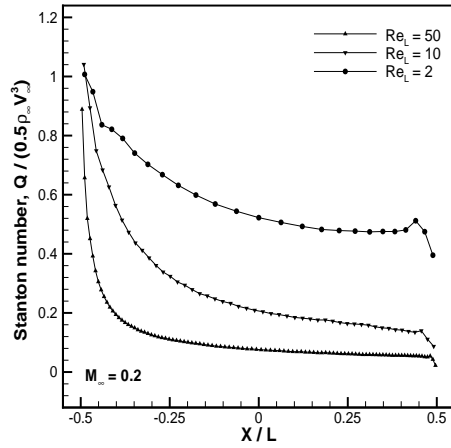

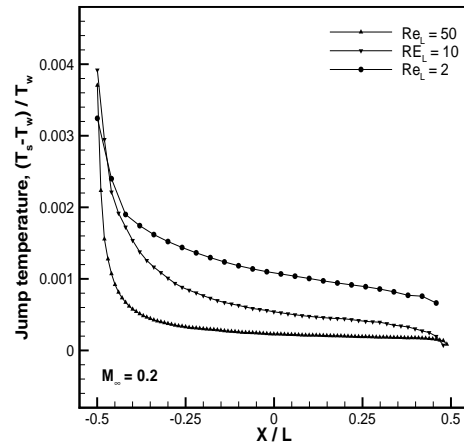**Figure 6.4. Reynolds number effect on Stanton number distributions**

Figure 6.5. Reynolds number effect on temperature jump distributions

6.1.4 Temperature Jump

The temperature jump phenomenon is not very obvious when the flow Mach number is small. However, we can still show the effect of the Reynolds number on this phenomenon. Figure 6.5 shows that the temperature jump increases when the flow Reynolds number decreases.

It is concluded that when the flow Reynolds number decreases, the slip velocity, the compressibility, the viscous heating and the temperature jump all increase for gas flows over a micro-scale flat plate, which shows that rarefied effects are important for low Reynolds number flows.

6.2 Drag on a Micro-Scale Flat Plate

The drag on a flat plate is one of the most important physical quantities for flows over a flat plate. It has been shown that the drag only depends on the Reynolds number for high Reynolds number flows. However, the behavior of the drag is not clear yet for low Reynolds number flows.

For low Reynolds number flows in the slip regime, Schaaf (1950) solved a Rayleigh problem (Equation 6.1) for incompressible flows with a first-order slip boundary condition, and obtained a relationship (Equation 6.2) between a normalized drag $C_D \cdot M$ on a flat plate and a non-dimensional parameter $\sqrt{\text{Re}}/M$. Later, Mirels (1951) extended the calculation to include the effect of compressibility and introduced an empirical relation to match with the Blasius solution (Equation 6.3) for high Reynolds number flows. The Mirels (1951) formulation is very similar to the Schaaf (1950) formulation except that the independent variable $\sqrt{\text{Re}}/M$ has a different numerical factor, and Mirels (1950) also added a term to limit the local skin friction within the free-molecular value. However, it turns out that the Schaaf (1950) result (Equation 6.2) agrees better with the experimental data obtained by Schaaf and Sherman (1954) than Mirels (1951) result (Equation 6.4). This may be a coincidence because there are some approximations made in both procedures. First, the transformation from Rayleigh's problem to a flat plate is approximate. Second, the continuum equations cannot be used to solve the Rayleigh equation at very small times. Third, the effect of the trailing edge is not included in this Rayleigh problem. Hence, the analytic solutions can only be used for a reference.

$$\rho_\infty u_\infty \left(\partial u / \partial x \right) = \mu_\infty \left(\partial^2 u / \partial y^2 \right) \tag{6.1}$$

$$C_D M = \frac{2.67}{z^2} \left\{ e^{z^2} erfc(z) - 1 + \frac{2z}{\sqrt{\pi}} \right\}, \quad z = \frac{\sqrt{\text{Re}}}{1.5M} \tag{6.2}$$

$$C_D M = \frac{2.656}{z}, \quad z = \frac{\sqrt{\text{Re}}}{M} \tag{6.3}$$

$$C_D M = \frac{2.697}{z^2}\left\{e^{z^2} erfc(z) - 1 + \frac{2z}{\sqrt{\pi}} - 0.0718\right\}, \quad z = \frac{1.146\sqrt{Re}}{M} \qquad \textbf{(6.4)}$$

For small Reynolds number flows near the free-molecular regime, Liu (1959) proposed a physical theory for the drag on a flat plate. In this theory, some collisions between incident and reflected molecules are considered whereas other types of collisions are neglected. Liu (1959) showed (Equation 6.5) that the drag normalized by the free-molecular value depends not only on $\sqrt{Re}/M$ but also on G (Equation 6.6) which is a function of M and Re/M. The drag based on the formula of Liu (1959) is plotted in Figure 6.6. It shows when $\sqrt{Re}/M < 1.5$, flows with smaller M have large $C_D \cdot M$. However, when $\sqrt{Re}/M$ is not small, the near-free-molecule theory may not predict the drag correctly because a lot of simplications made in the theory can only be accepted when the flow Knudsen number is large.

$$C_D M = 1.349\left(1 - 0.188\left(\sqrt{Re}/M\right)^2 G\right) \qquad \textbf{(6.5)}$$

$$
\begin{aligned}
G(S, L/\lambda) = &\frac{5}{4\pi}\int_0^\infty \frac{e^{-(L/\lambda)t}}{1+t}\left[ctg^{-1}t - t\ln\frac{1+t^2}{t^2}\right]dt \\
&+ \frac{S}{\sqrt{\pi}}\int_0^\infty \frac{e^{-(L/\lambda)t}}{1+t}\left[\left(1+t^2\right)^{1/2} + \frac{t^2}{\left(1+t^2\right)^{1/2}} - 2t\right]dt \\
&- \frac{1}{8}\left(\frac{1}{2} + \frac{3}{\pi}\right)S^2\int_0^\infty \frac{e^{-(L/\lambda)t}}{1+t}\left[4t\ln\frac{1+t^2}{t^2} - 3ctg^{-1}t - \frac{t}{1+t^2}\right]dt \qquad \textbf{(6.6)} \\
&+ \frac{S^3}{5\sqrt{\pi}}\int_0^\infty \frac{e^{-(L/\lambda)t}}{1+t}\left[\left(1+t^2\right)^{1/2} + \frac{2t^2}{\left(1+t^2\right)^{1/2}} - \frac{t^4}{3\left(1+t^2\right)^{3/2}} - \frac{8t}{3}\right]dt,
\end{aligned}
$$

where, $S = 0.8367M$ and $L/\lambda = 0.6730Re/M$

In the following, the skin friction and the drag on a flat plate are calculated for Reynolds number between 0.2 and 100 at several Mach numbers. Comparisons among the IP, DSMC and Navier-Stokes results are shown in Figure 6.7 and Figure 6.8. In Figure 6.7, the IP results agree well with the DSMC results for the skin friction along the plate, while the results obtained from the Navier-Stokes equation with a slip boundary condition are a little smaller. In Figure 6.8, the IP method predicts almost the same drag
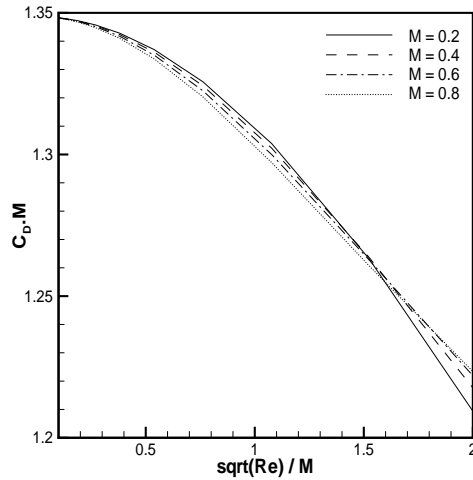
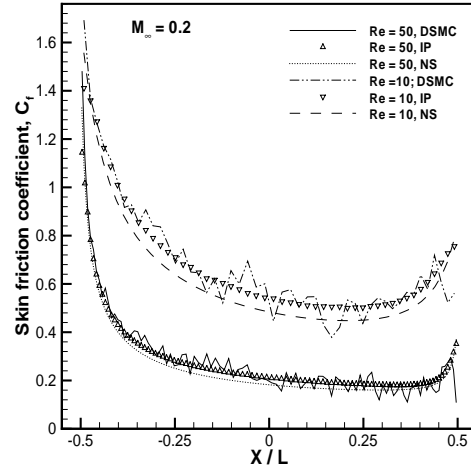**Figure 6.6. Drag predicted by Liu's near free molecular theory**

Figure 6.7. Comparison of skin friction among IP, DSMC and NS results

as the DSMC method when the flow Mach number is 0.8 for all Reynolds numbers. However, the drag of the DSMC results is not shown when the flow Mach number is 0.2 because the DSMC results exhibit a relatively large scatter as shown in Figure 6.7 for the skin friction. It is surprising that the overall drag predicted by the Navier-Stokes equation is so close to the IP profile although the difference of the skin friction between the IP and N-S results increases when the flow Reynolds number decreases.
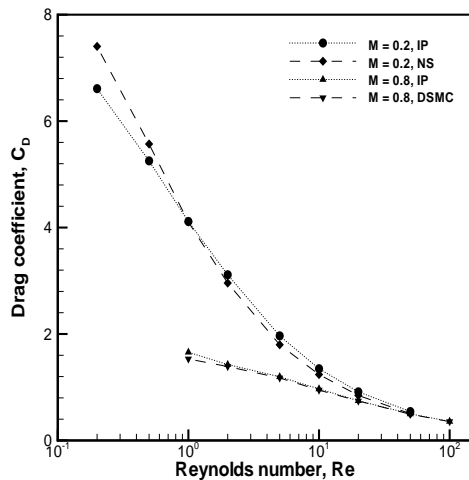

Figure 6.8. Comparison of drag on the flat plate between IP and DSMC and between IP and NS results
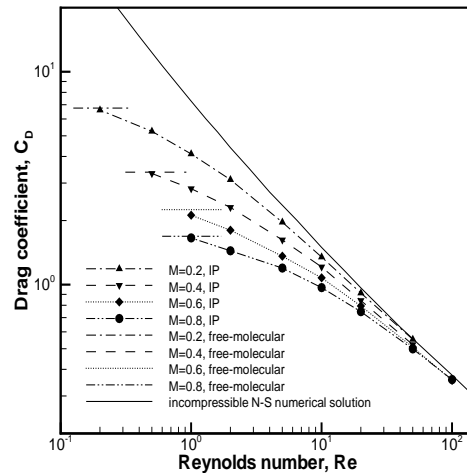

Figure 6.9. Drag on the plate depends on Mach number and Reynolds number as predicted by the IP method

The drag predicted by the IP method at different Mach numbers is shown in Figure 6.9.

Clearly, the drag on the plate depends not only on the flow Reynolds number, but also on

the flow Mach number. Comparison between the IP results and the experimental data

(Schaaf and Sherman, 1954) is shown in Figure 6.10, and the agreement is quite good. If

the relationship obtained by Schaaf (1950, Equation 6.2) or Mirels (1951, Equation 6.4)

is followed, both the IP results and the experimental data, however, do not collapse well

to a single curve. As the near free molecular theory of Liu (1959) shows that the

normalized drag coefficient or $C_D \cdot M$ is a function of the product of $\sqrt{Re}/M$ and G, the

present results suggest that $C_D \cdot M$ for the current range of $\sqrt{Re}/M$ may depend not

only on $\sqrt{Re}/M$. Careful examination of the drag in the $C_D \cdot M \sim \sqrt{Re}/M$ plot shows

that the profiles can be grouped with the flow Mach number. Therefore, plotting $C_D \cdot M$

with a variable combining $\sqrt{Re}/M$ and M was studied. Surprisingly, the normalized

drag coefficient or $C_D \cdot M$ profiles collapse very well with a variable similar to

$\sqrt{Re}/M^{0.8}$ for both the IP results and the experimental data as shown in Figure 6.11.

This may indicate that $\sqrt{Re}/M^{0.8}$ is the dominant variable for the drag of flows over a

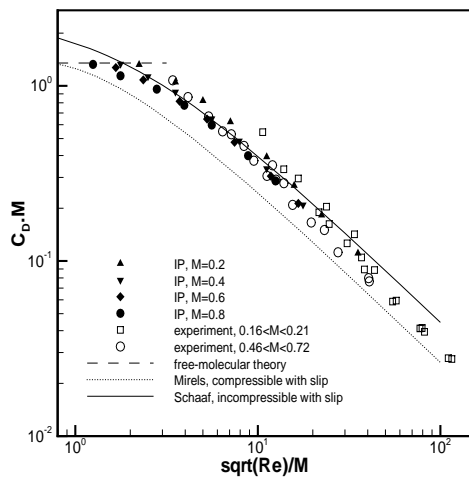flat plate in the slip flow regime and the transitional flow regime. A fitting formula is also

**Figure 6.10. Drag on the plate from
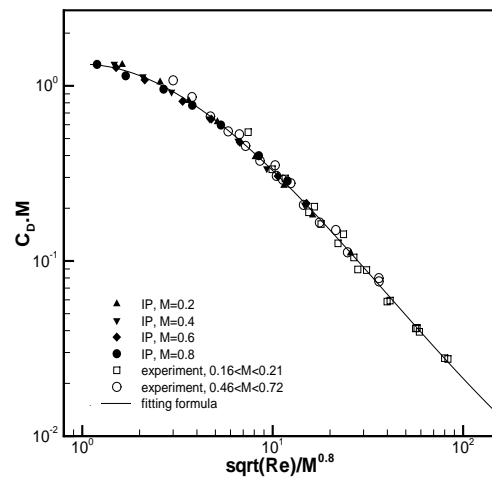the IP results and the experimental data
as $C_D \cdot M \sim \sqrt{Re}/M$**

**Figure 6.11. Drag on the plate from
the IP results and the experimental data
as $C_D \cdot M \sim \sqrt{Re}/M^{0.8}$**

given in Figure 6.11 for the simulated and measured drags as Equation 6.7 when $1 < \sqrt{\mathrm{Re}}/M^{0.8} < 100$.

$$\ln(C_D \cdot M) = 0.285 - 0.333 \times \ln^2\left(\sqrt{\mathrm{Re}}/M^{0.8}\right) + 0.030 \times \ln^3\left(\sqrt{\mathrm{Re}}/M^{0.8}\right) \qquad \textbf{(6.7)}$$

6.3 Fluid Mechanics of Air Flows over a Micro-Scale Airfoil

Experiments (Sunada et al., 1997) have shown that conventional streamlined airfoils do not perform as well as a flat plate with a thickness ratio of 5% at flow Reynolds number of 4×10^3. A comparison of the lift slope for several airfoils is shown in Figure 6.12. In this section, the fluid mechanics of a 5% flat plate is investigated at even smaller Reynolds numbers.
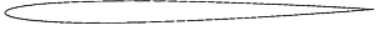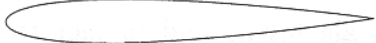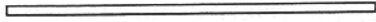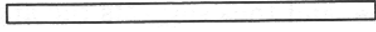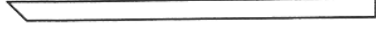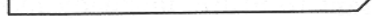
airfoil	lift slope
NACA0006	3.7
NACA0009	2.9
NACA0012	2.0
2.5% flat plate	5.2
5% flat plate	5.8
5% sharp LE	5.7
5% sharp TE	5.6

**Figure 6.12. Comparison of lift slope of airfoil
at a Reynolds number of 4×10^3, after Sunada et al. (1997)**

The flat plate in the present simulation has a 30 μm chord length, a 1.5 μm thickness and an infinite wingspan. The temperature of the plate is kept at 295K, and full thermal accommodation is assumed for the plate. The free stream is air with a Mach number of 0.2 and a temperature of 295K. The simulations adopt 1.0 atmosphere, 0.1 atmosphere and 0.01 atmosphere as the free stream pressure. The angle of attack is also varied from 0° to 50° using increments of 10°. The hybrid continuum/particle approach is

used to simulate the flows. When the free stream pressure is 1.0 atm, the flow in the domain near both ends of the plate is solved using the IP method, whereas the flow in the rest of the computational domain is calculated using the Navier-Stokes solver. The interface employs three levels of buffer cells and three levels of reservoir cells. When the free stream pressure is 0.1 atm or 0.01 atm, the hybrid approach is only used for the flow to reach a steady state, and thereafter all the computational domain is simulated with the IP method.

The flow patterns when p_∞=1.0 atm (Re=135.7) are illustrated in Figures 6.13-6.16 for flows using different angles of attack. Figure 6.13 shows the pressure field and some streamlines around the airfoil. Clearly, the pressure increases where the flow faces the airfoil, and drops where the flow leaves the airfoil. There is no flow separation when the angle of attack (α) is equal to or less than 10°. However, when α=20°, the flow begins to separate near the left end of the upper edge because of the strong local adverse pressure gradient (Figure 6.15). When α=30°, another separation occurs near the right end of the plate. The flow is then dominated by the two separated regions or two vortices. The downstream vortex becomes stronger when the angle of attack increases (α=40°), and this vortex almost eats away the upstream vortex when α=50°. The flow above the upper edge of the plate can also be illustrated by the profiles of the velocity component parallel to the plate as shown in Figure 6.14. A typical boundary layer is observed when α=0° as the boundary layer thickness increases along the plate (the leading edge is a singularity point for boundary layer theory). The gas velocity within the boundary layer decreases with an increasing angle of attack because the adverse pressure gradient increases. When the angle of attack is large enough (α=20°), the velocity at a certain location (e.g., X/L=0.3) becomes negative and the flow begins to separate. The distributions of the pressure coefficient and the skin friction coefficient along the plate are shown in Figure 6.15 and Figure 6.16. These data are used to calculate the aerodynamic characteristics of the airfoil.

The flow patterns when p_∞=0.1 atm (Re=13.57) are shown in Figures 6.17-6.20, and those when p_∞=0.01 atm (Re=1.357) are shown in Figures 6.21-6.24. Compared to the flows when p_∞=1.0 atm, these flows under lower pressures exhibit very different flow behavior. First, the boundary layer thickness increases although the slip velocity increases. Secondly, the pressure gradient near the left end of the plate decreases although the overall pressure variation increases. Next, only a weak flow separation occurs at a very large angle of attack (α=50°) when p_∞=0.1, and there is no separation when p_∞=0.01 atm for the angle of attack up to 50°. Finally, the skin friction increases by a significant amount, which means that the importance of the viscous diffusion increases so as to prevent flows from being separated. Therefore, it can be anticipated that the aerodynamic characteristics of the micro-scale airfoil at low Reynolds number flows are very different from those at high Reynolds number flows.

Figure 6.13. Pressure field and streamlines for flows over a 5% flat plate when M∞=0.2, ReL=135.7, with angle of attack ranging from 0° to 50°

Plate-parallel velocity profile when M$_\infty$=0.2, Re$_L$=135.7, and α=0°

Plate-parallel velocity profile when M$_\infty$=0.2, Re$_L$=135.7, and α=10°

Plate-parallel velocity profile when M$_\infty$=0.2, Re$_L$=135.7, and α=20°

Plate-parallel velocity profile when M$_\infty$=0.2, Re$_L$=135.7, and α=30°

Plate-parallel velocity profile when M$_\infty$=0.2, Re$_L$=135.7, and α=40°

Plate-parallel velocity profile when M$_\infty$=0.2, Re$_L$=135.7, and α=50°

Figure 6.14. Profiles of the velocity component parallel to the plate for flows over a 5% flat plate when M$_\infty$=0.2, Re$_L$=135.7, with angle of attack ranging from 0° to 50°

Figure 6.15. Distributions of the pressure coefficient for flows over a 5% flat plate when M∞=0.2, Re_L=135.7, with angle of attack ranging from 0° to 50°

Figure 6.16. Distributions of the skin friction coefficient for flows over a 5% flat plate when M∞=0.2, ReL=135.7, with angle of attack ranging from 0° to 50°

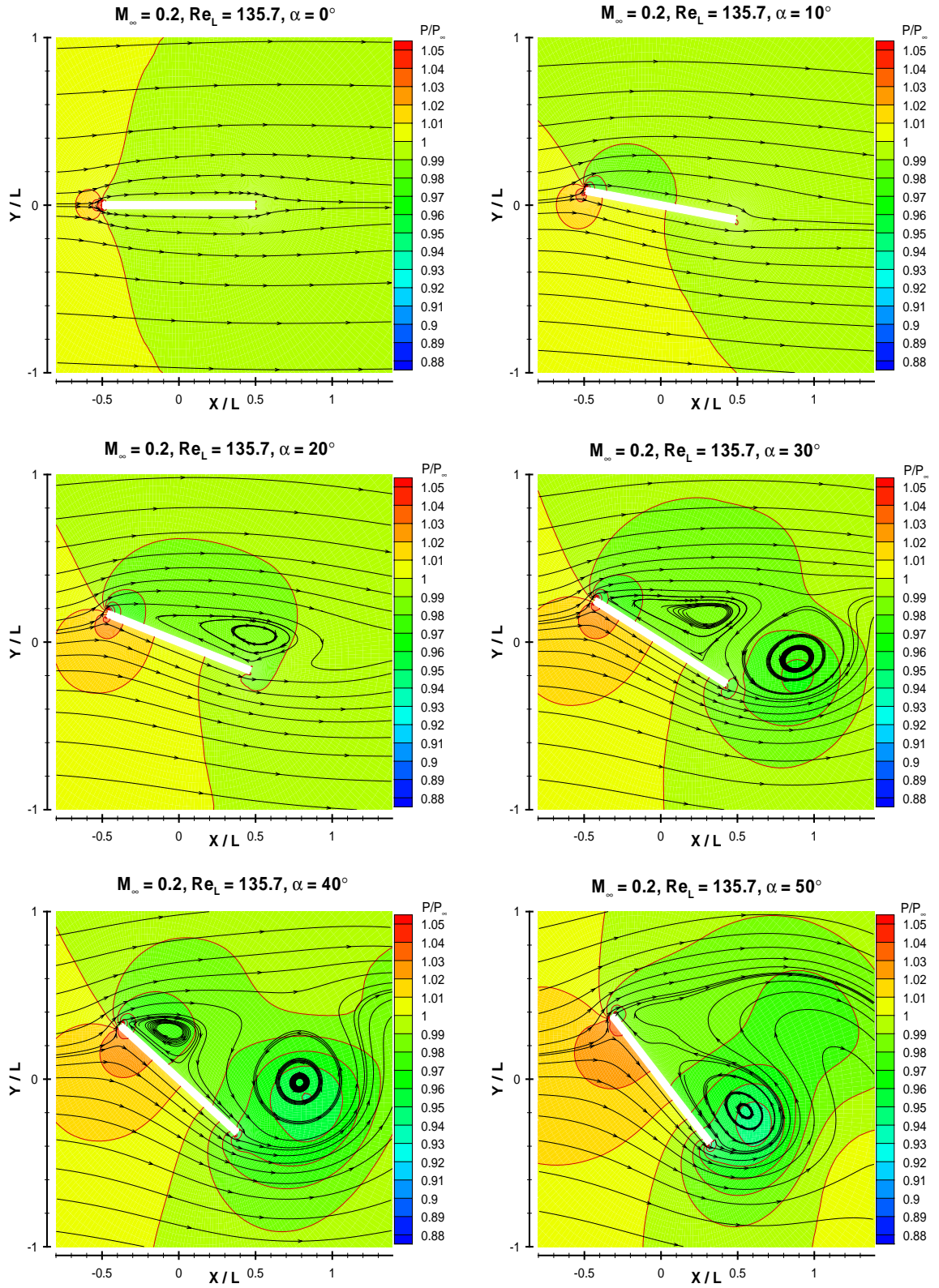**Figure 6.17. Pressure field and streamlines for flows over a 5% flat plate when M∞=0.2, ReL=13.57, with angle of attack ranging from 0° to 50°**

Plate-parallel velocity profile when M$_\infty$=0.2, Re$_L$=13.57, and α=0°

Plate-parallel velocity profile when M$_\infty$=0.2, Re$_L$=13.57, and α=10°

Plate-parallel velocity profile when M$_\infty$=0.2, Re$_L$=13.57, and α=20°

Plate-parallel velocity profile when M$_\infty$=0.2, Re$_L$=13.57, and α=30°

Plate-parallel velocity profile when M$_\infty$=0.2, Re$_L$=13.57, and α=40°

Plate-parallel velocity profile when M$_\infty$=0.2, Re$_L$=13.57, and α=50°
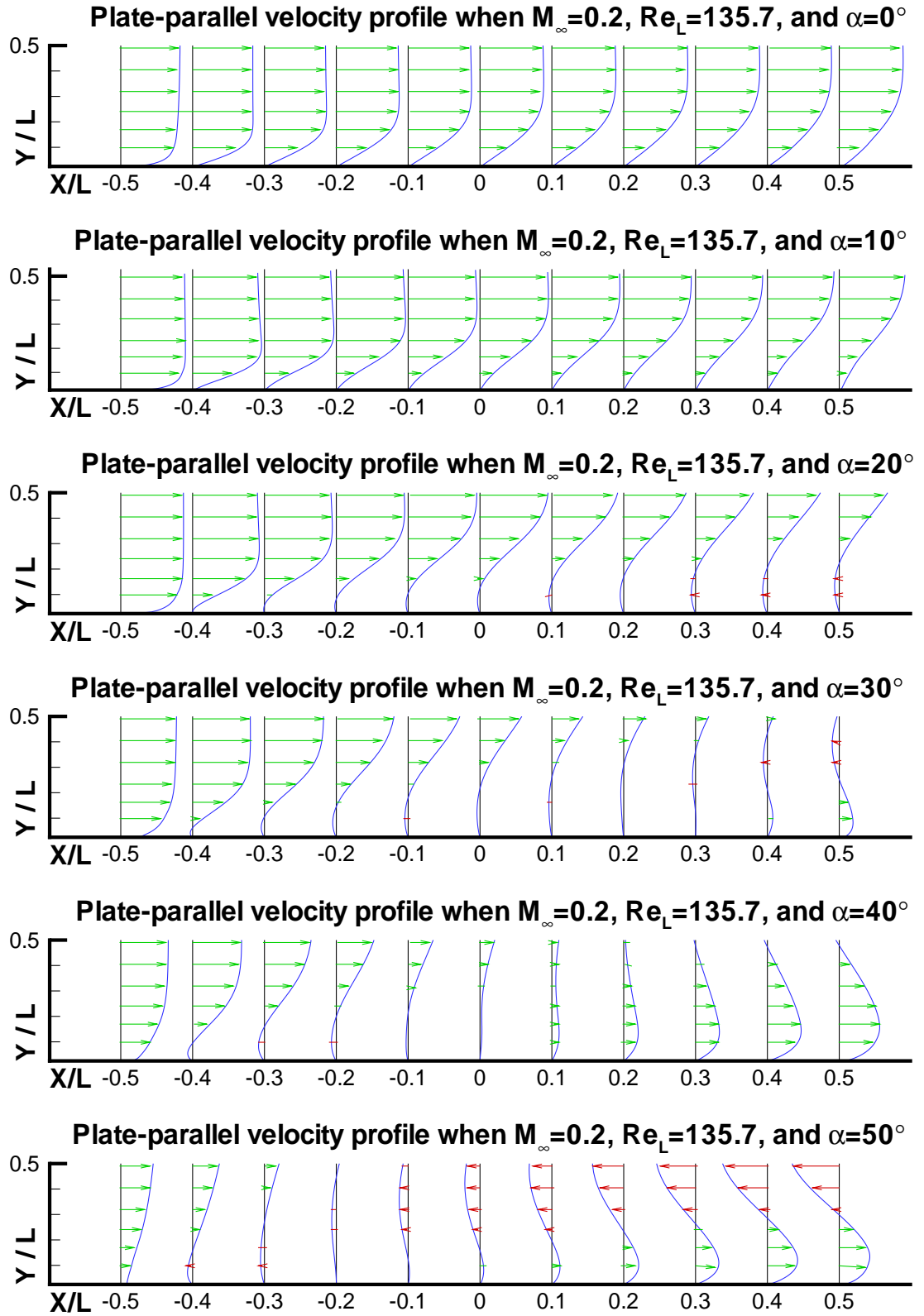
Figure 6.18. Profiles of the velocity component parallel to the plate for flows over a 5% flat plate when M$_\infty$=0.2, Re$_L$=13.57, with angle of attack ranging from 0° to 50°
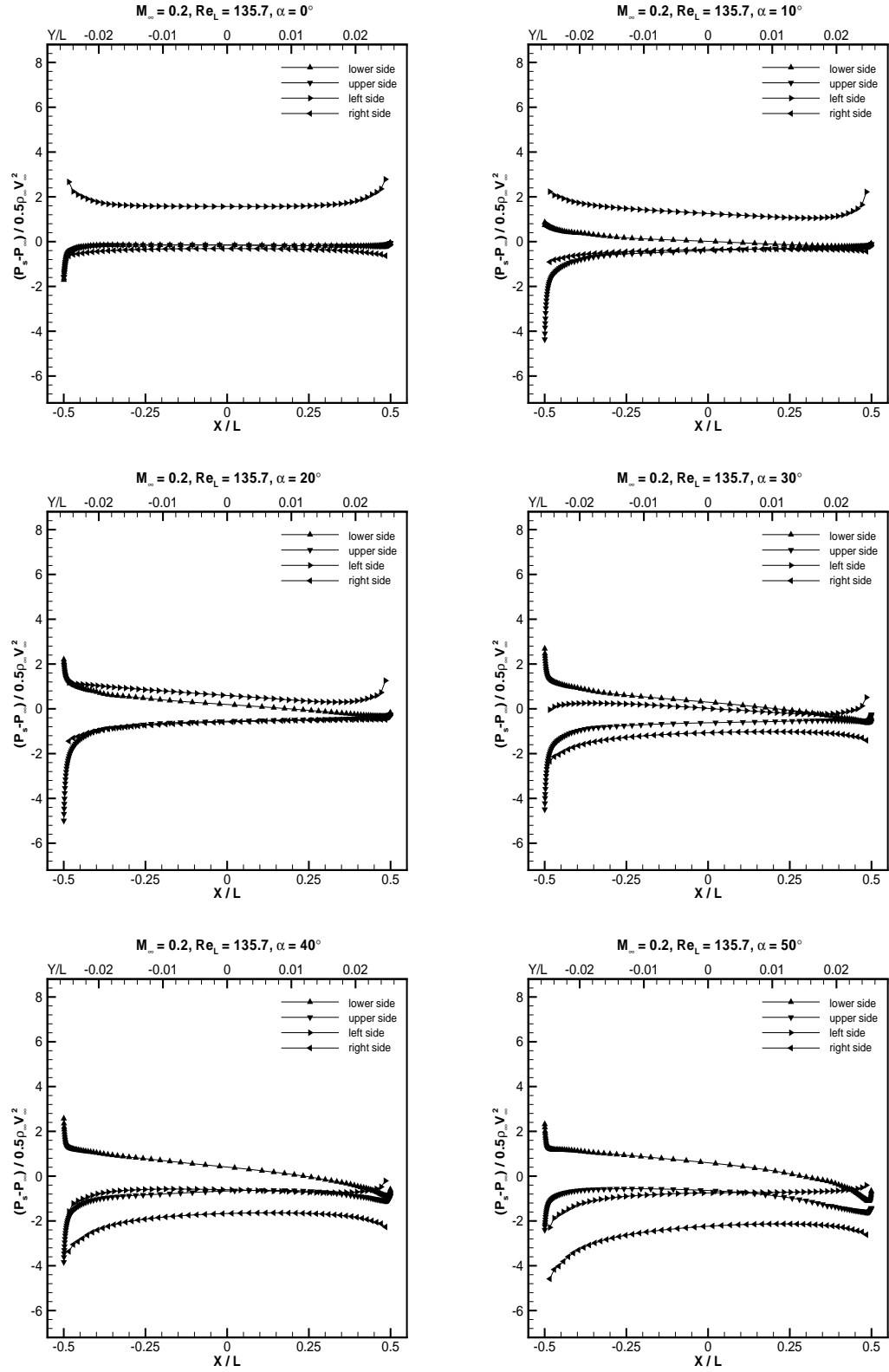
Figure 6.19. Distributions of the pressure coefficient for flows over a 5% flat plate when M∞=0.2, Re_L=13.57, with angle of attack ranging from 0° to 50°

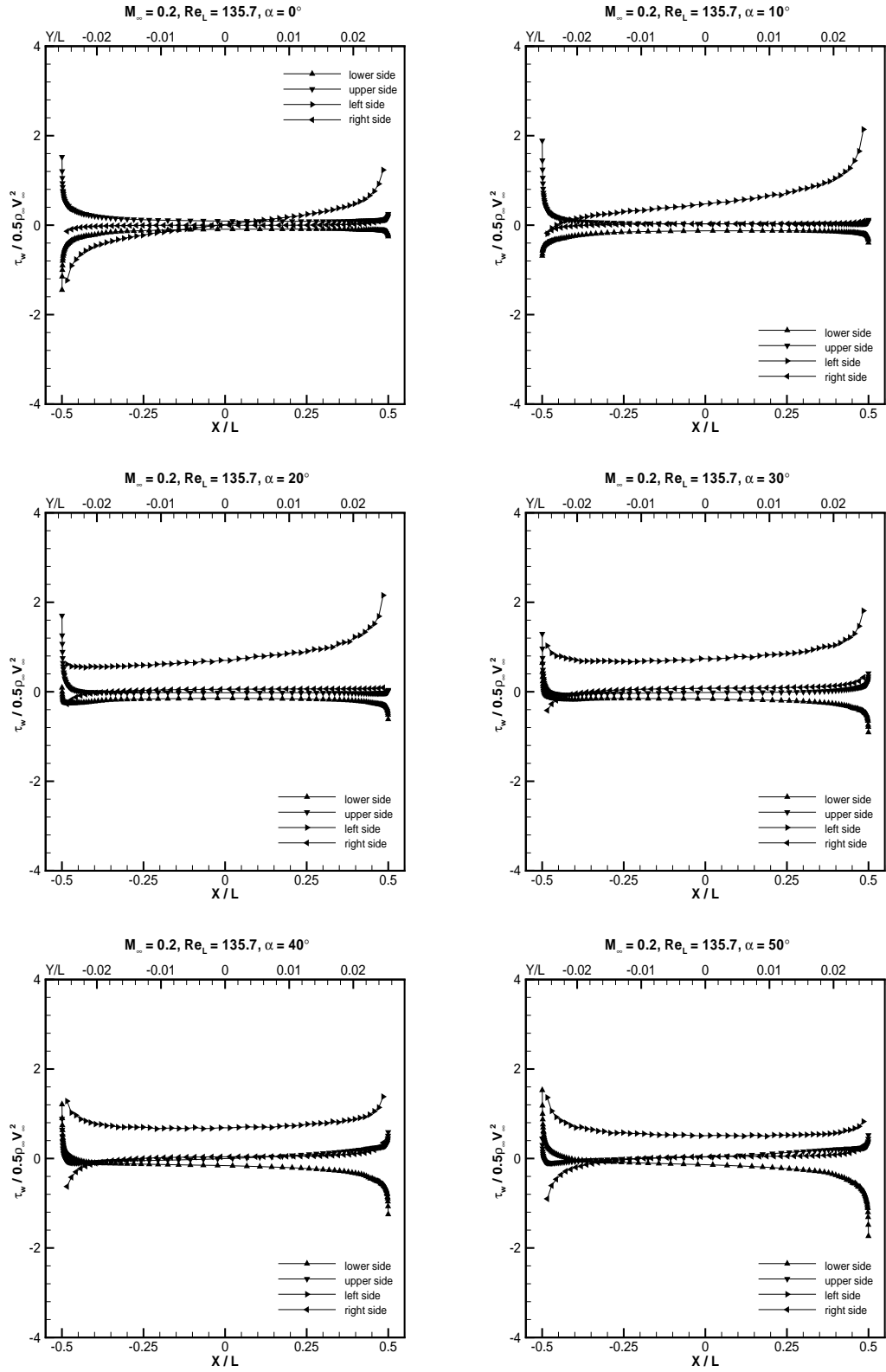**Figure 6.20. Distributions of the skin friction coefficient for flows over a 5% flat plate when M∞=0.2, ReL=13.57, with angle of attack ranging from 0° to 50°**
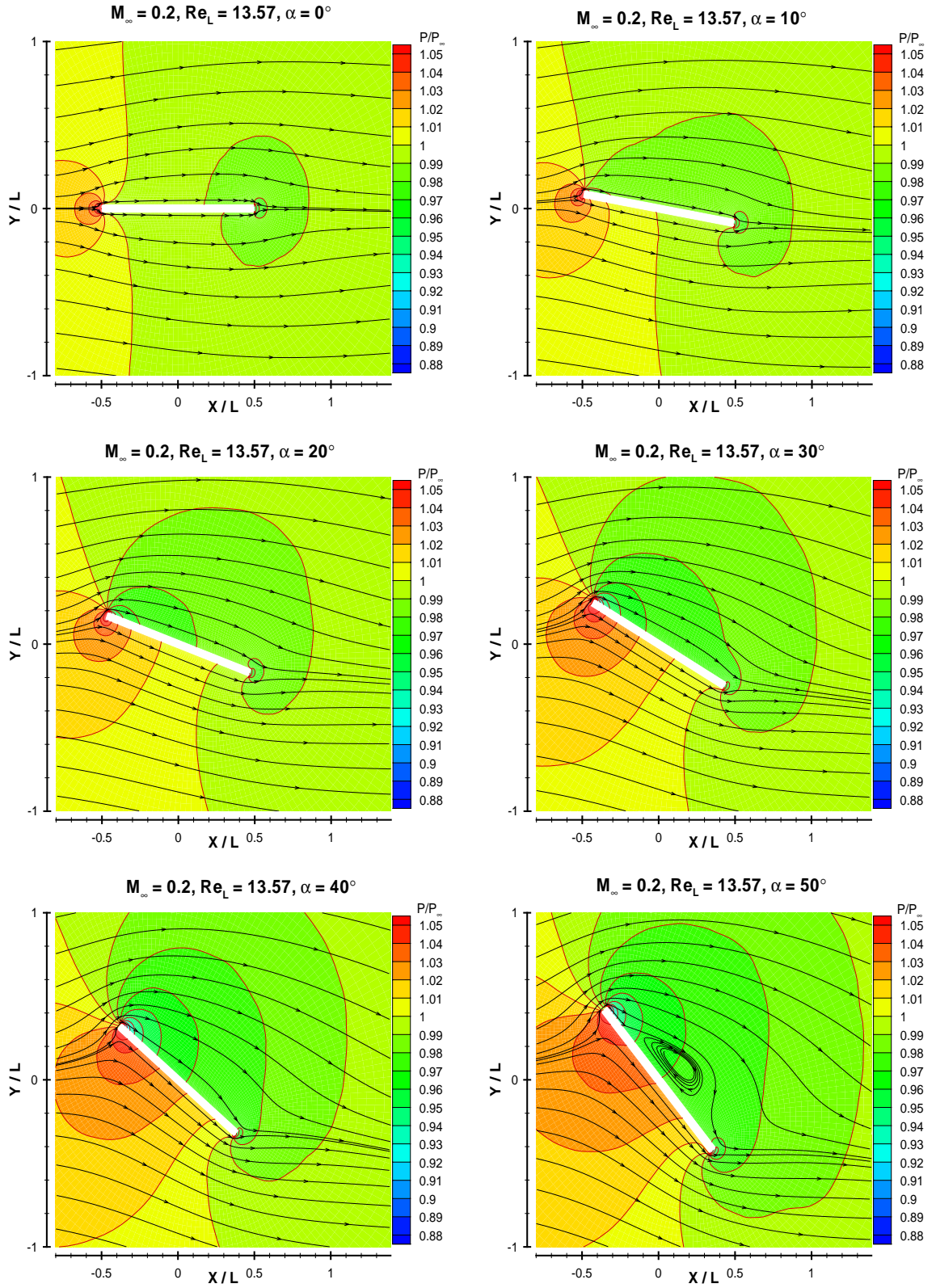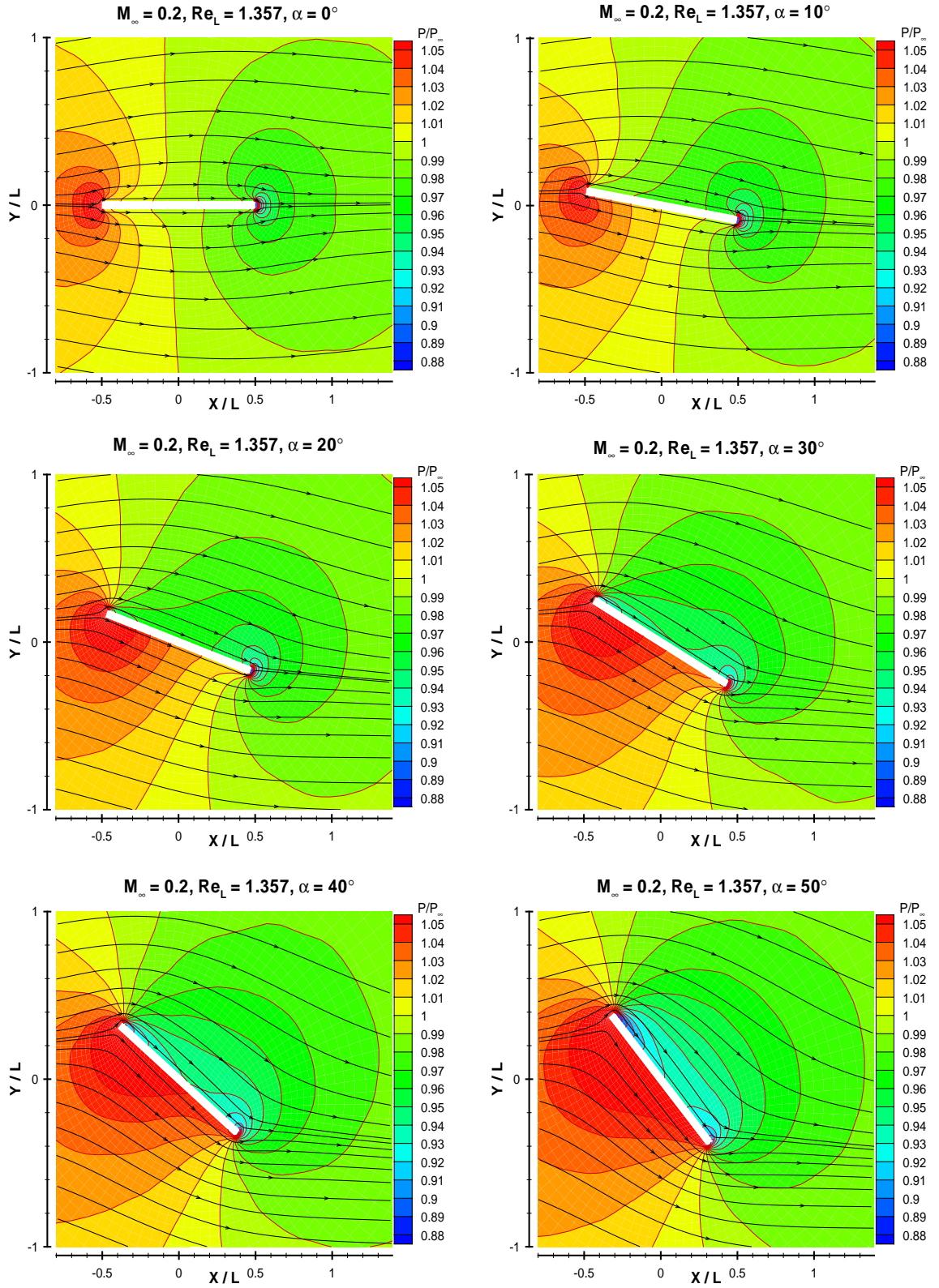
Figure 6.21. Pressure field and streamlines for flows over a 5% flat plate when M∞=0.2, ReL=1.357, with angle of attack ranging from 0° to 50°

Plate-parallel velocity profile when M$_\infty$=0.2, Re$_L$=1.357, and α=0°

Plate-parallel velocity profile when M$_\infty$=0.2, Re$_L$=1.357, and α=10°

Plate-parallel velocity profile when M$_\infty$=0.2, Re$_L$=1.357, and α=20°

Plate-parallel velocity profile when M$_\infty$=0.2, Re$_L$=1.357, and α=30°

Plate-parallel velocity profile when M$_\infty$=0.2, Re$_L$=1.357, and α=40°

Plate-parallel velocity profile when M$_\infty$=0.2, Re$_L$=1.357, and α=50°
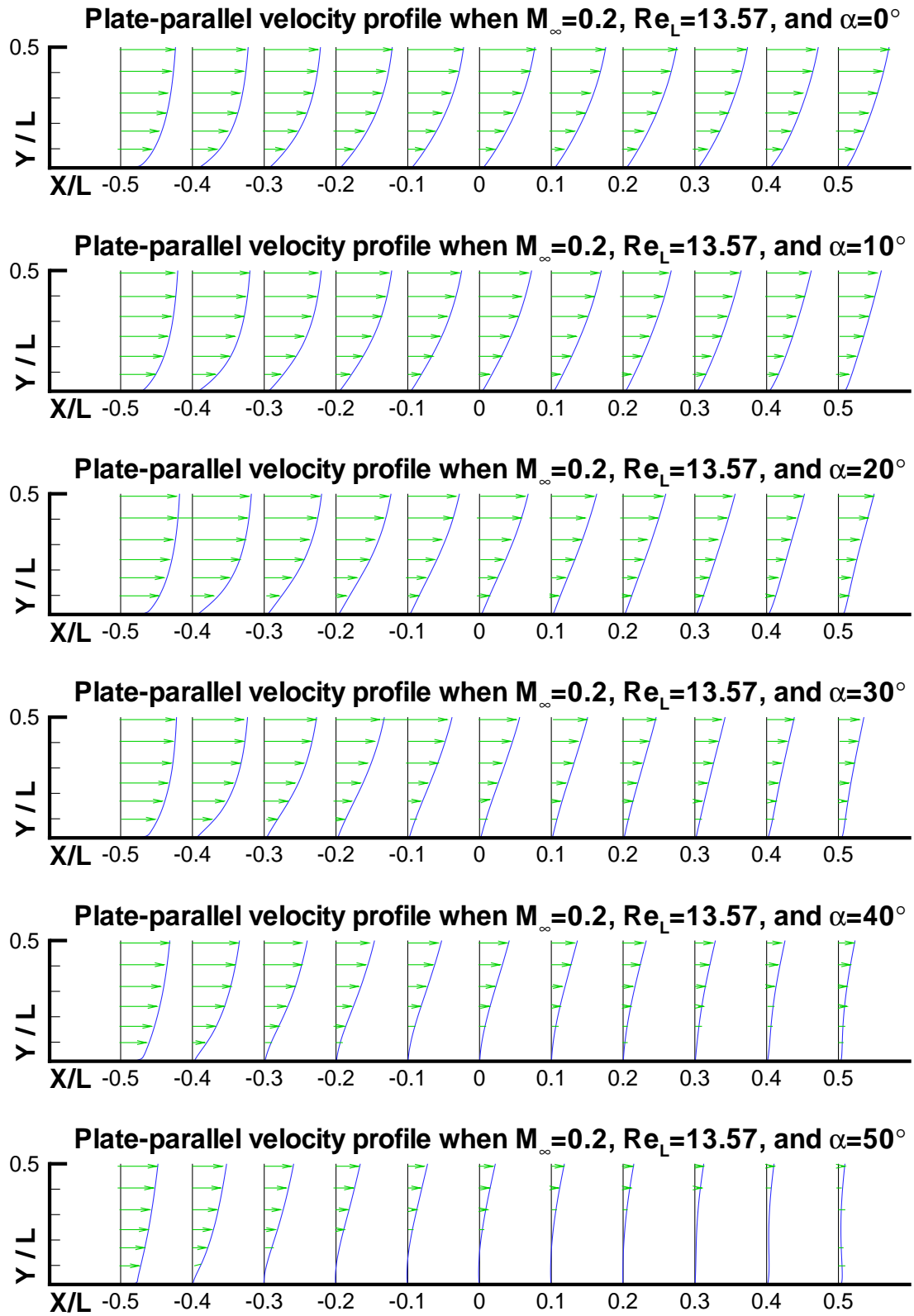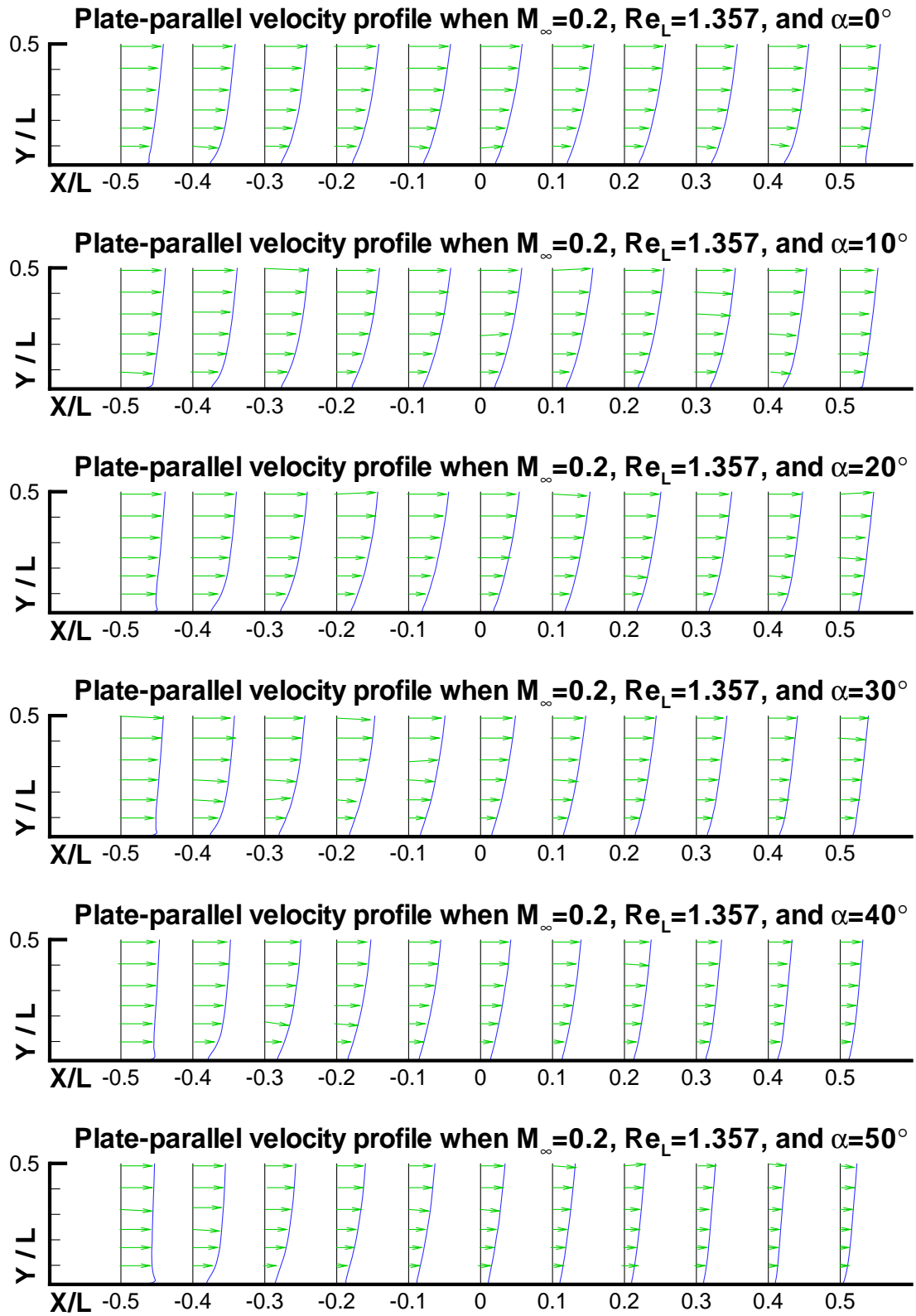
Figure 6.22. Profiles of the velocity component parallel to the plate for flows over a 5% flat plate when M$_\infty$=0.2, Re$_L$=1.357, with angle of attack ranging from 0° to 50°
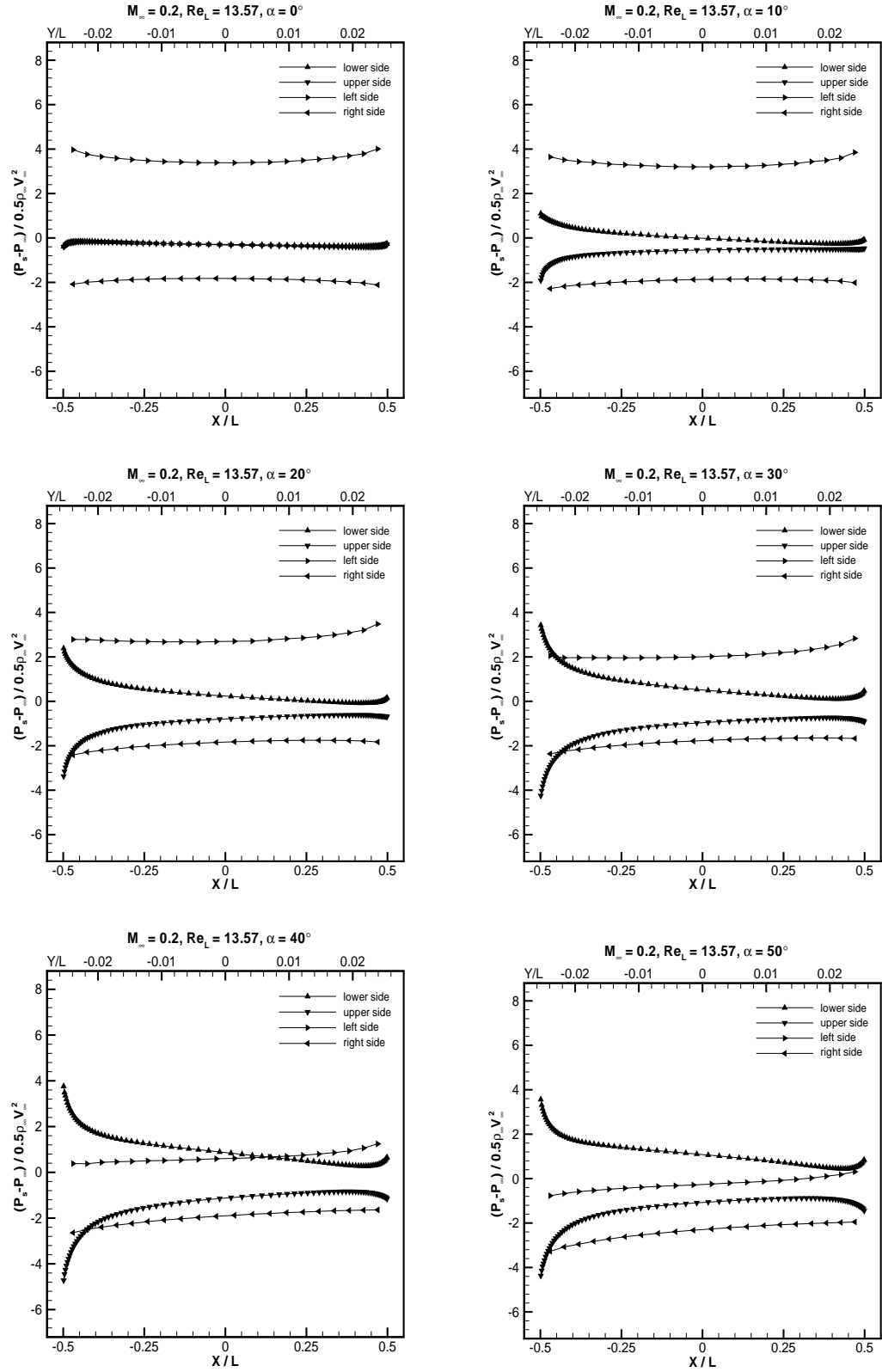
Figure 6.23. Distributions of the pressure coefficient for flows over a 5% flat plate when M∞=0.2, ReL=1.357, with angle of attack ranging from 0° to 50°

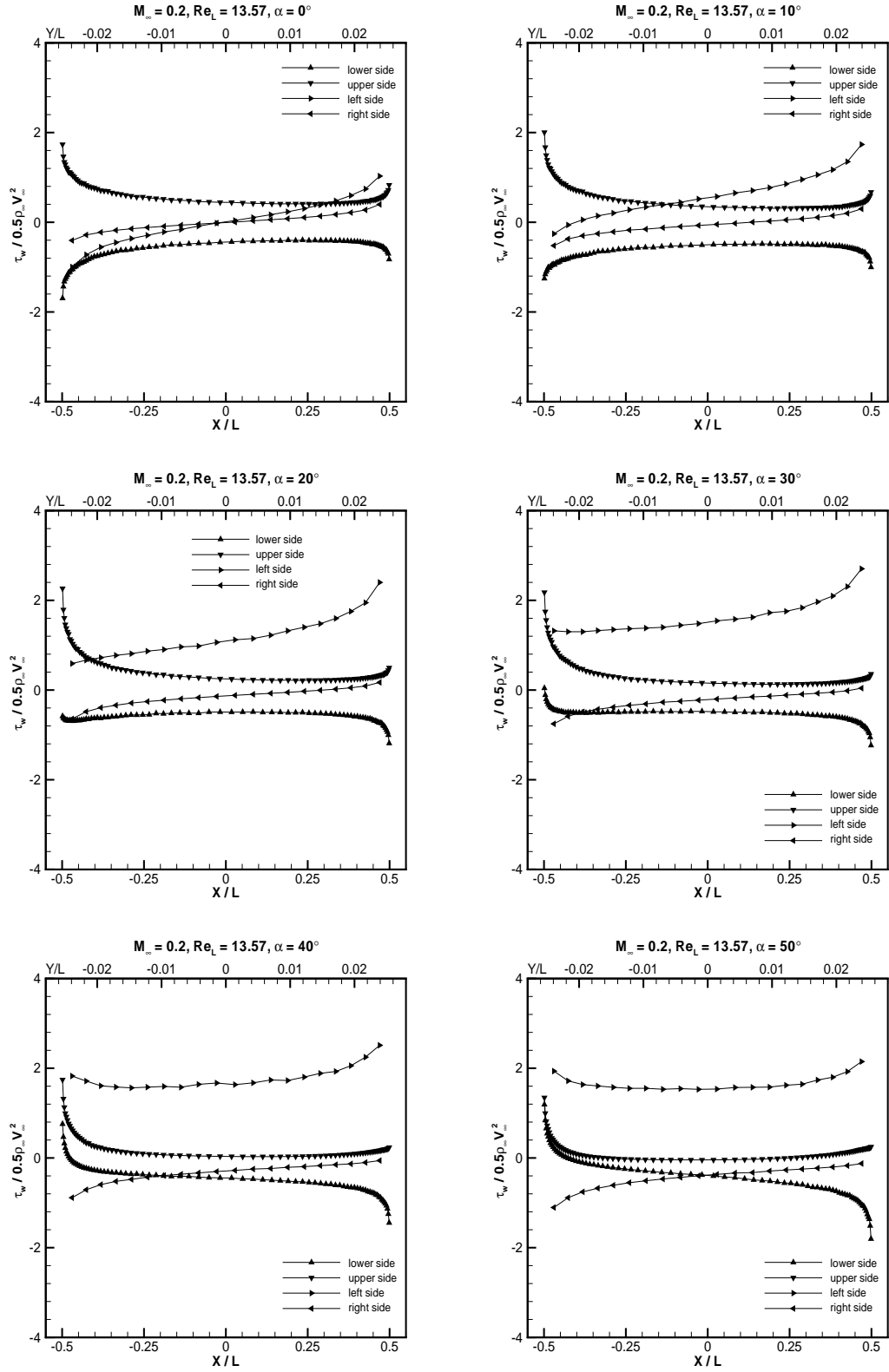**Figure 6.24. Distributions of the skin friction coefficient for flows over a 5% flat plate when M∞=0.2, ReL=1.357, with angle of attack ranging from 0° to 50°**

6.4 Aerodynamic Characteristics of a Micro-Scale Airfoil
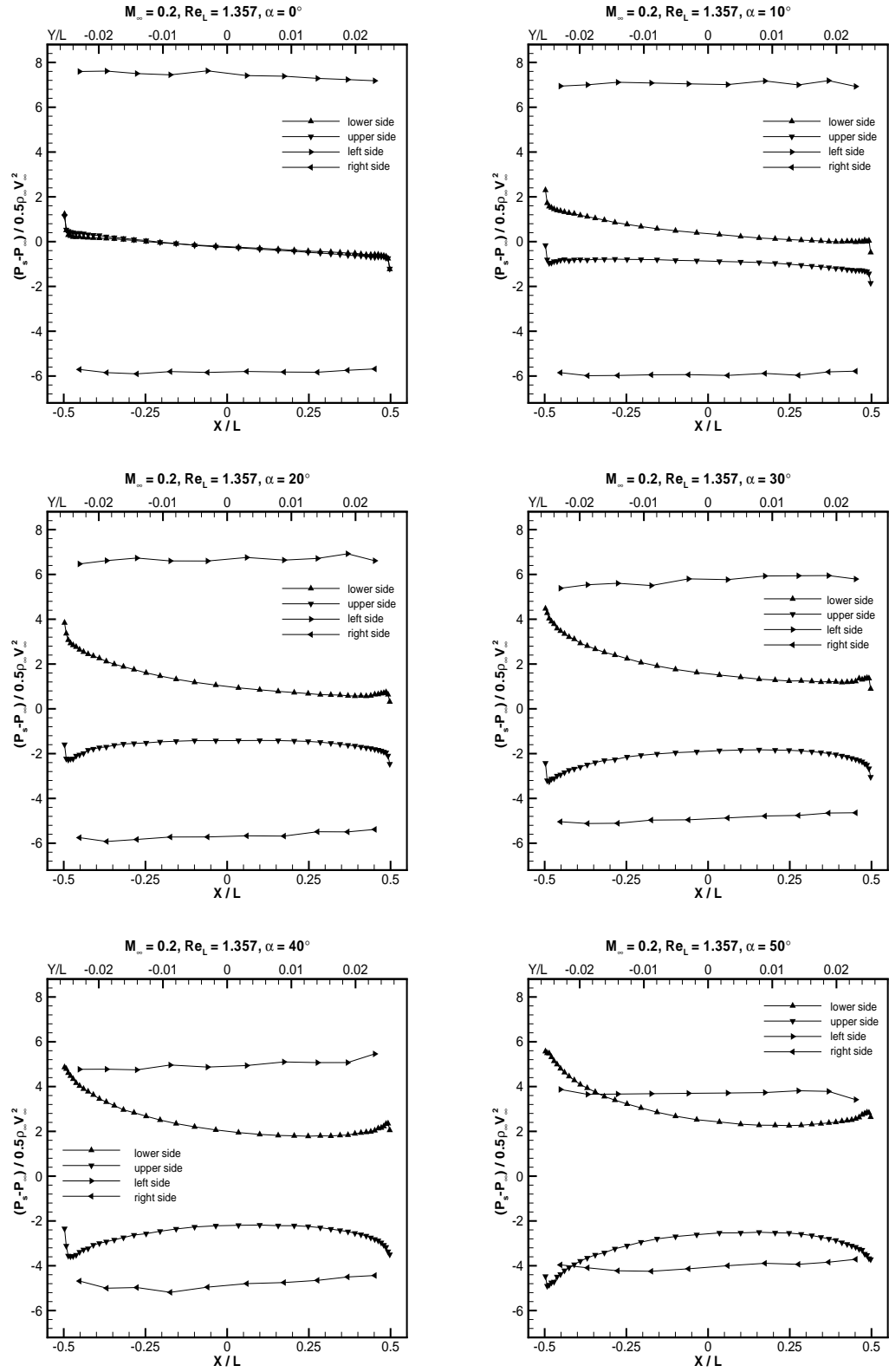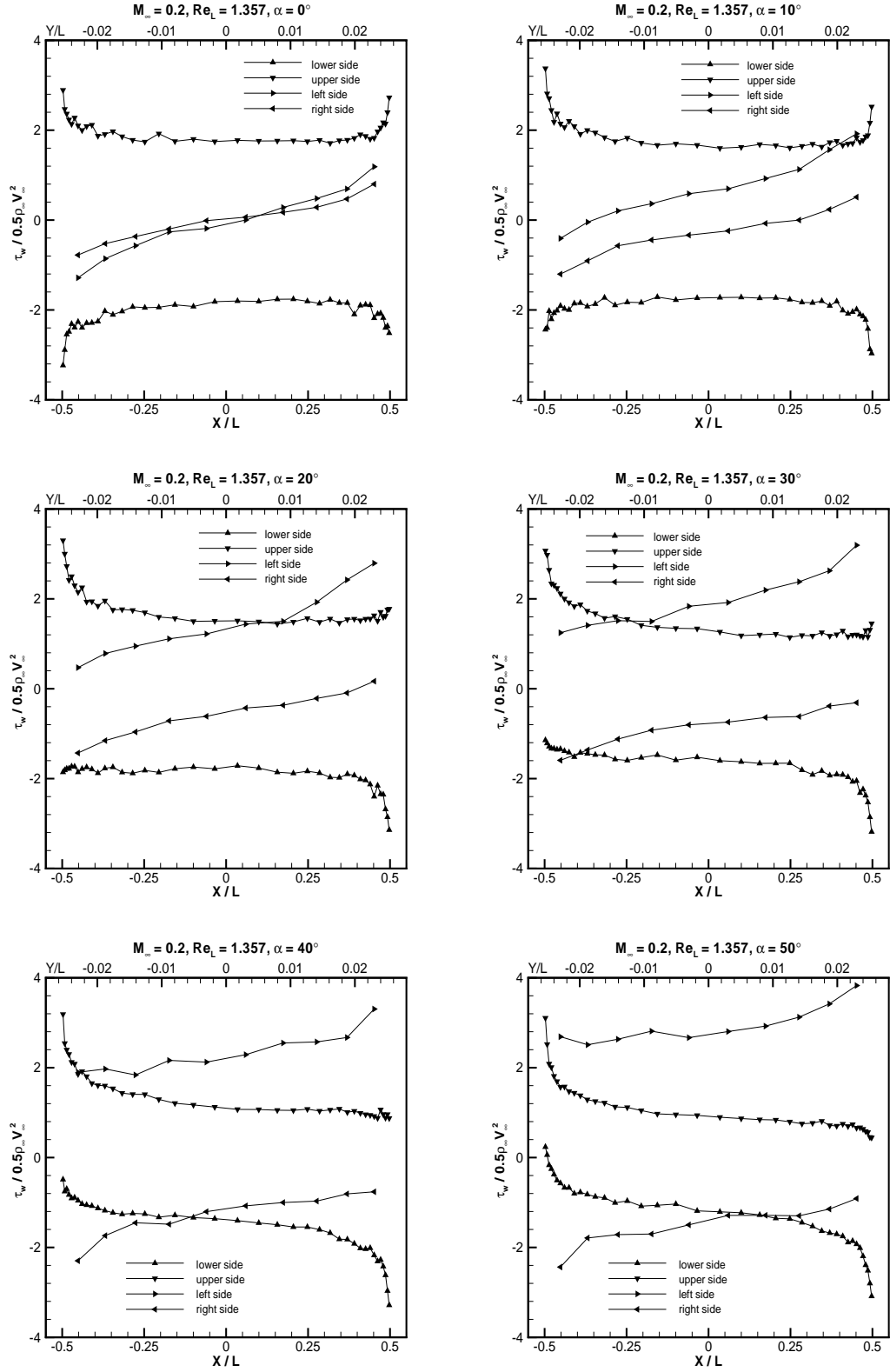
The airfoil theory for invisid flows indicates that the lift slope for a thin airfoil is 2π. However, the lift slope decreases when the flow Reynolds number decreases for conventional streamlined airfoils (Sunada et al., 1997). Sunada concluded that a flat plate with a thickness ratio of 5% has larger lift than conventional streamlined airfoils. In this section, we compare the aerodynamic characteristics of a 5% flat plate for several Reynolds number flows.

Sunada et al. (1997) conducted experiments on a 5% flat plate at the chord Reynolds number of 4×10^3 by towing the airfoil through water in a tank. We plot his experimental data in Figure 6.25. It was estimated that the measurement error is within 18 percent for the lift coefficient and the drag coefficient. The figure shows that the lift slope is 5.8 and the drag coefficient is less than 0.1 at small angle of attack.
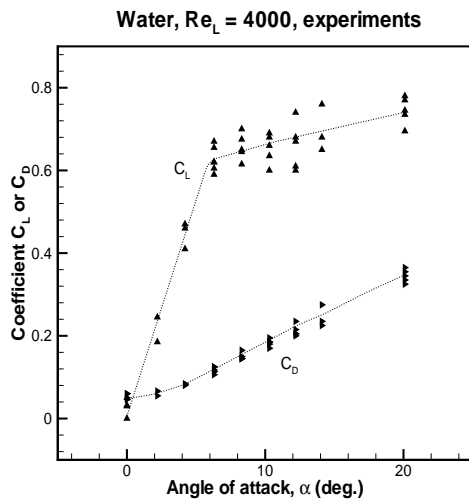
Figure 6.25. Measured drag coefficient and lift coefficient after Sunada, et al. (1997) when the Reynolds number is 4×10^3

Figure 6.26. Drag coefficient and lift coefficient from IP when the Reynolds number is 137.5

The lift coefficient and the drag coefficient calculated for the current simulations are plotted in Figures 6.26-6.28. Figure 6.26 shows the results when Re=135.7. The lift slope is about 3.0 and the drag coefficient is about 0.4 at small angle of attack. The lift

does not increase linearly because the flow is separated when the angle of attack is 20° or larger. Figure 6.27 shows the results when Re=13.57. Here, the lift slope is about 2.8 and the drag coefficient is a little larger than 1 at small angle of attack. Also, the ratio of lift to drag is less than 1 because of the large drag coefficient. Figure 6.28 shows the results when Re=1.357. Here, the lift slope is about 4.2 and the drag coefficient is larger than 4.

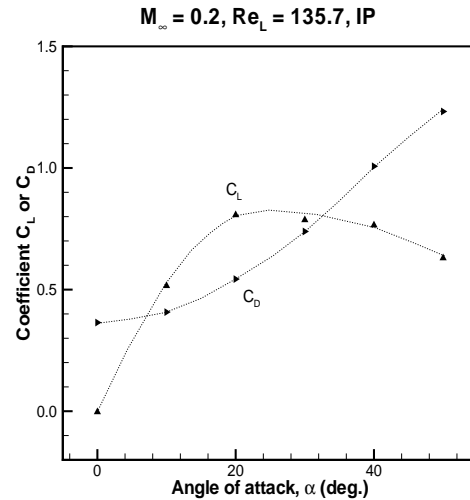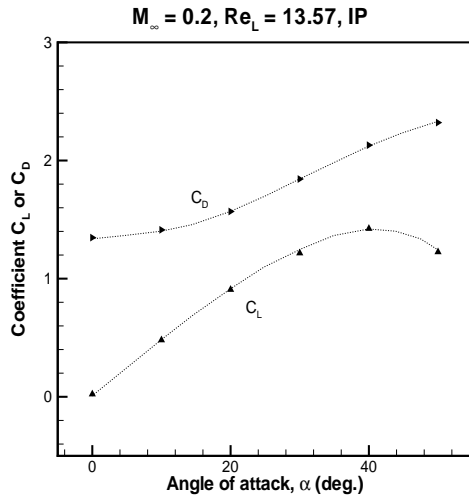**Figure 6.27. Drag coefficient and lift coefficient from IP when the Reynolds number is 13.57**
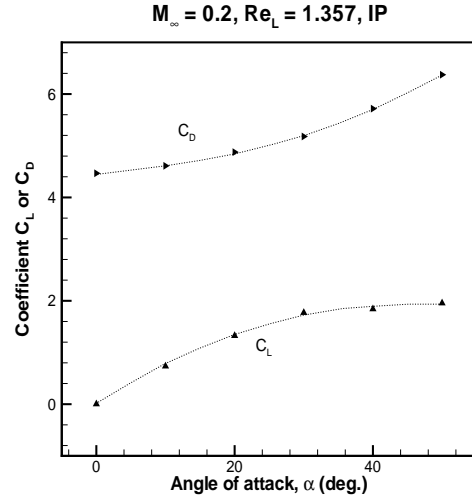
Figure 6.28. Drag coefficient and lift coefficient from IP when the Reynolds number is 1.375

We also calculate the lift coefficient and the drag coefficient of the 5% flat plate under the free molecular condition with Equation 6.8 and Equation 6.9, where α is the angle of attack and $s = \sqrt{V_\infty^2/(2RT)}$. Figure 6.29 shows that the lift slope is as high as 16.5 and the drag coefficient is larger than 7.9. The ratio of lift to drag, however, is less than 1.

$$C_L = \cos\alpha\left[\frac{erf(s\sin\alpha)}{s^2}+\sqrt{\pi}\,\frac{\sin\alpha}{s}\right]-0.05\sin\alpha\left[\frac{erf(s\cos\alpha)}{s^2}+\sqrt{\pi}\,\frac{\cos\alpha}{s}\right] \quad \textbf{(6.8)}$$

$$C_D = \frac{2}{\sqrt{\pi}}\left[\frac{e^{-s^2\sin^2\alpha}}{s}+\sqrt{\pi}\sin\alpha\left(1+\frac{1}{2s^2}\right)erf(s\sin\alpha)+\pi\frac{\sin^2\alpha}{2s}\right]$$

$$+0.05\frac{2}{\sqrt{\pi}}\left[\frac{e^{-s^2\cos^2\alpha}}{s}+\sqrt{\pi}\cos\alpha\left(1+\frac{1}{2s^2}\right)erf(s\cos\alpha)+\pi\frac{\cos^2\alpha}{2s}\right] \quad \textbf{(6.9)}$$
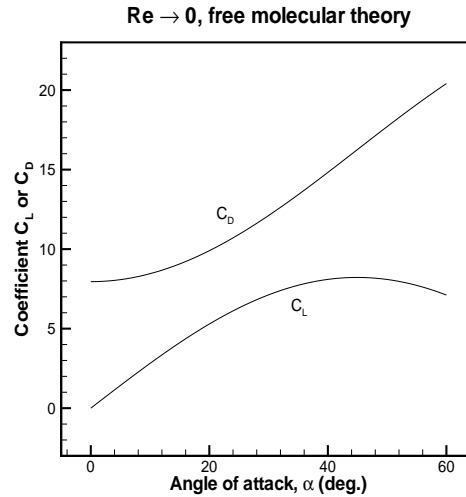
Figure 6.29. Drag and lift coefficients predicted by the free molecular theory

The Reynolds number effects on the lift slope and drag coefficient of the 5% flat plate airfoil are illustrated in Figure 6.30. The results show that there is a minimum lift slope near Reynolds number of 10 for the aerodynamic characteristics of the airfoil, while the drag coefficient keeps increases when the Reynolds number decreases.
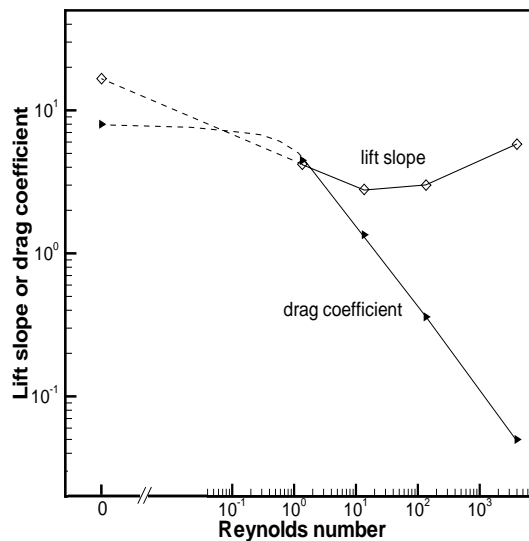
**Figure 6.30. Reynolds number effects on the lift slope and drag coefficient
of the 5% flat plate airfoil**

6.5 Conclusions

It is very important to investigate micro-scale gas flows because understanding of these flows will improve current and potential applications of rapidly emerging micro systems. Studies were performed for flows over a flat plate having a zero thickness and for the aerodynamic characteristics of a flat plate having a thickness ratio of 5% at low Reynolds numbers. It was found that the normalized drag coefficient on the flat plate varies according to $\sqrt{\mathrm{Re}}/M^{0.8}$. It was concluded that there is a minimum lift slope for the 5% flat plate at a Reynolds number near 10, and the drag coefficient monotonically increases with decreasing Reynolds number.

CHAPTER VII

SUMMARY AND CONCLUSIONS

7.1 Summary

The overall objective of the present study was to develop a numerical approach for modeling micro-scale gas flows. The first phase of the study developed an information preservation (IP) method with evaluations. The development included: a principle for updating preserved macroscopic information, an energy flux model for the preserved temperature, a collision model for the preserved macroscopic information, and an implementation of the IP method for general 2D flows. The evaluation of the IP method was performed for several benchmark problems, including thermal Couette flow, high-speed Couette flow, Rayleigh flow, and a flow over a NACA0012 airfoil. The second phase of the study introduced a hybrid continuum/particle approach. Two key issues of a hybrid approach were discussed. One is the information exchange between the two coupled approaches. The other is the continuum breakdown parameter and its cutoff value. The hybrid approach was implemented based on a DSMC code. The final phase of the study applied the hybrid approach simulating flows over a micro-scale flat plate with zero thickness and 5% thickness. Drag on a flat plate was studied for various free stream Mach numbers and Reynolds numbers. Aerodynamic characteristics of the 5% flat plate were also investigated for low Reynolds numbers.

7.2 Conclusions

The results of this study are based on the development of the IP method, the work on the hybrid approach, and the study of flows over a micro-scale flat plate. The major conclusions of the study are as follows:

(1) The information preservation method is developed and implemented for general two-dimensional micro-scale gas flows. The method exhibits much smaller statistical scatter and costs less computational time compared with the DSMC method for low-speed flows. The IP method reduces a sample size by at least three orders of magnitude compared with the DSMC method when simulating subsonic gas flows.

(2) Preserved macroscopic information in the IP method can be described by the transfer equation in kinetic theory with certain forms of microscopic quantities. There is no need to preserve density for simulated particles. The preserved macroscopic velocity and temperature can be updated by particle collisions, particle motion, and pressure effects.

(3) The preserved macroscopic information in the IP method does not have all details of particle microscopic information. Therefore, an energy flux model is proposed to resolve the difference of the translational energy flux between the microscopic reality and the IP representation. The model allows a particle to transport this difference when it crosses a surface while overall energy conservation is implemented.

(4) The collision effects on preserved macroscopic information can be described by a phenomenological collision model. Within this model, collisions equalize the preserved macroscopic information with a weight depending on the collision deflection angle. The shear stress and heat flux of a flow can be correctly modeled.

(5) A continuum/particle hybrid approach is introduced and implemented that couples the IP method and a continuum solver using a continuum/particle interface. The continuum solver that solves the Navier-Stokes equations can use particle cells as ghost cells, and particles can be generated from the continuum domain by either using a flux

balanced condition or by implementing buffer cells and reservoir cells. As a result, this coupling of the two methods is strong, efficient, and adaptive.

(6) The continuum/particle interface is determined using a continuum breakdown parameter. Parameters that combine all terms in the Chapman-Enskog expansion can better indicate the breakdown of the continuum equations than the gradient-length local Knudsen number. The cutoff value of a breakdown parameter, however, depends on the implementation of the information exchange between the two coupled solvers. Using more buffer and reservoir cells can improve the quality of particles that enter into the particle domain from the continuum domain, and thus increase the cutoff value, which may increase the computational efficiency of the hybrid approach.

(7) The hybrid approach speeds up simulations because the time spent on a computational cell in a continuum domain is much less than the time spent on a cell in a particle domain. Therefore, the computational efficiency of the hybrid approach depends on the ratio of the continuum cell number to the particle cell number. However, buffer cells and reservoir cells cost extra time for a hybrid simulation.

(8) The IP method predicts very similar results to the DSMC method when simulating thermal Couette flow (heat transfer between two parallel plates), high-speed Couette flow, Rayleigh flow, and a flow over a NACA0012 airfoil. For the thermal Couette flows, the temperature jump and the normalized heat transfer increase when the flow Knudsen number increases. In addition, the thermal accommodation coefficient of the plates plays an important role on the heat transfer between two plates. For the high-speed Couette flows, the slip velocity, the viscous heating, and the flow temperature increase when the flow Knudsen number increases.

(9) Studies on flow over a flat plate show that rarefied effects become significant when the Reynolds number is small. Such effects include the velocity slip, the compressibility, the viscous heating, and the temperature jump. Drag on the flat plate having a zero thickness depends not only on the flow Reynolds number, but also on the

flow Mach number. Decreasing the flow Reynolds number or the flow Mach number increases the drag coefficient on a flat plate. It is found that the normalized drag coefficient depends on $\sqrt{\text{Re}}/M^{0.8}$ when this parameter is between 1 and 100.

(10) Many results are obtained for flow over a flat plate having a 5% thickness. Such results include: when the free stream pressure decreases, the boundary layer thickness increases; the slip velocity increases; the overall pressure variation increases; the pressure gradient decreases near the leading edge of the plate; flow separation is delayed or even disappeared; and the skin friction increases. For the aerodynamic characteristics of the 5% flat plate, the slope of the lift coefficient decreases from 3.0 at Re=135.7 to 2.8 at Re=13.57 and then increases to 4.2 at Re=1.357. There is a minimum slope of the lift coefficient at the Reynolds number near 10, whereas the drag coefficient monotonically increases when the Reynolds number decreases.

7.3 Recommendations for Further Study

The IP method is still a new method for simulating micro-scale gas flows. Several aspects can be developed by further study. First, new models may be required to better resolve the translational energy flux differences between microscopic reality and the IP representation. Second, a better method is required to solve the continuum equations at rarefied conditions. Third, the IP method can be implemented for 3D flows with parallelization. Fourth, the IP method may be developed to simulate multiple-species gases. Finally, there is need to thoroughly investigate the effects of computational parameters within their physical limits for the IP method. Such parameters include the cell size, the time step, and the number of particles in a cell.

The hybrid approach is also a new technique for simulating flows. In order to obtain maximum benefit from a hybrid approach, there is still a need to investigate the breakdown parameter for continuum equations when simulating general micro-scale flows. It is also important to investigate the way of generating particles from the

continuum domain because this will affect the cutoff value for a continuum breakdown parameter in any implementation.

The present study of flow over micro-scale flat plates shows that the hybrid approach is able to simulate such flows. Therefore, by using the present IP or hybrid methods, many micro-scale gas flows can be studied, which will increase our understanding of micro-scale gas flows.

BIBLIOGRAPHY

Aktas, O. and Aluru, N.R. (2002) A Combined Continuum/DSMC Technique for Multiscale Analysis of Microfluidic Filters. Journal of Computational Physics, Vol. 178, pp. 342-372.

Alder, B. (1997) Highly Discretized Dynamics. Physica A, Vol. 240, pp. 193-195.

Aluru N.R. and Li, G. (2001) Finite Cloud Method: A True Meshless Technique Based on Reproducing Kernel Approximation. International Journal for Numerical Methods in Engineering, Vol. 50(10), pp. 2373-2410.

Arkilic, E.B. (1997) Measurement of the Mass Flow and Tangential Momentum Accommodation Coefficient in Silicon Micromachined Channels. *Ph.D. Thesis*, MIT, Cambridge.

Babovsky H. and Illner, R. (1989) A Convergence Proof for Nanbu's Simulation Method for the Full Boltzmann Equation. SIAM Journal on Numerical Analysis, Vol. 26, pp. 45-65.

Bayt, R. (1999) Analysis, Fabrication and Testing of a MEMS-based Micro Propulsion System. *Ph.D. Thesis*, MIT, Cambridge.

Beskok, A. (1996) Simulations and Models for Gas Flows in Microgeometries. *Ph.D. Thesis*, Princeton University, Princeton.

Beskok, A. (2001) Physical Challenges and Simulation of Micro Fluidic Transport. AIAA Paper No. 2001-0718.

Beskok, A. and Karniadakis, G.E. (1999) A Model for Flows in Channels, Pipes, and Ducts at Micro and Nano Scales. Microscale Thermophysical Engineering, Vol. 3, pp. 43-77.

Bhatnagar, P.L., Gross, E.P. and Krook, M. (1954) Model for Collision Processes in Gases, I. Small Amplitude Processes in Charged and Neutral One-Component Systems. Physics Review, Vol. 94, pp. 511-524.

Bird, G.A. (1970) Breakdown of Translational and Rotational Equilibrium in Gaseous Expansions. AIAA Journal, Vol. 8, pp. 1998-2003.

Bird, G.A. (1976) *Molecular Gas Dynamics*. Clarendon Press, Oxford.

Bird, G.A. (1978) Monte Carlo Simulation of Gas Flows. Annual Review of Fluid Mechanics, Vol.10, pp. 11-31.

Bird, G.A. (1981) Monte Carlo Simulation in an Engineering Context. <u>Progress in Astronautics and Aeronautics</u>, Vol., 74, pp. 239-255.

Bird, G.A. (1994) *Molecular Gas Dynamics and the Direct Simulation of Gas Flows*. Oxford Science Publications, New York.

Bird, G.A. (1998) Recent Advances and Current Challenges for DSMC. <u>Computers & Mathematics with Applications</u>. Vol. 35, pp. 1-14.

Bird, G.A. (2001) Forty Years of DSMC, and Now? In *Rarefied Gas Dynamics: 22nd International Symposium*, edited by T.J. Bartel and M.A. Gallis, Sydney, pp. 372-380.

Blankinship, S. (2001) New Miniturbine Takes Aim at Microturbine Market. <u>Power Engineering</u>, Vol. 105(10), pp. 77-77.

Bourgat, J.F., Tallec, P.L. and Tidriri, M.D. (1996) Coupling Boltzmann and Navier-Stokes Equations by Friction. <u>Journal of Computational Physics</u>, Vol. 127, pp. 227-245.

Boyd, I.D., Chen, G. and Candler, G.V. (1995) Predicting Failure of the Continuum Fluid Equations in Transitional Hypersonic Flows. <u>Physics of Fluids</u>, Vol. 7, pp. 210-219.

Cai, C., Boyd, I.D., Fan, J. and Candler, G.V. (2000) Direct Simulation Methods for Low-Speed Microchannel Flows. <u>Journal of Thermophysics and Heat Transfer</u>, Vol. 14(3), pp. 368-378.

Chapman, S. and Cowling, T.G. (1970) *The Mathematical Theory of Non-Uniform Gases*, 3rd edition. Cambridge Univ. Press, Cambridge, UK.

Choi, J., Jeon, W.P., and Choi, H. (2002) Control of Flow Around an Airfoil Using Piezoceramic Actuators. <u>AIAA Journal</u>, Vol. 40(5), pp. 1008-1010.

Choi, Y.H. and Merkle, C.L. (1993) The Application of Preconditioning in Viscous Flows. <u>Journal of Computational Physics</u>, Vol. 105, pp. 207-223.

Dietrich, S. and Boyd, I.D. (1996) Scalar and Parallel Optimized Implementation of the Direct Simulation Monte Carlo Method. <u>Journal of Computational Physics</u>, Vol. 126, pp. 328-342.

Ehrfeld, W. and Ehrfeld, U. (2001) Progress and Profit Through Micro Technologies, Commercial Applications of MEMS/MOEMS. In *MEMS Components and Applications for Industry, Automobiles, Aerospace, and Communication*, Ed. H. Helvajian, S.W. Janson and F. Larmer, pp. xi-xx.

Epstein, A.H., and Senturia, S.D. (1997) Microengineering: Macro Power from Micro Machinery. <u>Science</u>, Vol. 276, pp. 1211.

Fan J. (2002) A Generalized Soft-Sphere Model for Monte Carlo Simulation. Physics of Fluids, Vol. 14, pp.4256-4265.

Fan J. and Shen C. (1999) Statistical Simulation of Low-Speed Unidirectional flows in Transition Regime. In *Proceedings of the 21th International Symposium on Rarefied Gas Dynamics*, edited by R. Brum, et al., Marseille, France, pp. 245-252.

Fan J. and Shen C. (2001) Statistical Simulation of Low-Speed Rarefied Gas Flows. Journal of Computational Physics, Vol. 167, pp. 393-412.

Fan, J., Boyd, I.D., Cai, C., Hennighausen, K. and Candler, G.V. (2001) Computation of Rarefied Flows Around a NACA 0012 Airfoil. AIAA Journal, Vol. 39(4), pp. 618-625.

Fan, L.S., Tai, Y.C. and Muller, R.S. (1988) IC-Processed Electrostatic micromotors. In *Tech. Dig. Int. Electron Dev. Meet.(IEDM)*, San Francisco, pp. 666-669.

Flekkøy, E.G., Wagner, G. and Feder, J. (2000) Hybrid Model for Combined Particle and Continuum Dynamics. Europhysics Letters, Vol. 52(3), pp. 271-276.

Freeman, D.M., Aranyosi, A.J., Gordon, M.J. and Hong, S.S. (1998) Multidimensional Motion Analysis of MEMS Using Computer Microvision. In Solid-State Sensor and Actuator Workshop, Hilton-Head Island, pp. 150-155.

French, P.J. (2000) MEMS/MOEMS Technology Capabilities and Trends. In *MEMS and MOEMS Technology and Applications*, Ed. P.R. Choudhury, pp.1-40.

Gad-el-Hak, M. (1999) The Fluid Mechanics of Microdevices - The Freeman Scholar Lecture. Journal of Fluids Engineering, Vol. 121, pp. 5-33.

Gad-el-Hak, M. (2001) Flow Control: The Future. Journal of Aircraft, Vol. 38(3), pp. 402-418.

Garcia, A.L., Bell, J.B., Crutchfield, W.Y. and Alder, B.J. (1999) Adaptive Mesh and Algorithm Refinement Using Direct Simulation Monte Carlo. Journal of Computational Physics, Vol. 154, pp. 134-155.

Gombosi, T.I. (1994) *Gaskinetic Theory*. Cambridge University Press, Cambridge, UK.

Hadjiconstantinou, N.G. (1999) Hybrid Atomistic-Continuum Formulations and the Moving Contact-Line Problem. Journal of Computational physics, Vol. 154, pp. 245-265.

Hagleitner C., Hierlemann A., Lange, D., Kummer A., Kerness N., Brand O., and Baltes H. (2001) Smart Single-Chip Gas Sensor Microsystem. Nature, Vol. 414(6861), pp. 293-296.

Haile, J.M. (1993) *Molecular Dynamics Simulation: Elementary Methods*. Wiley-Interscience, New York.

Harley, J.C., Huang, Y., Bau, H.H. and Zemel, J.N. (1995) Gas Flow in Micro-Channels. Journal of Fluid Mechanics, Vol. 284, pp. 257-274.

Hash, D.B. and Hassan, H.A. (1996a) A Decoupled DSMC/Navier-Stokes Analysis of a Transitional Flow Experiment. *AIAA Paper* No. 96-0353.

Hash, D.B. and Hassan, H.A. (1996b) Assessment of Schemes for Coupling Monte Carlo and Navier-Stokes Solution Methods. Journal of Thermophysics and Heat Transfer, Vol. 10, pp. 242-249.

Hash, D.B. and Hassan, H.A. (1997) Two-Dimensional Coupling Issues of Hybrid DSMC/Navier-Stokes Solvers. *AIAA Paper* No. 97-2507.

Hennighausen K. (2001) Fluid Mechanics of Microscale Flight. *Ph.D. Thesis*, University of Minnesota, Minneapolis.

Hirsh, C. (1991) *Numerical Computation of Internal and External Flows, II*. John Wiley & Sons, West Sussex, England.

Ho, C.-M., and Tai, Y.-C. (1998) Micro-Electro-Mechanical Systems (MEMS) and Fluid Flows. Annual Review of Fluid Mechanics, Vol. 30, pp. 579-612.

Ivanov, M.S. and Gimelshein, S.F. (1998) Computational Hypersonic Rarefied Flows. Annual Review of Fluid Mechanics, Vol. 30, pp. 469-505.

Kaplan, C.R. and Oran, E.S. (2002) Nonlinear Filtering for Low-Velocity Gaseous Microflows. AIAA Journal, Vol. 40, pp.82-90.

Karniadakis, G.E. and Beskok, A. (2002) *Micro Flows: Fundamentals and Simulation*. Springer-Verlag New York, Inc., New York.

Karniadakis, G.E. and Sherwin, S.J. (1999) *Spectral/Hp Element Methods for CFD*. Oxford University Press, New York.

Kogan, M.N. (1973) Molecular Gas Dynamics. Annual Review of Fluid Mechanics, Vol. 5, pp. 383-404.

Kolesar, E.S. and Restin, R.R. (1998) Review and Summary of a Silicon Micromachined Gas Chromatography System. IEEE Transactions on Components Packaging and Manufacturing Technology Part B-Advanced Packaging, Vol. 21(4), pp. 424-328.

Kosuge, S., Aoki, K. and Takata, S. (2001) Heat Transfer in a Gas Mixture Between Two Parallel Plates: Finite-Difference Analysis of the Boltzmann Equation. In *Rarefied Gas Dynamics: 22nd International Symposium*, edited by T.J. Bartel and M.A. Gallis, Sydney, pp.289-296.

Liou W.W. and Fang Y. (2000) Implicit Boundary Conditions for Direct Simulation Monte Carlo Method in MEMS Flow Predictions. Computer Modeling in Engineering & Science, Vol. 1, pp. 119-128.

Liou W.W. and Fang Y. (2001) The Development of a Burnett Equations Solver for Microfluid Flow and Heat Transfer Simulations. *AIAA Paper* No. 2001-3046.

Liu, V.C. (1959) On the Drag of a Flat Plate at Zero Incidence in Almost-Free-Molecule Flow. Journal of Fluid Mechanics, Vol., 5, pp. 481-496.

Lofdahl, L. and Gad-el-Hak, M. (1999) MEMS Applications in Turbulence and Flow Control. Progress in Aerospace Sciences, Vol. 35(2), pp. 101-203.

Lumpkin, F.E., III, Stuart, P.C. and LeBeau, G.J. (1996) Enhanced Analyses of Plume Impingement During Shuttle-Mir Docking Using a Combined CFD and DSMC Methodology. *AIAA Paper* No. 96-1877.

MacCormack, R.W. (1969) Effect of Viscosity in Hypervelocity Impact Cratering. *AIAA Paper* No. 69-354.

MacCormack, R.W. and Candler, G.V. (1989) The Solution of the Navier-Stokes Equations Using Gauss-Seidel Line Relaxation. Computers & Fluids, Vol. 17, pp. 135-150.

McNeely, M. (1998) Microturbine designed for Mechanical Drive Applications. Diesel Progress North American Edition, Vol. 64(5), pp. 38(2).

Mirels, H. (1951) Estimate of Slip Effect on Compressible Laminar-Boundary-Layer Skin Friction. *NACA TN* 2609.

Morris D.L., Hannon, L. and Garcia, A.L. (1992) Slip Length in a Dilute Gas. Physical Review A, Vol. 46, pp. 5279-5281.

Muntz, E.P. (1989) Rarefied Gas Dynamics. Annual Review of Fluid Mechanics, Vol. 21, pp. 387-417.

Myong, R.S. (2001) A Computational Method for Eu's Generalized Hydrodynamic Equations of Rarefied and Microscale Gasdynamics. Journal of Computational Physics, Vol. 168, pp. 47-72.

Nanbu, K. (1980) Direct Simulation Scheme Derived from the Boltzmann Equation. I. Multicomponent Gases. Journal of the Physical Society of Japan, Vol. 45, pp. 2042-2049.

Oh, C.K. and Oran, E.S. (1998) A New Hybrid Algorithm: Navier-Stokes as a DSMC Filter. *AIAA Paper* No. 98-0849.

Ohwada, T. (1993) Structure of Normal Shock Waves: Direct Numerical Analysis of the Boltzmann Equation for Hard-Sphere Molecules. Physics of Fluids A, Vol. 5, pp. 217.

Ohwada, T. (1996) Heat Flow and Temperature and Density Distributions in a Rarefied Gas Between Parallel Plates with Different Temperatures. Finite-Difference Analysis of the Nonlinear Boltzmann Equation for Hard-Sphere Molecules. Physics of Fluids, Vol. 8, pp. 2153-2160.

Ohwada, T., Aoki, K. and Sone, Y. (1989) Heat Transfer and Temperature Distribution in a Rarefied Gas Between Two Parallel Plates with Different Temperatures: Numerical Analysis of the Boltzmann Equation for a Hard Sphere Molecule. In Rarefied Gas Dynamics: Theoretical and Computational Techniques, edited by Muntz, E.P., et al., Washington, pp. 70.

Oran, E.S., Oh, C.K. and Cybyk, B.Z. (1998) Direct Simulation Monte Carlo: Recent Advances and Applications. Annual Review of Fluid Mechanics, Vol. 30, pp. 403-441.

Pan, L.S., Liu, G.R., Khoo, B.C. and Song, B. (2002) Modified Direct Simulation Monte Carlo Method for Low-Speed Microflows. Journal of Micromechanics and Microengineering, Vol. 10, pp. 21-27.

Pan, L.S., Ng, T.Y., Xu, D. and Lam, K.Y. (2001) Molecular Block Model Direct Simulation Monte Carlo Method for Low Velocity Microgas Flows. Journal of Micromechanics and Microengineering, Vol. 11, pp. 181-188.

Peyret, R. and Taylor, T.D. (1983) *Computational Methods for Fluid Flow*. Springer-Verlag, Berlin.

Pong, K.C., Ho, C.M., Liu, J. and Tai, Y.C. (1994) Non-linear Pressure Distribution in Uniform Microchannels. In *Application of Microfabrication to Fluid Mechanics, ASME Winter Annual Meeting*, Chicago, pp. 51-56.

Reddy, J.N. and Gartling, D.K. (1994) *The Finite Element Method in Heat Transfer and Fluid Dynamics*. CRC Press, Boca Raton.

Rossi, C., Do, C.T., Esteve D. and Larangot B. (2001) Design, Fabrication and Modeling of MEME-Based Microthrusters for Space Application. Smart Materials & Structures, Vol. 10(6), pp. 1156-1162.

Roveda, R., Goldstein, D.B. and Varghese, P.L. (1998) Hybrid Euler/Particle Approach for Continuum/Rarefied Flows. Journal of Spacecraft and Rockets, Vol. 35(4), pp. 258-265.

Roveda, R., Goldstein, D.B. and Varghese, P.L. (2000) Hybrid Euler/Direct Simulation Monte Carlo Calculation of Unsteady Slit Flow. Journal of Spacecraft and Rockets, Vol. 37(6), pp. 753-760.

Salomons E. and Mareschal M. (1992) Usefulness of the Burnett Description of Strong Shock Waves. Physical Review Letters, Vol. 69, pp. 269-272.

Schaaf, S.A. (1950) A Note on the Flat Plate Drag Coefficient. *Report* No. HE-150-66, Institute of Engineering Research, University of California, Berkley.

Schaaf, S.A. and Sherman, F.S. (1954) Skin Friction in Slip Flow. Journal of the Aeronautical Science, Vol. 21, pp. 85-90.

Senturia, S.D. (2001) *Microsystem Design*. Kluwer Academic Publishers, Norwell.

Shen, C., Jiang, J.Z. and Fan, J. (2001) Information Preservation Method for the Case of Temperature Variation. In *Rarefied Gas Dynamics: 22nd International Symposium*, edited by T.J. Bartel and M.A. Gallis, Sydney, pp.185-192.

Sone, Y., Ohwada, T. and Aoki, K. (1989) Temperature Jump and Knudsen Layer in a Rarefied Gas over a Plate Wall: Numerical Analysis of the Linearized Boltzmann Equation for Hard-Sphere Molecules. Physics of Fluids A, Vol. 1, pp. 363.

Sun, Q., Boyd, I.D. and Candler, G.V. (2002) Numerical Simulation of Gas Flow over Microscale Airfoils. Journal of Thermophysics and Heat Transfer, Vol. 16, pp. 171-179.

Sun, Q., Boyd, I.D. and Fan, J. (2001) Development of an Information Preservation Method for Subsonic, Micro-Scale Gas Flows. In *Rarefied Gas Dynamics: 22nd International Symposium*, edited by T.J. Bartel and M.A. Gallis, Sydney, pp. 547-533.

Sunada, S., Sakaguchi, A. and Jawachi, K. (1997) Airfoil Section Characteristics at a Low Reynolds Number. Journal of Fluids Engineering. Vol. 119, pp. 129-135.

Tallec, P.L. and Mallinger F. (1997) Coupling Boltzmann and Navier-Stokes Equations by Half Fluxes. Journal of Computational Physics, Vol. 136, pp. 51-67.

Teagan, W.P. and Springer, G.S. (1968) Heat-Transfer and Density-Distribution Measurements Between Parallel Plates in the Transition Regime. The Physics of Fluids, Vol. 11, pp. 497-606.

Tiwari, S. (1998) Coupling of the Boltzmann and Euler Equations with Automatic Domain Decomposition. Journal of Computational Physics, Vol. 144, pp. 710-726.

Tiwari, S. and Klar, A. (1998) An Adaptive Domain Decomposition Procedure for Boltzmann and Euler Equations. Journal of Computational and Applied Mathematics, Vol. 90, pp. 223-237.

Versteeg, H.K. and Malalasekera, W. (1996) *An Introduction to Computational Fluid Dynamics*. Addison-Wesley Pub. Co., New York.

Wadsworth, D.C. and Erwin, D.A. (1990) One-Dimensional Hybrid Continuum/Particle Simulation Approach for Rarefied Hypersonic Flows. *AIAA Paper* No. 90-1690.

Wadsworth, D.C. and Erwin, D.A. (1992) Two-Dimensional Hybrid Continuum/Particle Approach for Rarefied Flows. *AIAA Paper* No. 92-2975.

Wang X. (2002) FastStokes: A Fast 3-D Fluid Simulation Program for Micro-Electro-Mechanical Systems. *Ph.D. Thesis*, MIT, Cambridge.